Plyn	Zastoupení (objemova procenta, ppm objemova)
dusík	78,08 %
kyslík	20,94 %
argon	0,93 %
kysličník uhličitý	0,03 %
neon	18,18 ppmv
helium	5,24 ppmv
krypton	1.14 ppmv
xenon	0.087 ppmv
vodík	0,5 ppmv
metan	2,0 ppmv
propan	2,0 ppmv
kyslíčník dusný	0,5 ppmv
ozón	0,04 pmv
voda	5 300 ppmv

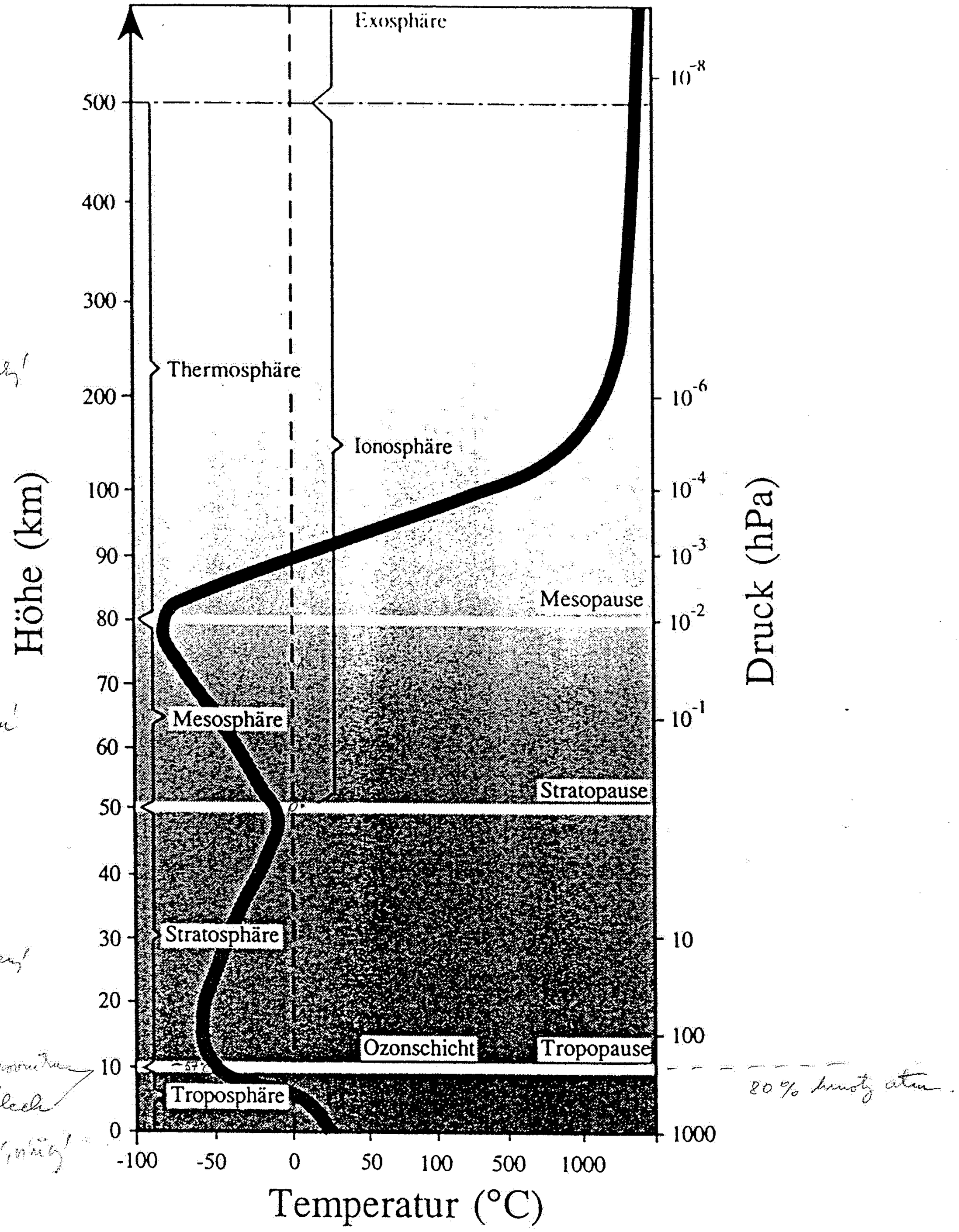

Abb. 2.1
Die Atmosphäre der Erde ist etwa 500 km mächtig. Der Temperaturverlauf in ihr ist durch die schwarze Linie angezeigt. Das uns direkt betreffende Wetter konzentriert sich in der Troposphäre.

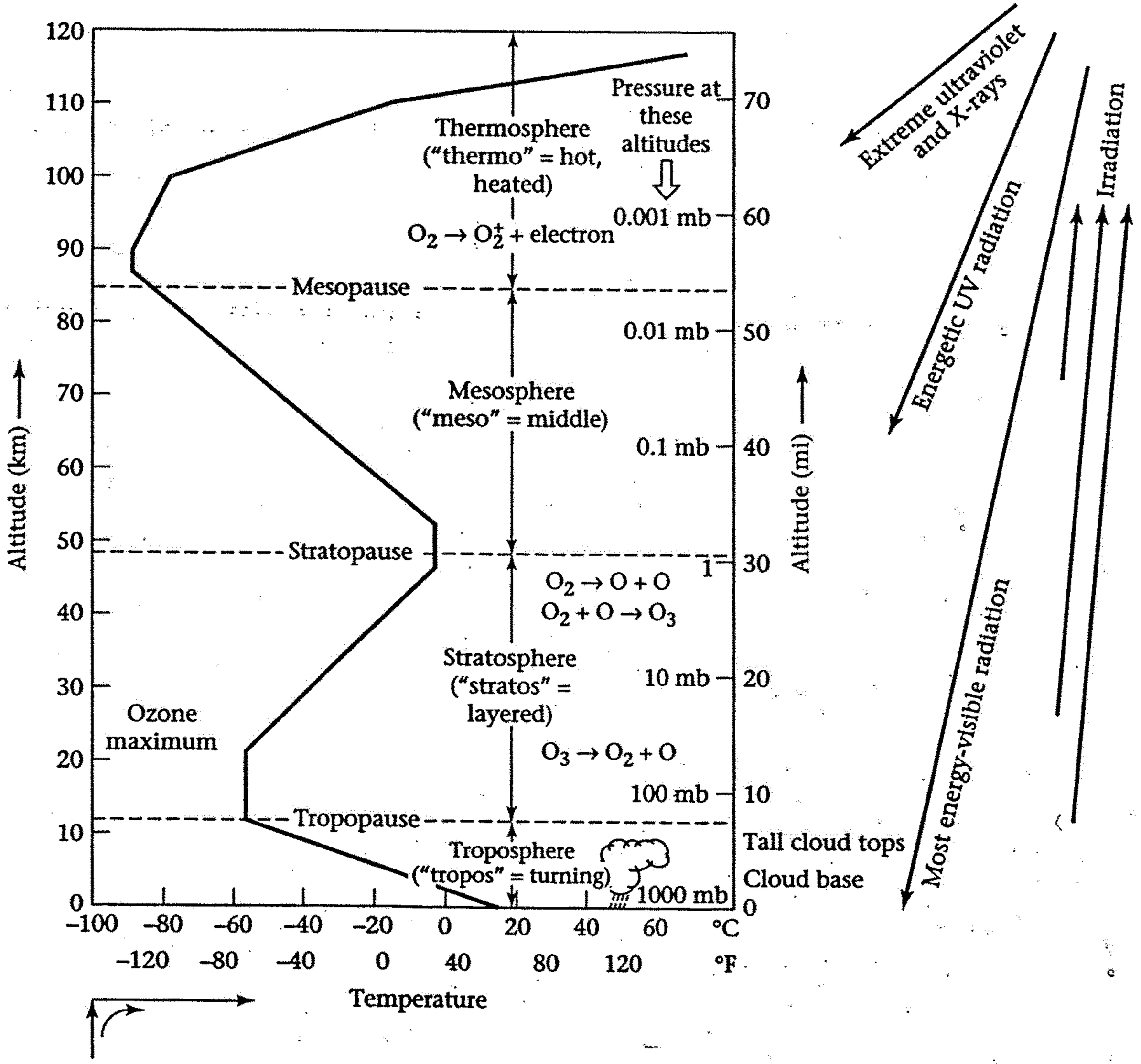

Figure 13.4. An expanded display of the variation of atmospheric temperature with altitude, showing how the temperature maxima correspond to absorption of the Sun's radiative energy, and also how the temperature patterns define the major atmospheric layers or "spheres": the troposphere, stratosphere, mesosphere, and thermosphere. Approximately the lowest kilometer of the troposphere is not named a separate sphere; however, this region, the "planetary boundary layer," exhibits strong effects from the daily cycle of solar cooling and heating. The troposphere above this region generally varies only a degree or so due to the daily cycle of heating; however, it does vary greatly with the effect of passing weather systems. km = kilometers, ml = millibars, mi = miles. (*Source:* Adapted from D. C. Ahrens, *Meteorology today; an introduction to weather, climate, and environment,* West Publishing Company, 5th edition, 1994.)

Figure 14.1. Air motions as they would occur on an imagined idealized Earth that does not spin on its axis, but is heated evenly in the tropics. In a direct circulation, as shown here, there is rising motion in the warm areas and sinking motion in the cooler areas. Poleward motions in the upper atmosphere and equatorward motions in the lower atmosphere act to enclose the circulation. Motions on the real Earth tend to begin in a similar manner near the Equator, where the effect of the Earth's rotation is small; similar cells, called Hadley cells, show this same direct circulation.

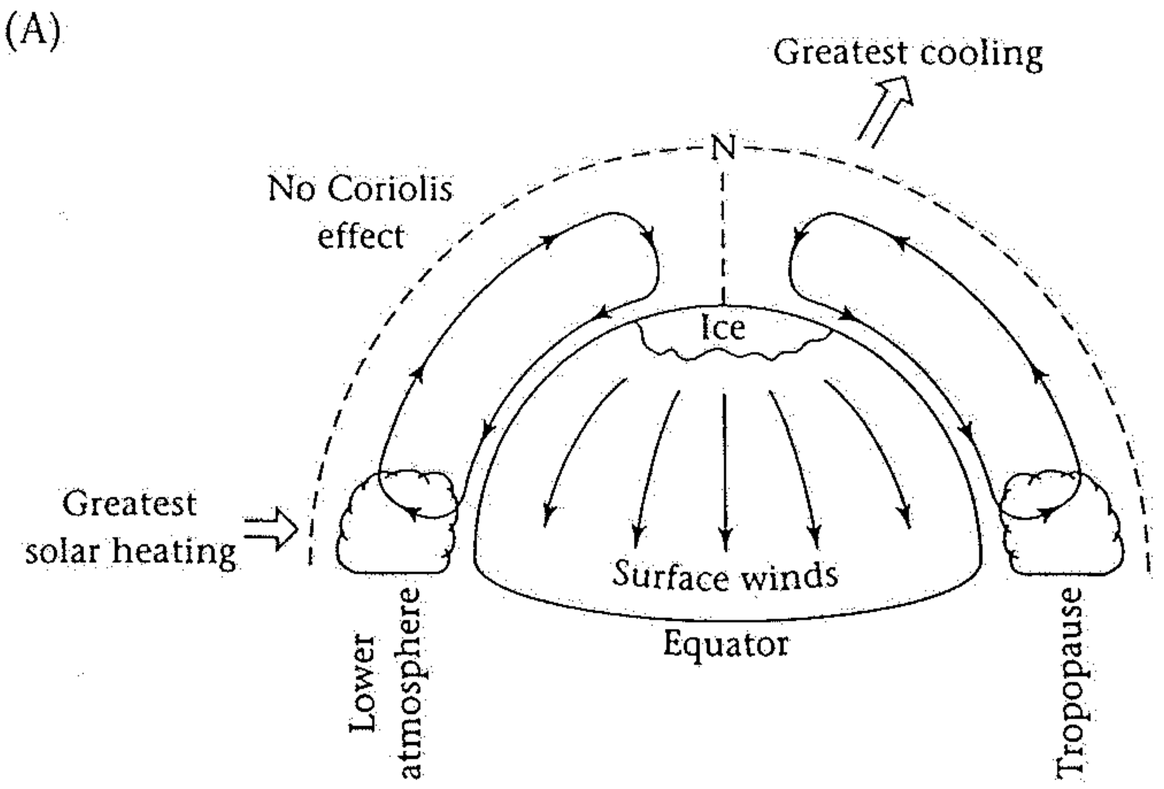

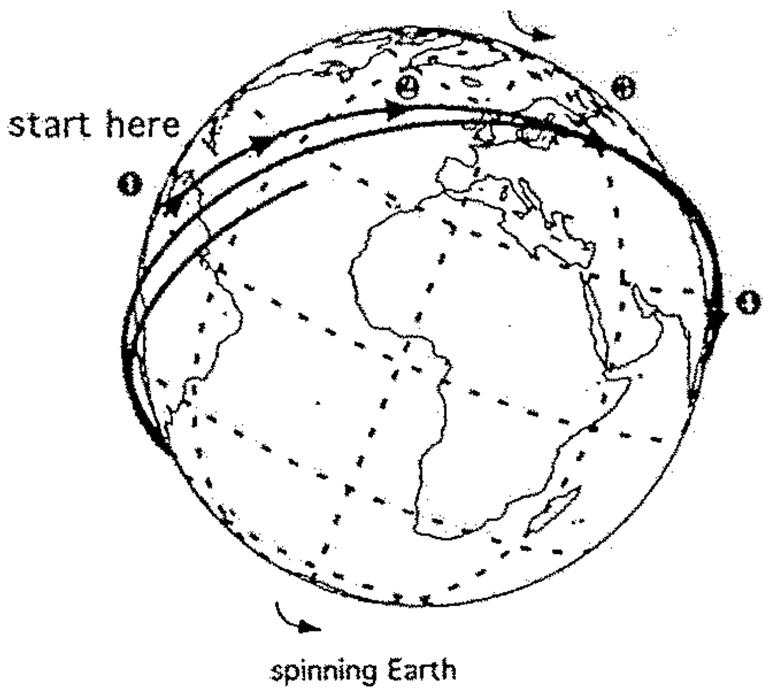

Figure 14.2. The Coriolis effect is observed when the reference point is the rotating coordinate frame defined by the spinning Earth. The left-hand figure shows a satellite in low Earth orbit, as seen from space. The satellite makes a simple circular orbit under the force of gravity alone. It was launched from the Earth and carries along some of the Earth's angular momentum plus whatever was added by the initial rocket power. The right-hand figure shows this motion from the perspective of someone moving with the reference frame of the rotating planet. As the satellite moves northward, some effect causes it to turn continuously to the right, passing regions on the Earth. The satellite is conserving angular momentum. The apparent rightward forcing then brings the satellite to a due west-east trajectory at the northernmost portion of its orbit. The satellite continues in a straight line; however, the parallels of Earth's latitude circles curve away from the straight-line motion of the satellite. Place a pencil along a latitude circle (tangent to it) to observe this effect clearly. Again there is apparent rightward motion in the flight track. Exactly the same laws of physics apply to a cannon projectile or an airplane flying within the atmosphere. The same laws of motion apply to air parcels, even as they are affected by pressure forces from surrounding parcels. In addition to the various reasons for these apparent forces, the basic physical laws of the rotating Earth's coordinate system dictate the following: There is an apparent "force," always to the right (in the Northern Hemisphere) and always proportional to the speed of the parcel. (*Source:* Adapted from J. T. Houghton, L. G. Meira Filho, B. A. Callander, N. Harris, A. Kattenberg, 2d K. Maskell, eds., *Climate change 1995: the science of climate change*, Cambridge University Press, 1996.)

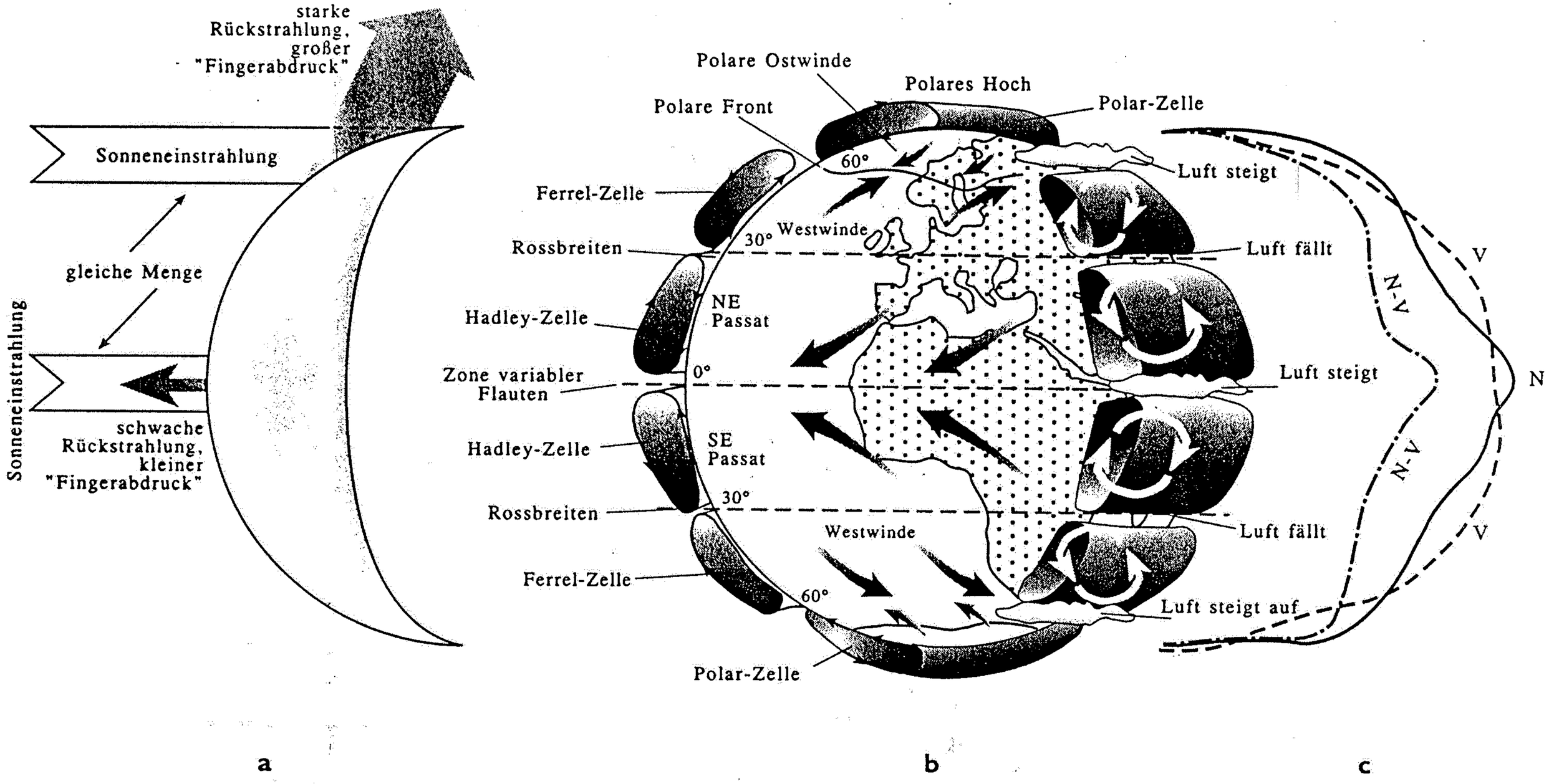

Abb. 2.2
Schema der Sonneneinstrahlung auf die Erdoberfläche sowie der Zirkulationssysteme und der Niederschlagsverteilung in der Troposphäre. **a)** Bei gleicher Menge der auf die Erdoberfläche treffenden Sonneneinstrahlung verteilt sie sich in hohen Breiten über eine größere Fläche als in niedrigen. Entsprechend größer ist die Albedo an den Polen und bedingt somit die geringere Erwärmung. **b)** Die großen atmosphärischen Zirkulationssysteme. Die Rossbreiten liegen unter den absteigenden Ästen der Hadley- und Ferrel-Zellen, die relativ kalte Luft herabführen. Das Meer ist hier oft aufgewühlt. Die häufigen Schaumkämme der stürmischen Wellen erinnerten die Seefahrer an die Mähnen galloppierender Pferde, daher der Name. Am Äquator liegt die Zone der variablen Flauten auf den Meeren unterhalb der Aufstiegszone erwärmter Luft und zwischen den beiden Hadley-Zellen. Die häufigen und langanhaltenden Flauten waren bei den Seeleuten der großen Segelschiffe gefürchtet. **c)** Relative Variation von Niederschlag *N*, Verdunstung *V* und Niederschlagsüberschuß bzw. -defizit *N-V* mit der geographischen Breite.

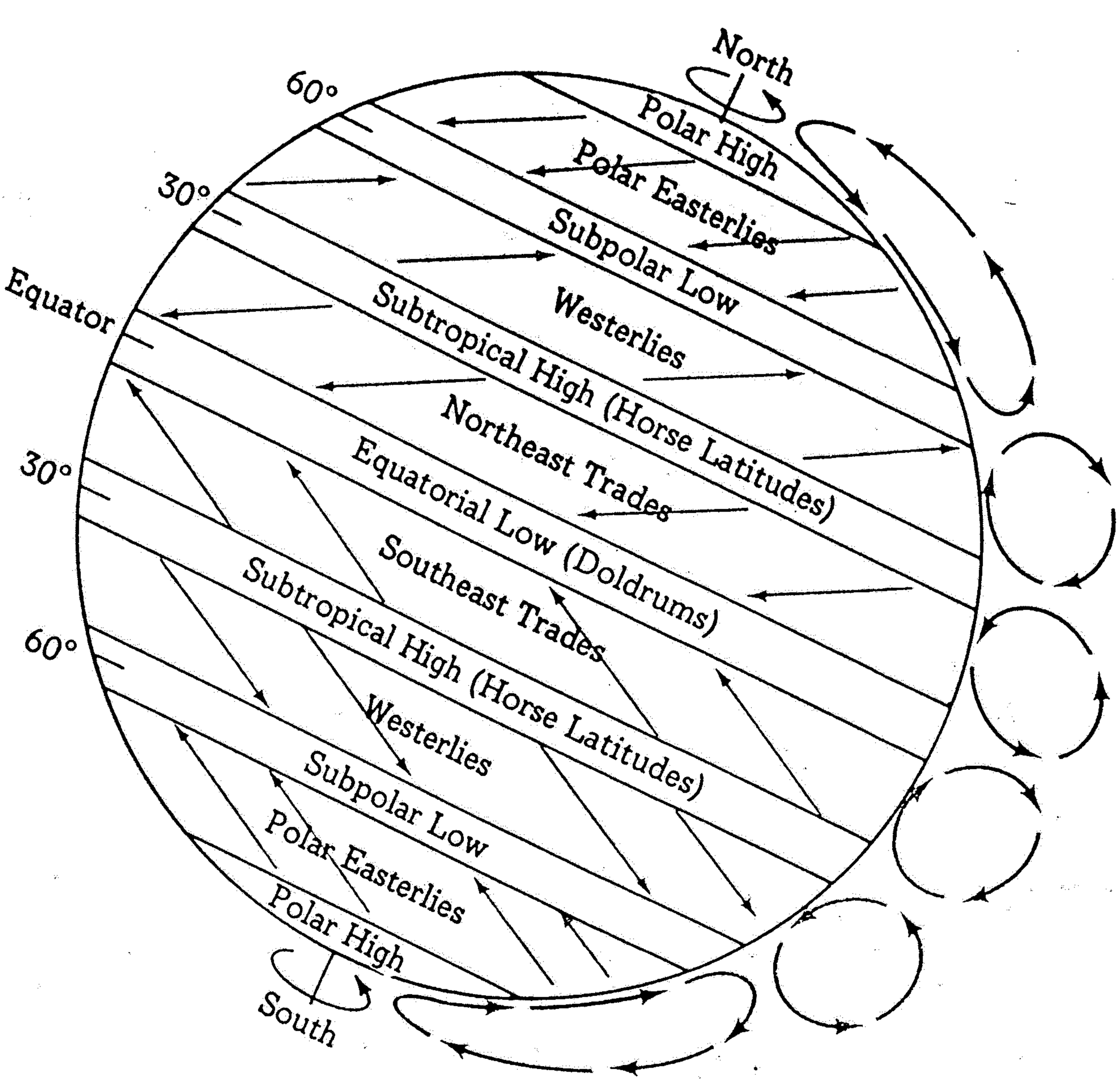

16.8 Idealized circulation of the atmosphere on a rotating globe completely covered with water. See text for discussion and relation to the major surface currents of the Earth.

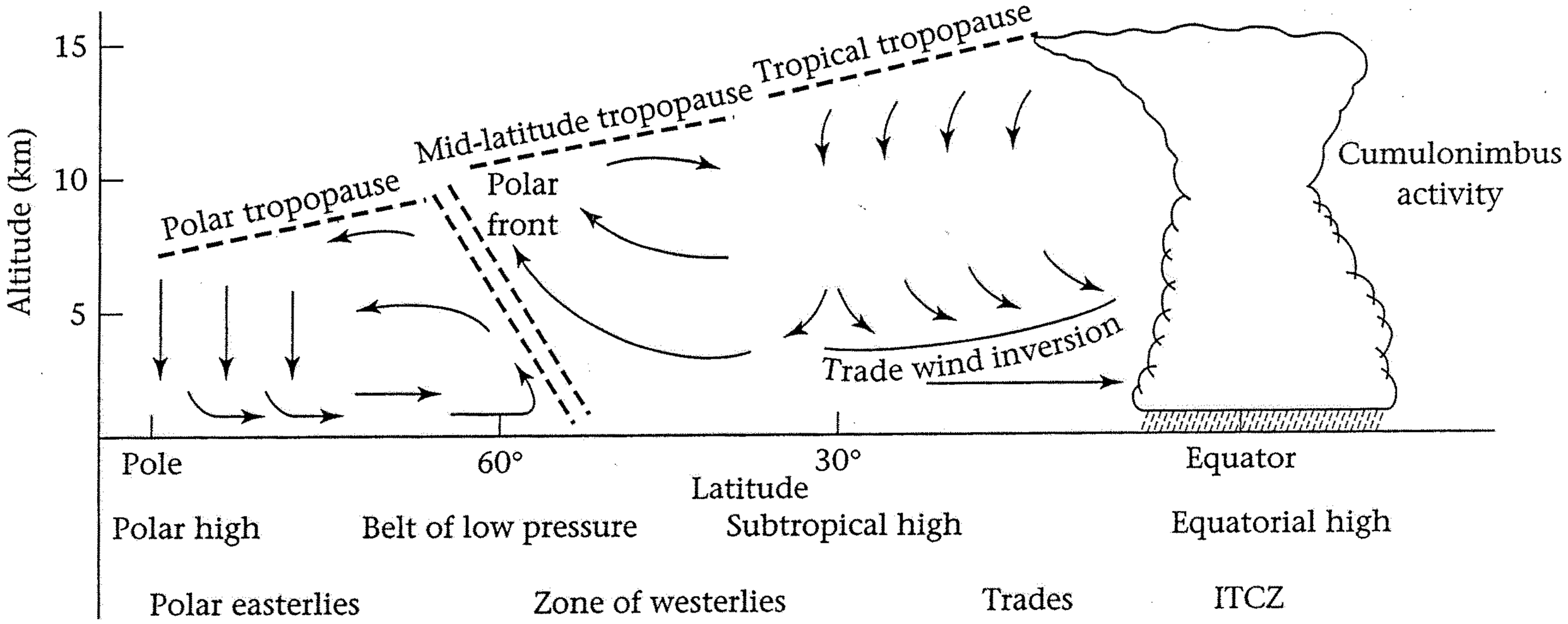

Figure 9.5. The general circulation of the atmosphere: the actual atmospheric circulation shown schematically in a vertical section from polar regions to the equator. ITCZ = intertropical convergence zone; km = kilometers. (*Source:* A. Goudie, *The nature of the environment*, 2nd ed. Copyright © Basil Blackwell Ltd., 1989. Used with permission.)

Figure 14.3. Motions of air into a low-pressure region in the Northern Hemisphere are shown at the right in (A) and at the left in (B). Air begins to move in from higher to lower air pressure, accelerated by the pressure-gradient force. However, the Coriolis effect acts continuously, causing the air to move to the right of the accelerating force; within hours, the motion becomes a slow spiral inward. The low-pressure region is called a *cyclone* because the air is moving cyclically, and in the same direction as the Earth's rotation. Similarly, in high-pressure regions, air moves outward from high to low pressure; however, the Coriolis effect moves it to the right to form nearly circular spiraling motions. These are called *anticyclones*: The motion is cyclic or nearly circular but is opposite to the direction of the Earth's spin. (*Source:* (A) Brian J. Skinner and Stephen C. Porter, *The blue planet*, Wiley, 1995, p. 342.)

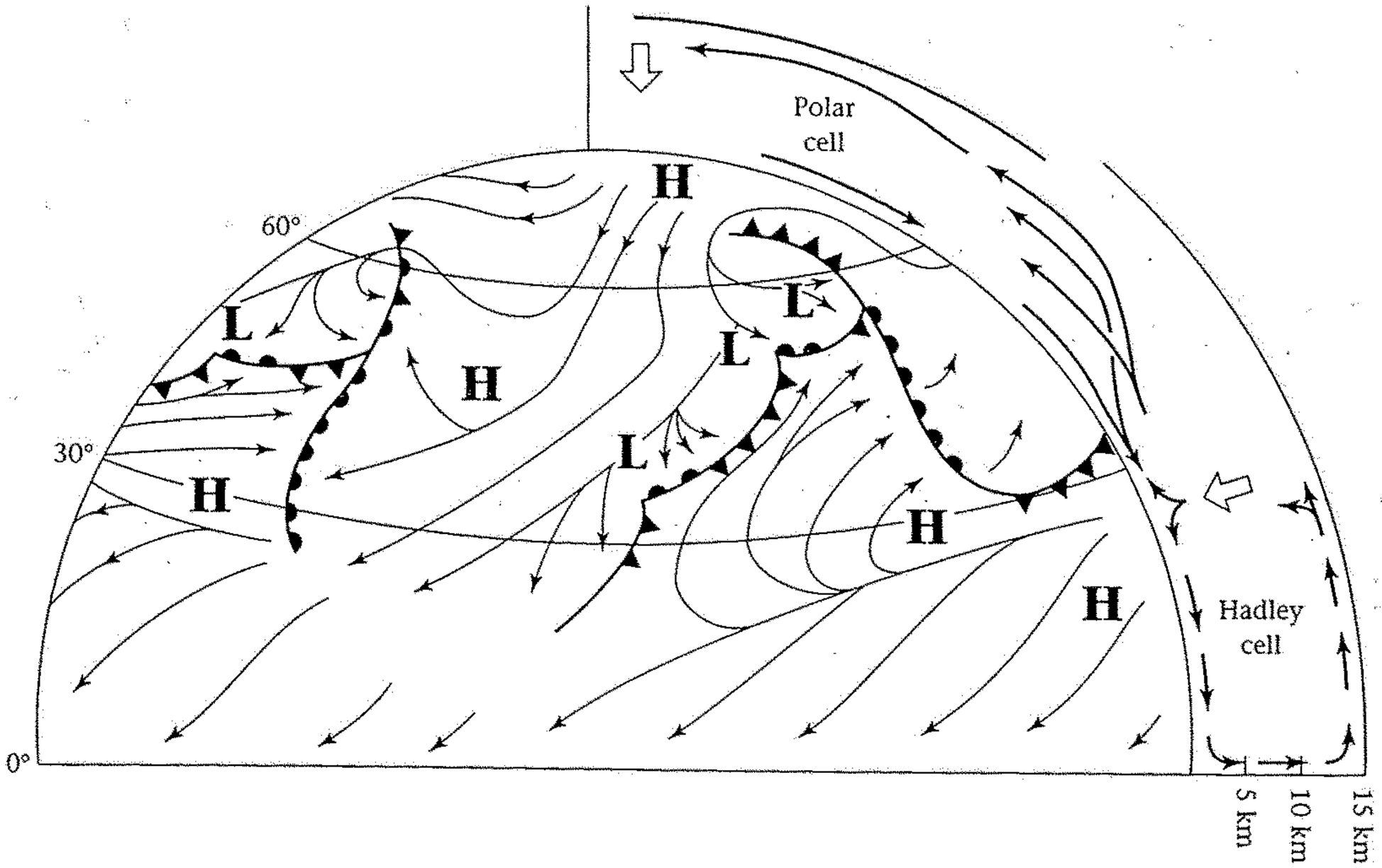

Figure 14.4. Typical coordinated motions and eddies in various regions of the globe. All winds are shown at the surface. Around the sides, cross sections show the vertical motions and great cells, such as the Hadley cells in the tropics. In the tropics, motions are driven by strong heating, and are *thermally direct.* At the poles, the strong chilling effects of the ice packs drive strong overturning motions. More complicated motions are typical in the mid-latitudes. From the Earth system perspective, these complicated motions are called *eddies,* or variations on the flow; from a more local perspective, they are *organized cyclonic storms*. These include winter storms and hurricanes or typhoons. Between these localized rainy regions are larger regions of fair weather, the great anticyclones, or high-pressure systems. (*Source:* Adapted from L. Musk, *Weather systems*, Cambridge University Press, 1988.)

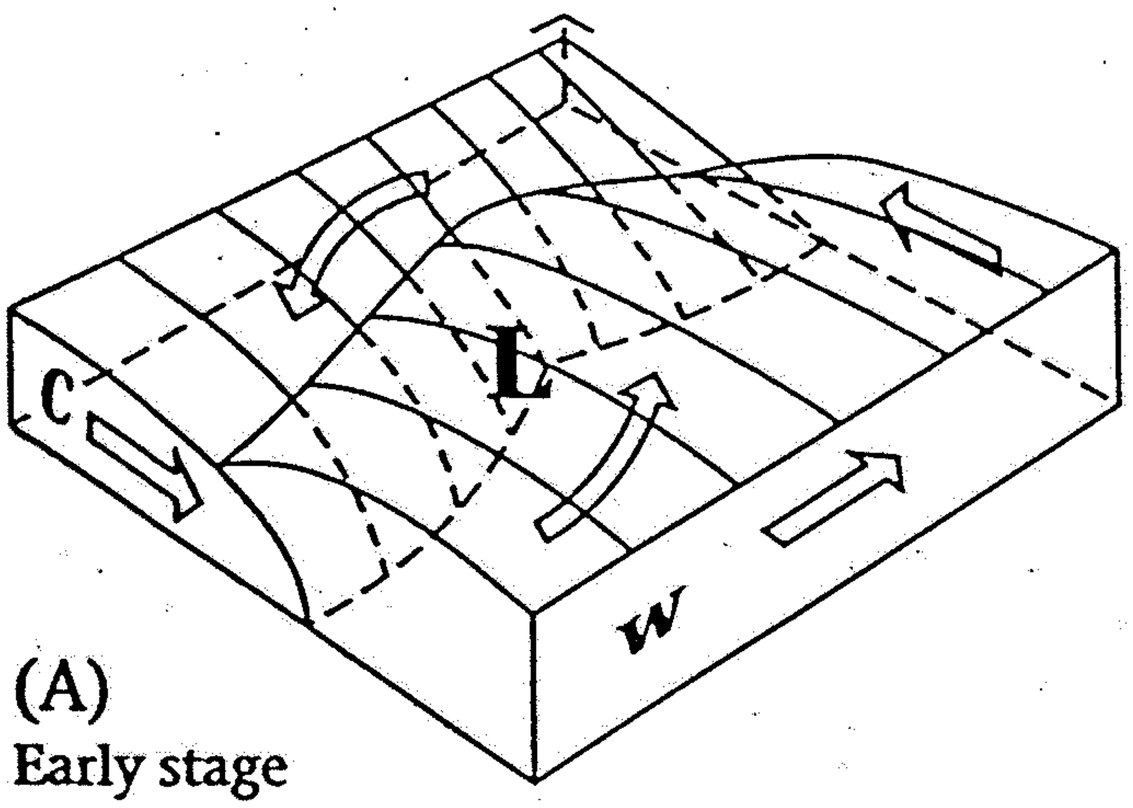

(A)
Early stage

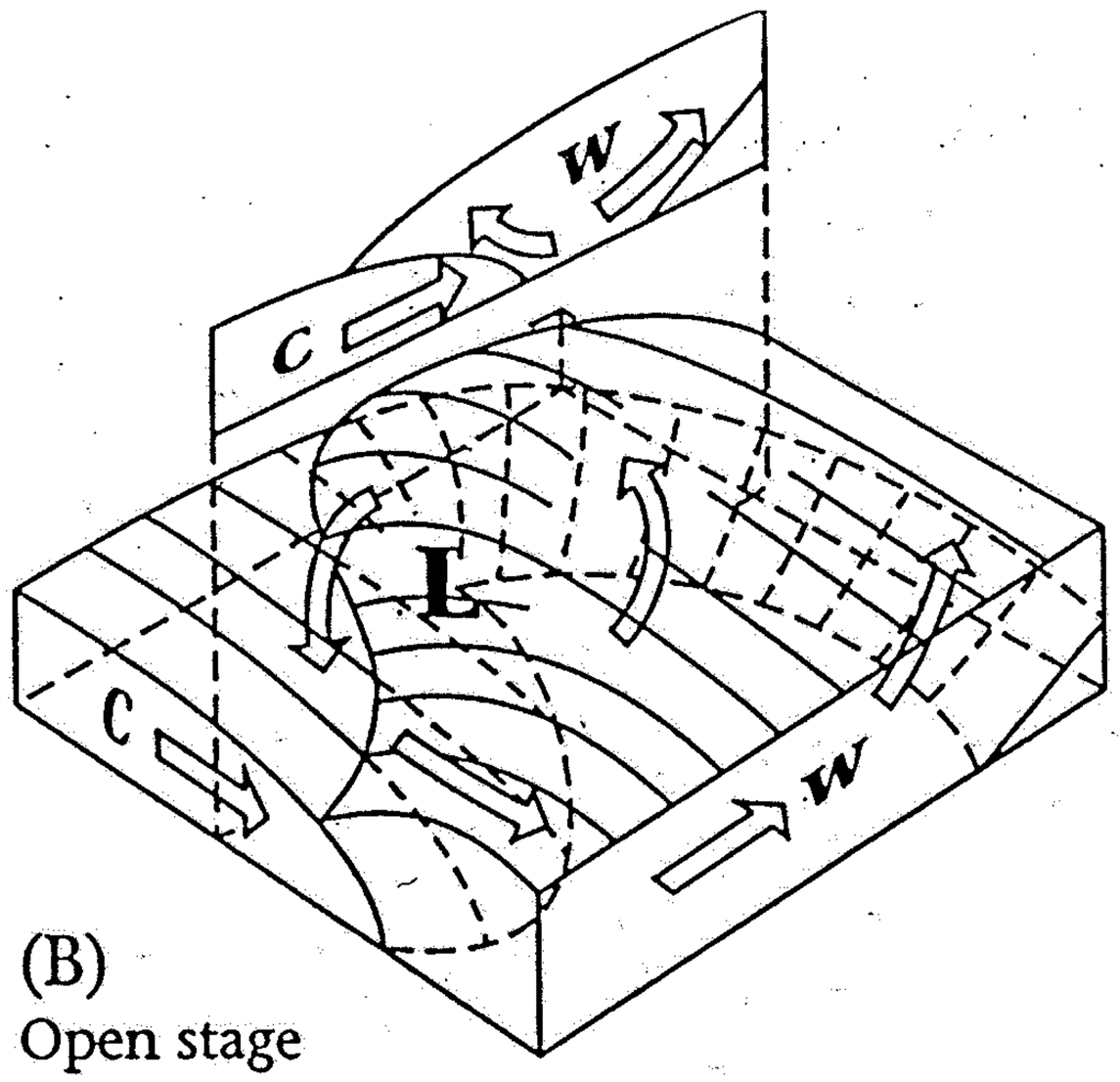

(B)
Open stage

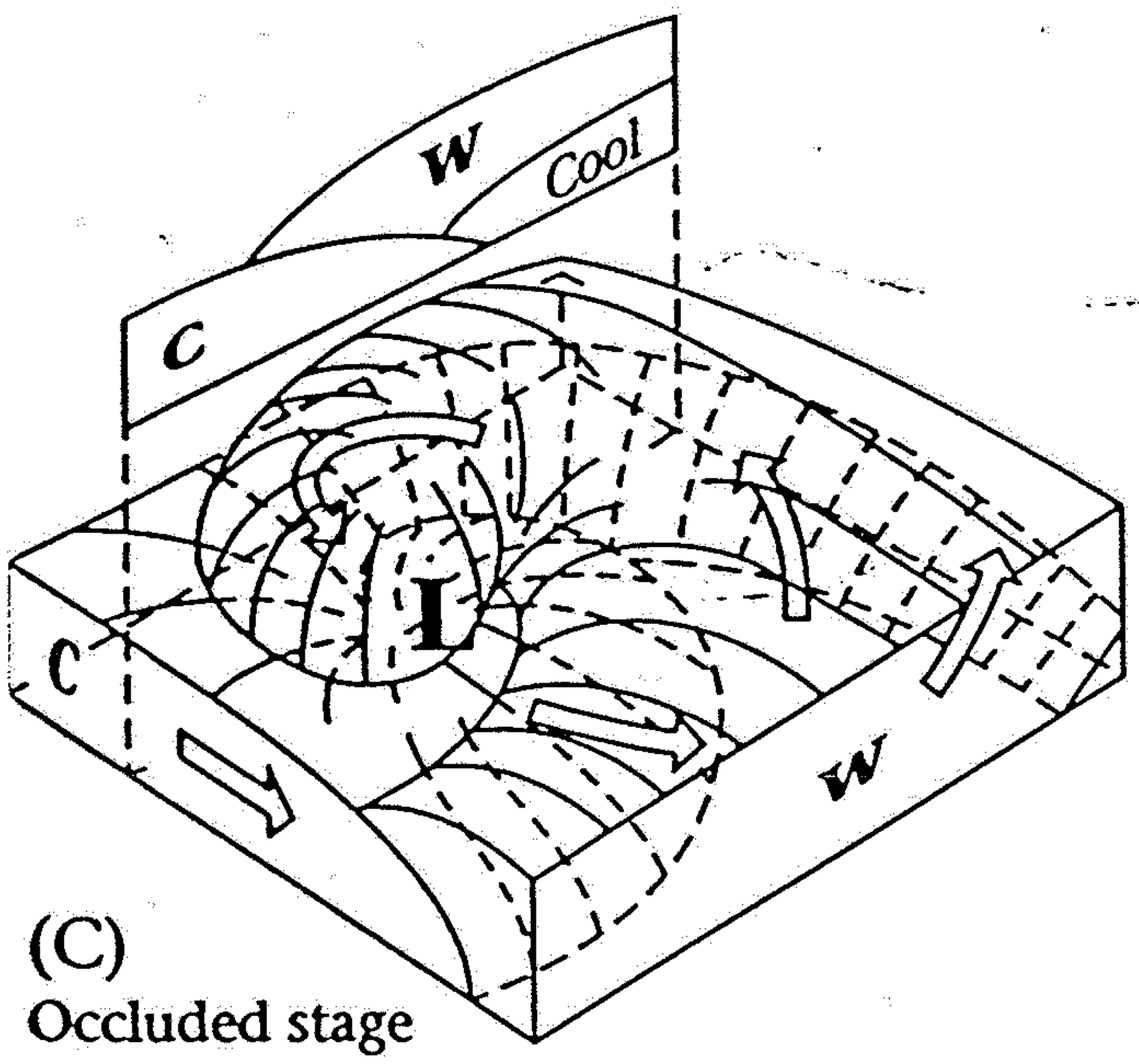

(C)
Occluded stage

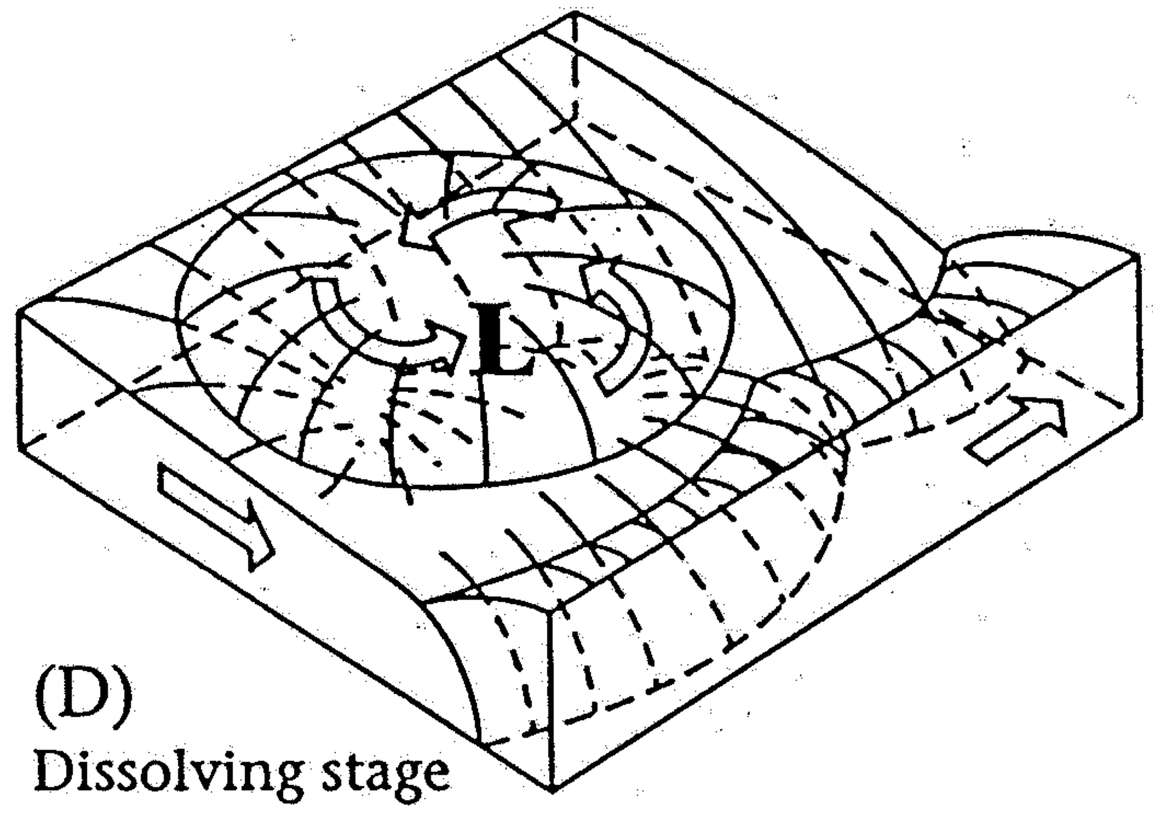

(D)
Dissolving stage

Figure 14.5. A simplified view of the development of a typical mid-latitude weather system, known as an *extratropical cyclonic storm*, also called a *winter storm*, although it can occur during any season. (A) The storm begins anywhere along a front, or boundary between cooler (polar-influenced) and warmer (more tropically influenced) air. These boundaries tend to be distinct. (B) Warm air flows in from the south and rises, producing an area of low pressure. (C) Meanwhile, cold air sinks as it flows around the storm from the north; eventually some air will curve around the rear of the storm, along what is called the *cold front*. Cold air occupies progressively more of the surface, whereas warm air collects aloft. (D) As a result of the Coriolis effect, warm and cold air tend to take spiraling paths around the low-pressure center.

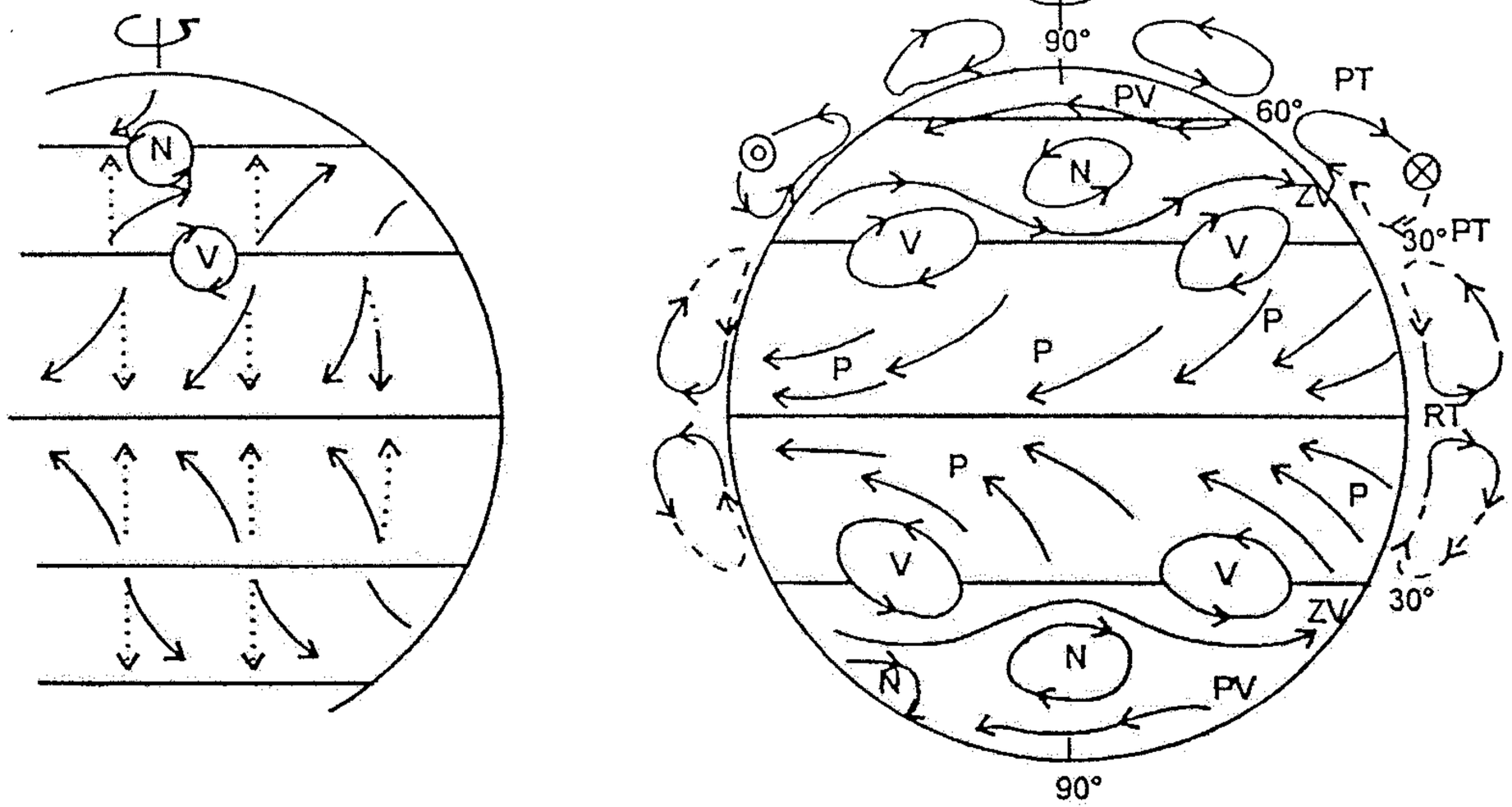

20.2 Všeobecná cirkulácia vzduchu. V - subtropická tlaková výš, N - tlaková níž, P - pasát, PT - pásmo tíšin, RT - rovníkové tíšiny, PV - východný polárny vietor, ZV - západný vietor. Otáčanie Zeme od-

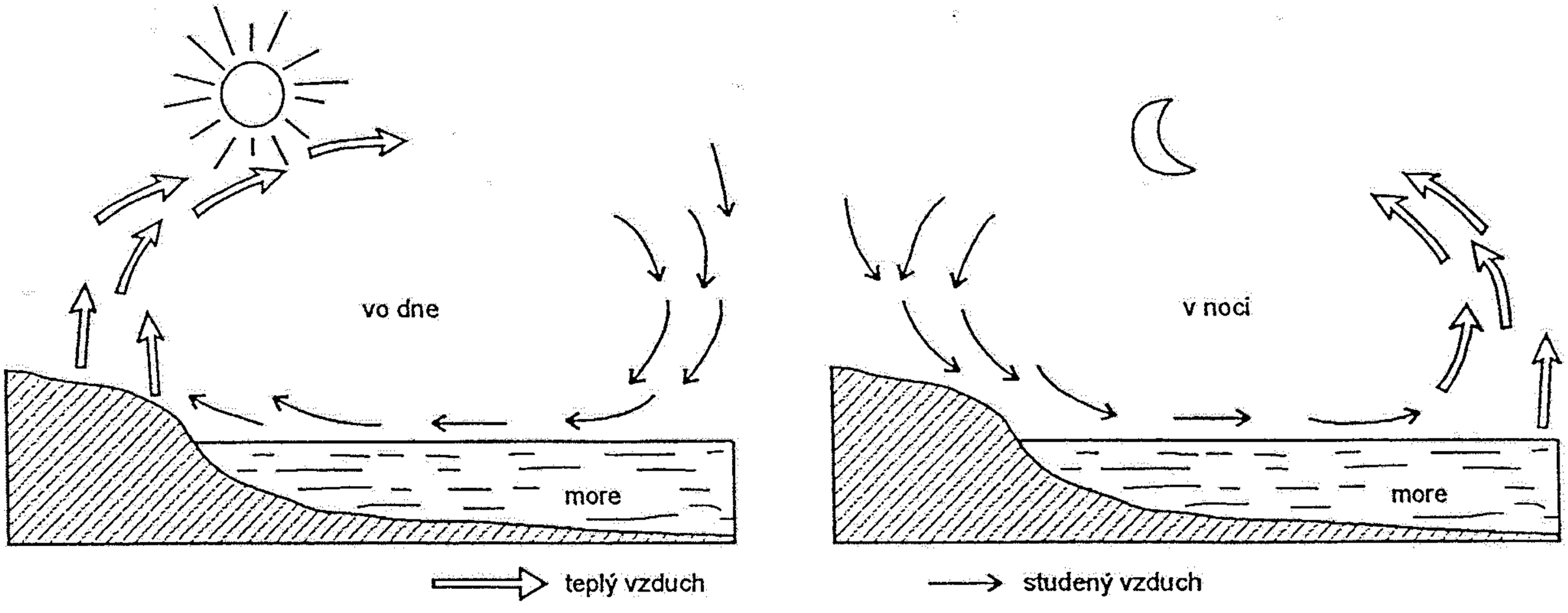

20.1 Pobrežný vietor - morská bríza

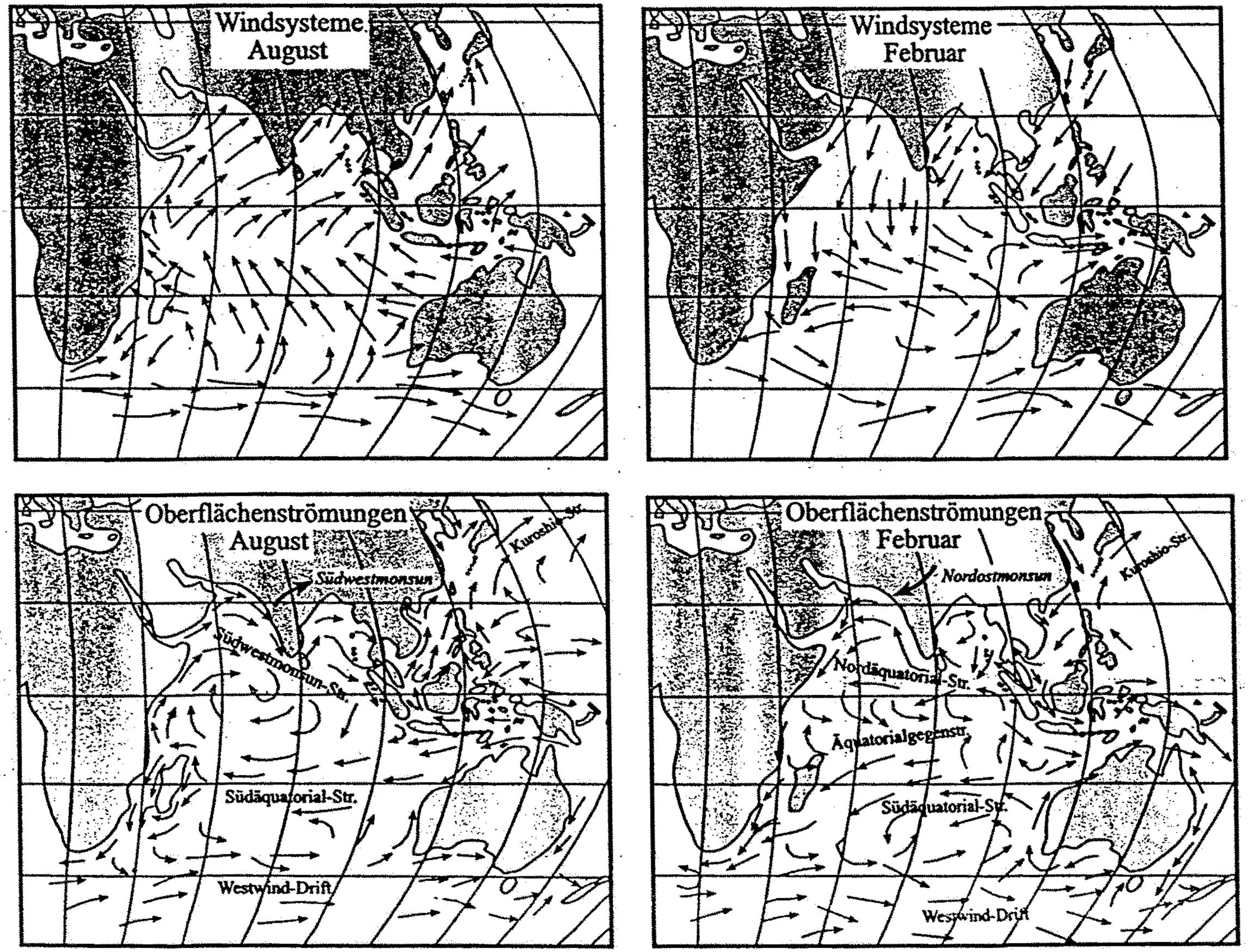

Abb. 2.4

Jahreszeitliche Variation der Monsunströmungen. **a)** August: Asien wärmt sich im Verlauf des Sommers auf, daher steigt die erwärmte Luft über der großen kontinentalen Landmasse auf und zieht Luft aus SW an. **b)** Infolge der gesteigerten Albedo über dem Kontinent wird Luft aus SW nachgesogen. Dieser Luftstrom bewegt sich nordostwärts nach Asien hinein und erzeugt vorher westlich von Indien im Indischen Ozean durch Reibungsübertragung die entsprechende Meeresströmung des SW-Monsunstroms, der an die Stelle des nördlichen Äquatorialstroms tritt. **c)** Februar: Kalte asiatische Luft weht im Winter als NE-Monsun aus NE über den Indischen Ozean, da nun hier in Äquatornähe infolge stärkerer Erwärmung Luftmassen aufsteigen. Infolge der niedrigen Albedo Asiens bildet sich **d)** der Nord-Äquatorialstrom wieder aus und der Indische Ozean zeigt Strömungsmuster wie die anderen Ozeane (nach GROSS, 1977).

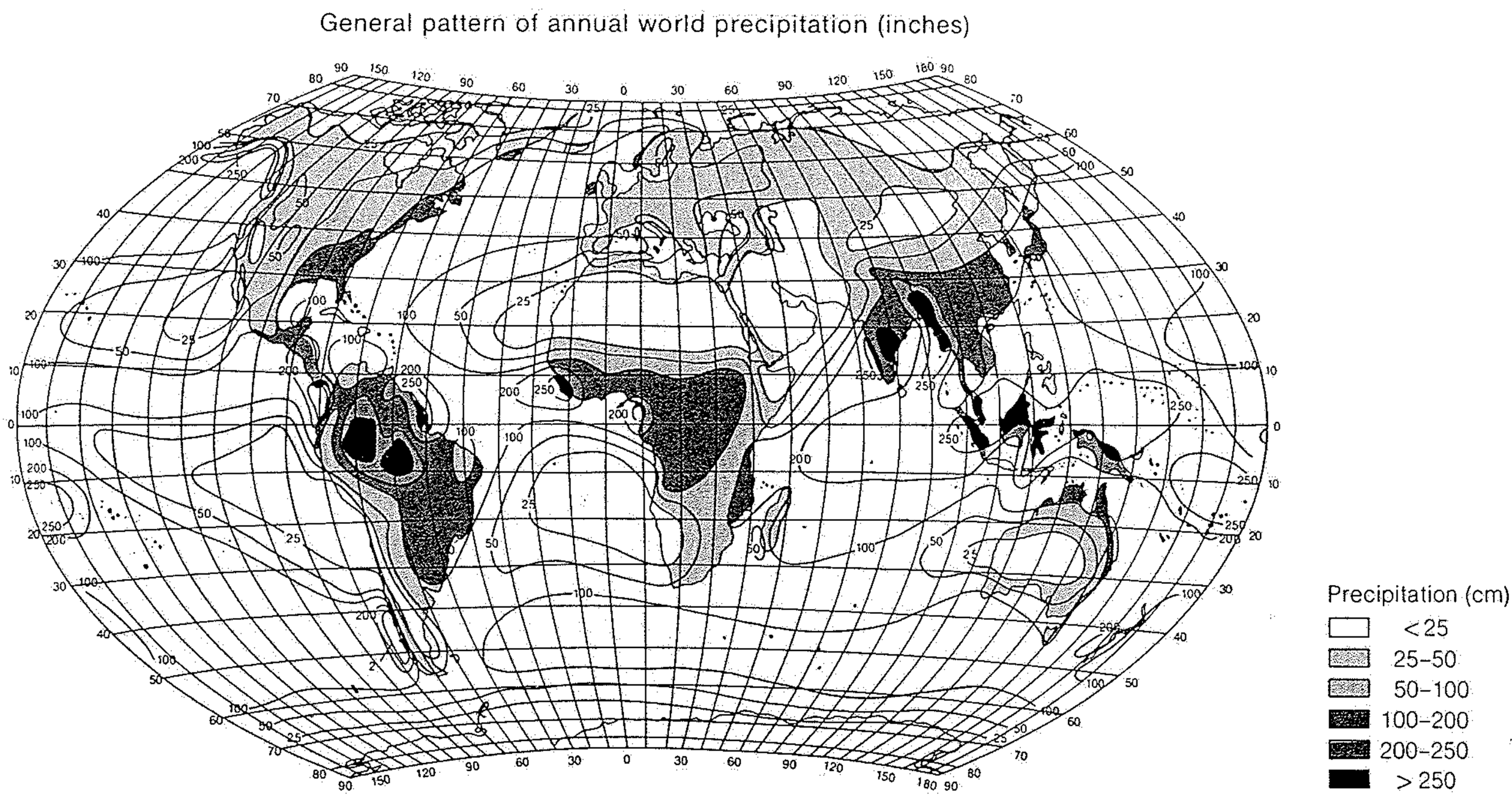

Figure 9-9

World distribution of average annual precipitation. [From *Climates of the World*, ESSA Environmental Data Service, Asheville, N.C., 1969.]

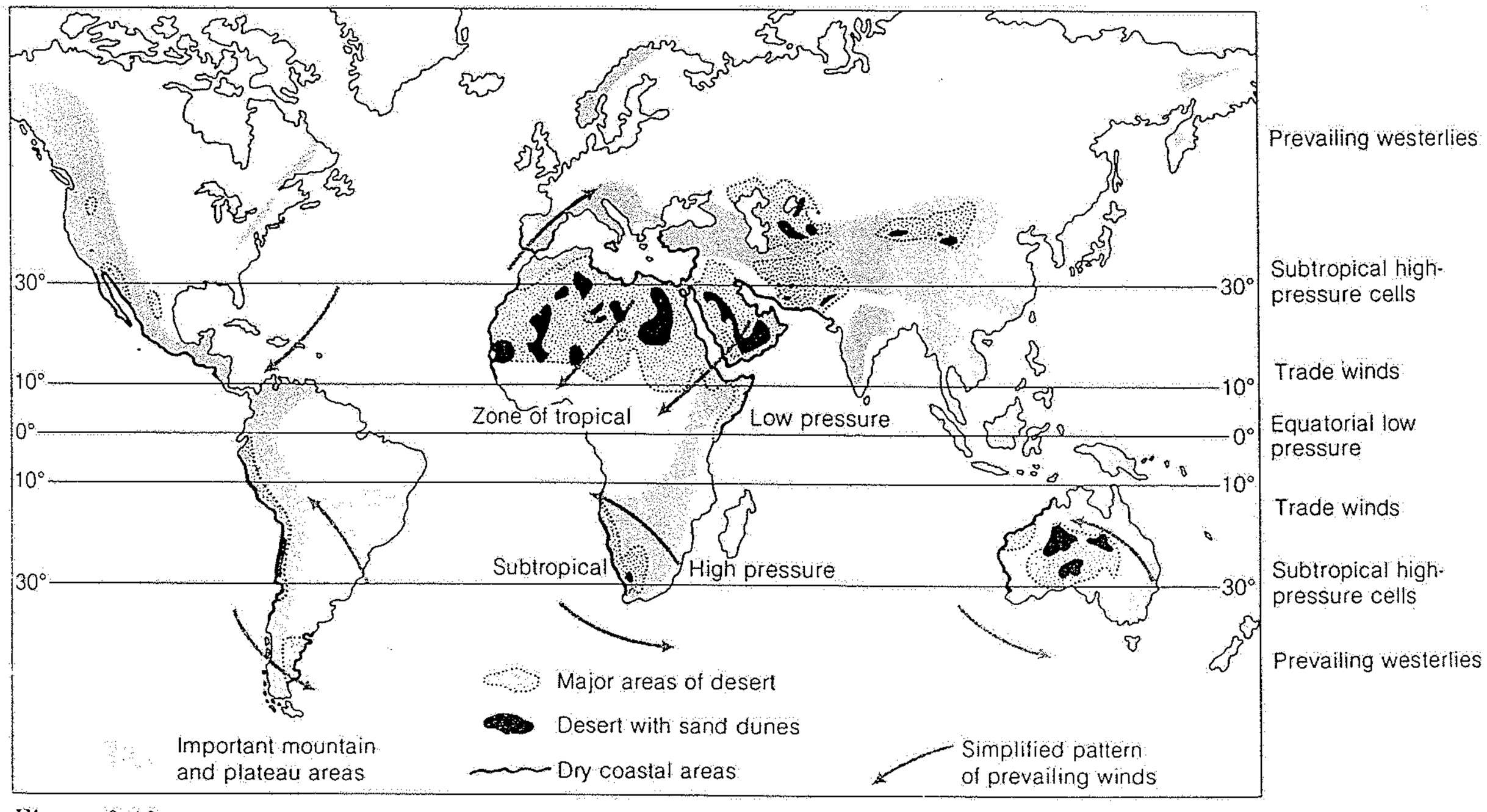

Figure 9-10

Major desert areas of the world in relation to prevailing wind directions and major topographic elevations. Sand dunes are only a small proportion of the total desert areas. [After *Desert Sedimentary Environments* by K. W. Glennie. Elsevier, 1970.]

Upraveno mezinárodní dohodou 1939

BEAUFORTOVA STUPNICE SÍLY VĚTRU

stupeň	označení v angličtině	rozpoznávací znaky	rychlost v m/s	rychlost v km/h
0	bezvětří - calm	Kouř stoupá kolmo vzhůru.	0,0 – 0,2	<1
1	vánek - light air	Směr větru je poznatelný podle pohybu kouře, vítr však neúčinkuje na větrnou korouhev.	0,3 – 1,5	1 – 5
2	slabý vítr - light breeze	Vítr je cítit ve tváři, listy stromů šelestí, korouhev se pohybuje.	1,6 – 3,3	6 – 11
3	mírný vítr - gentle breeze	Listy stromů a větvičky jsou v trvalém pohybu, vítr napíná praporky.	3,4 – 5,4	12 – 19
4	dosti čerstvý vítr - mod. breeze	Vítr zvedá prach a kousky papíru, pohybuje slabšími větvemi.	5,5 – 7,9	20 – 28
5	čerstvý vítr - fresh breeze	Listnaté keře se ohýbají, na stojatých vodách se tvoří vlnky se zpěněnými hřebeny.	8,0 – 10,7	29 – 38
6	silný vítr - strong breeze	Vítr pohybuje silnějšími větvemi, telegrafní dráty sviští, používání deštníku je nesnadné.	10,8 – 13,8	29 – 49
7	prudký vítr - moderate gale	Vítr pohybuje celými stromy, chůze proti větru je obtížná.	13,9 – 17,1	50 – 61
8	bouřlivý vítr - fresh gale	Vítr láme větve, normální chůze je nemožná.	17,2 – 20,7	62 – 74
9	vichřice - strong gale	Vítr způsobuje menší škody na stavbách (strhává komíny a střešní tašky).	20,8 – 24,4	75 – 88
10	silná vichřice - whole gale	Vítr vyvrací stromy; na pevnině se vyskytuje zřídka.	24,5 – 28,4	89 – 102
11	mohutná vichřice - storm	Působí rozsáhlé škody; vyskytuje se velmi zřídka.	28,5 – 32,6	103 – 117
12	orkán - hurricane	Ničivé účinky.	≧32,7	≧118

Beaufortova stupnice byla zavedena začátkem 19. stol. a založena na odhadu (posouzení) rychlosti větru podle typu (tvaru) a výšky vln, míry zpěnění moře (spršky) a viditelnosti - původní záměr byl cílen na stanovení povětrnostních podmínek lodní dopravy.

Údaje o rychlosti větru byly proto v původní verzi uvedeny v uzlech (knots) = počet námořních mil za hod.

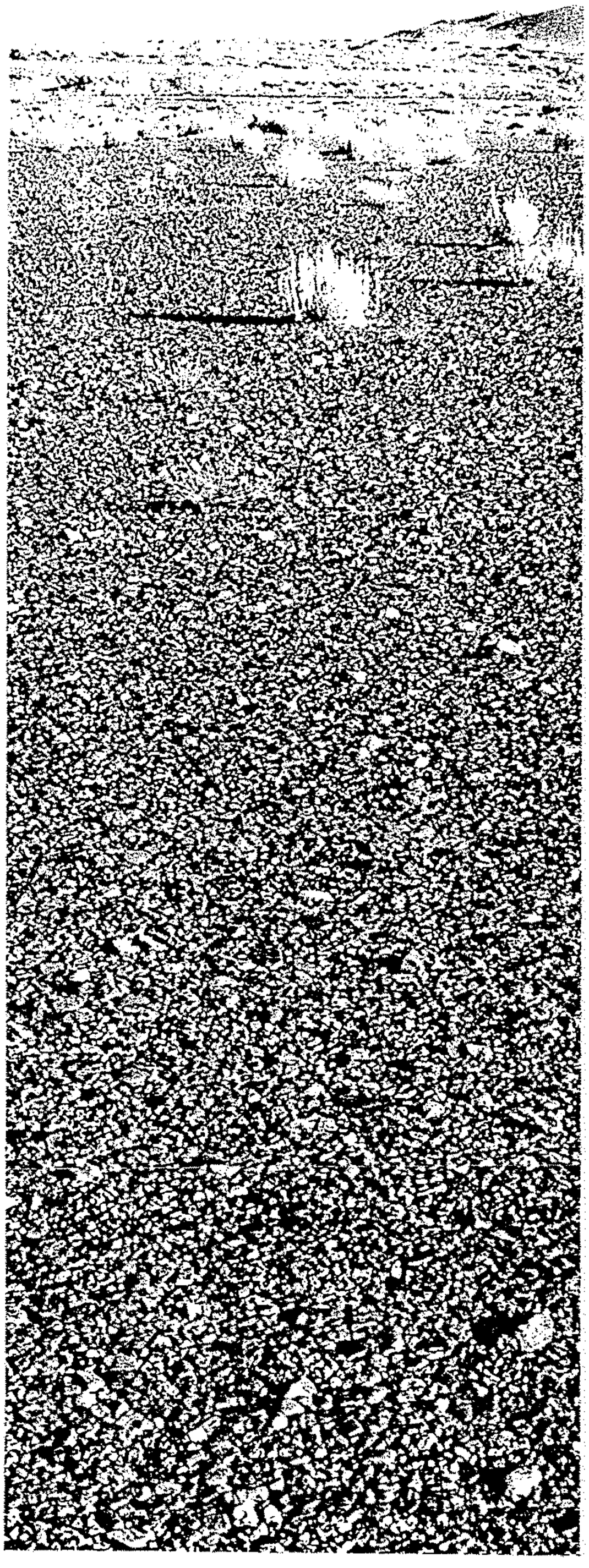

FIGURE 15–11
Deflation armor or desert pavement in the valley of the Little Colorado River, Arizona. (Photo by Tad Nichols, Tucson, Arizona.)

FIGURE 15–10
Desert pavement in Death Valley, California. Note how several of the pebbles have been faceted by sandblast. (Photo by Eliot Blackwelder.)

FIGURE 15–14
Concretions left on the rim of the Kharga Oasis, Western Desert, Egypt, by the deflation of finer sand grains, not so well cemented. (Photo by Tad Nichols, Tucson, Arizona.)

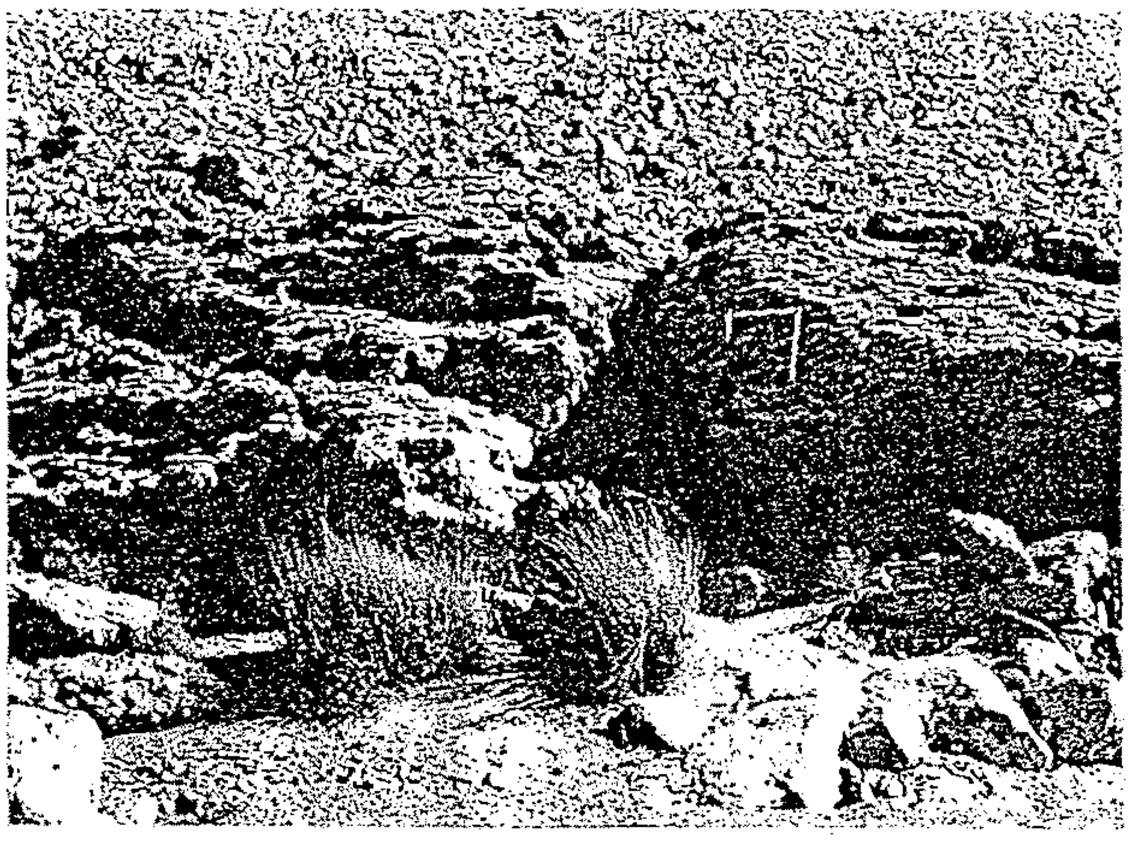

Fig. 3. Tafoni weathering in Cretaceous limestone in a branch valley of Wādī al Washkah. Oct. 1977.

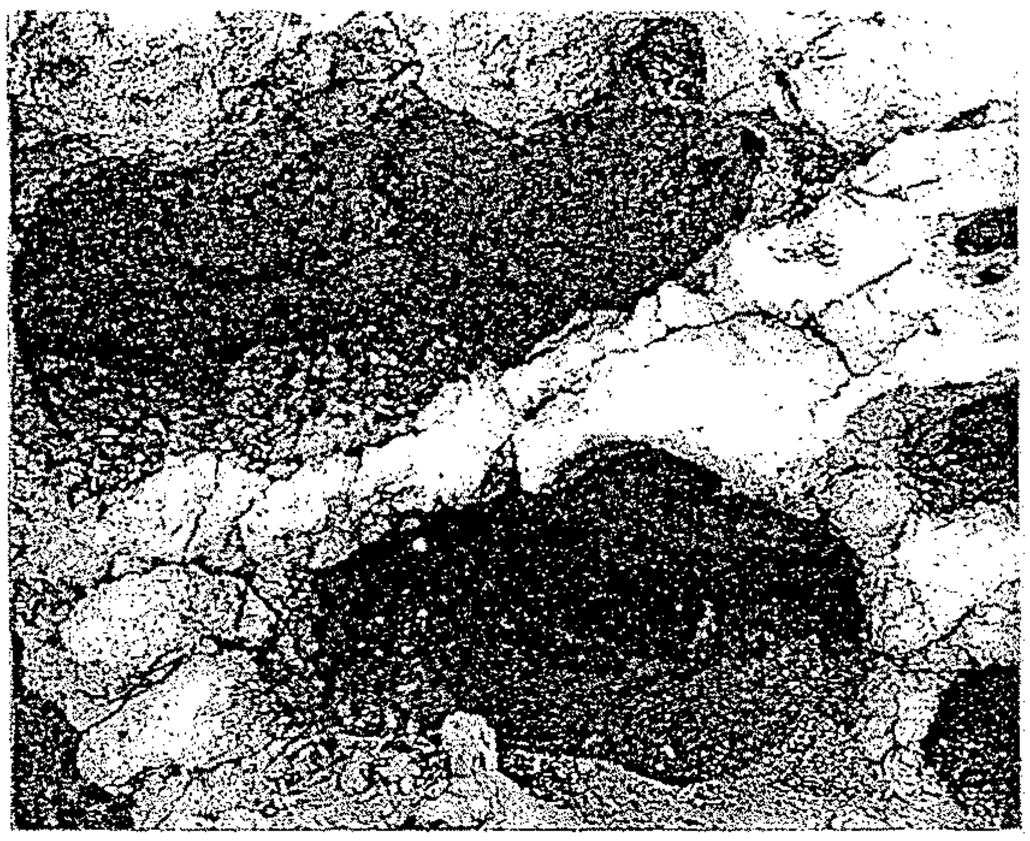

Fig. 4. Detail from Fig. 3. Fine material loosened by chemical weathering is still in the cavities. Oct. 1977.

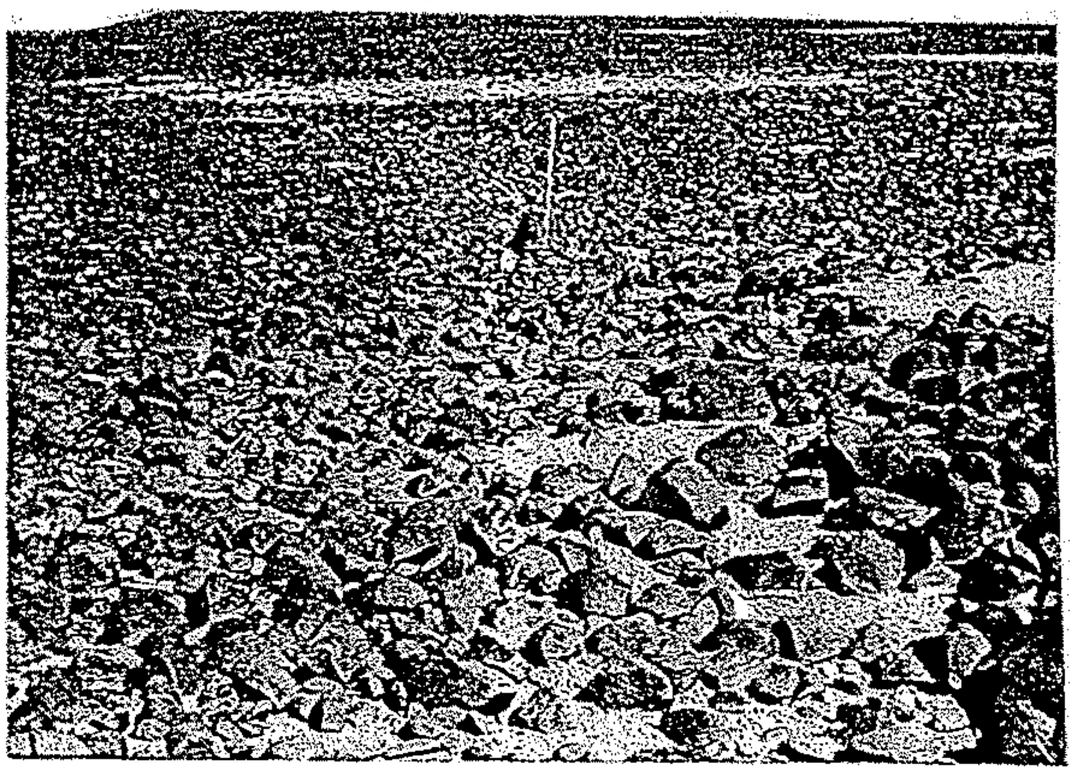

Fig. 18. Fine material fields on a basalt surface. Centre drainage channel is visible in which the basalts are heav weathered and rounded, without having been rolled. T drainage channel is recognizable by its lighter colour a rounded material. Nov. 1977.

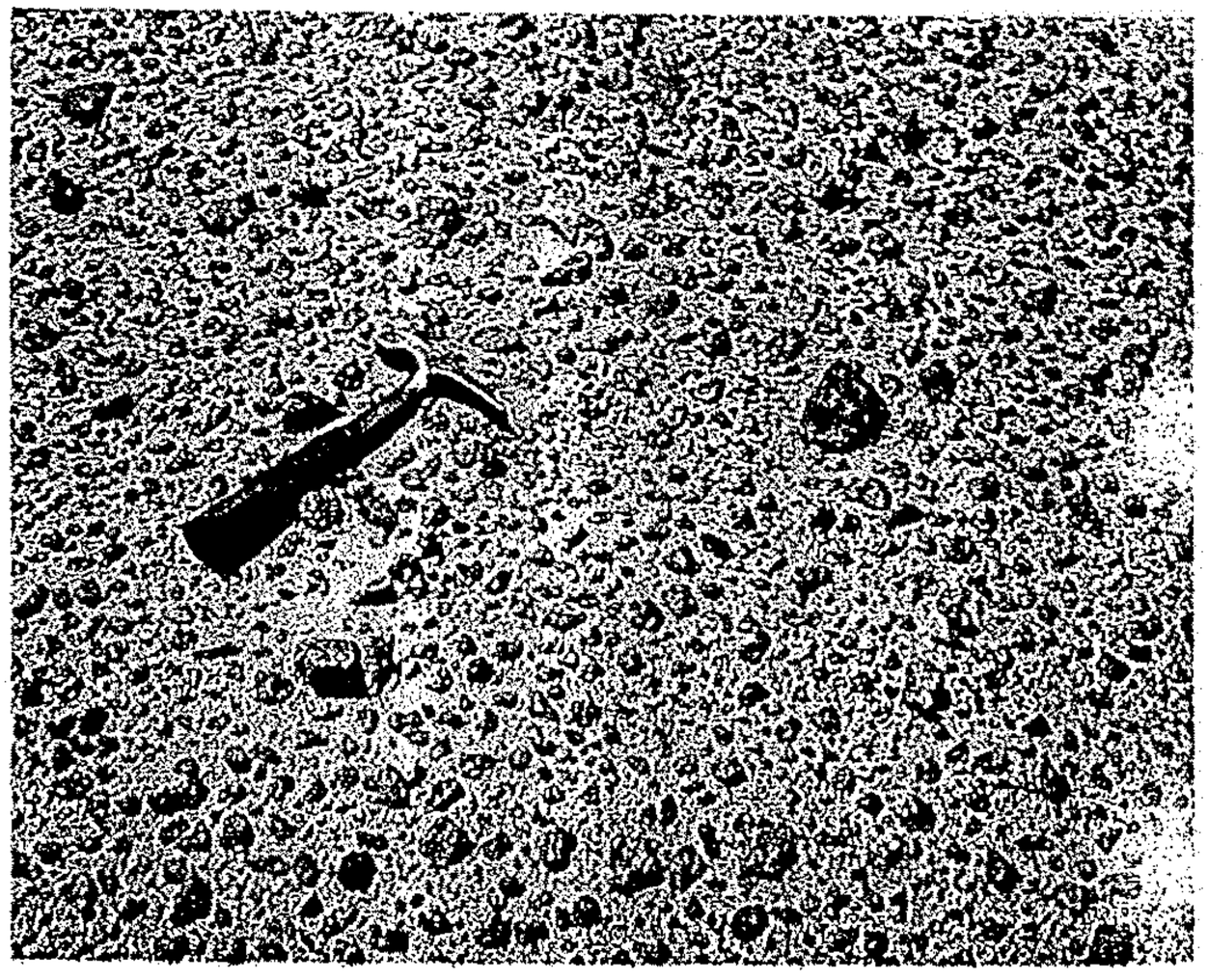

17.9 Stone-littered surfaces are common in the desert, as illustrated by this example from the Sahara. [Franklyn B. Van Houten.]

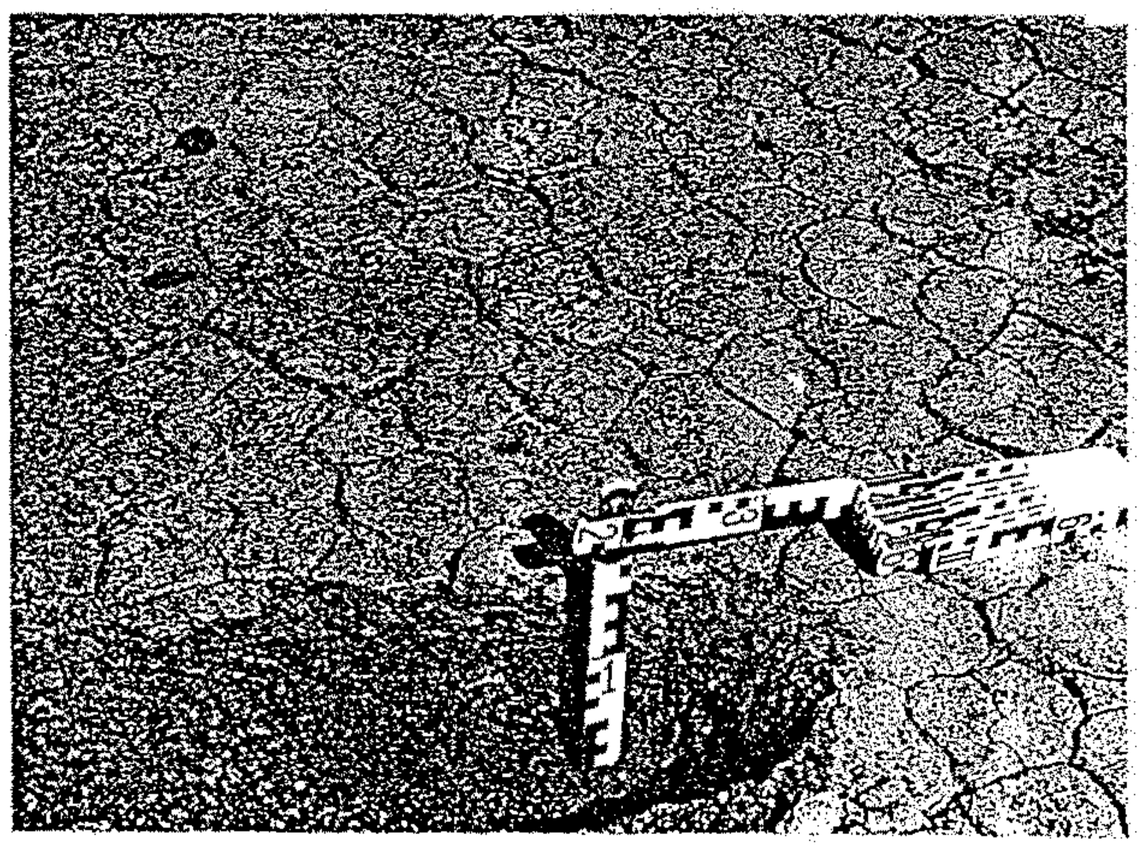

Fig. 19. Fine material and clay plane in basalt with mud cracks (Fig. 18). The fact that the cracks are not deep shows that after rainfall moisture never penetrates far. Nov. 1977.

Fig. 17. 3–4 cm deep moisture penetration of a pediment after rainfall on 12.11.1977. Photo 13.11. 1977.

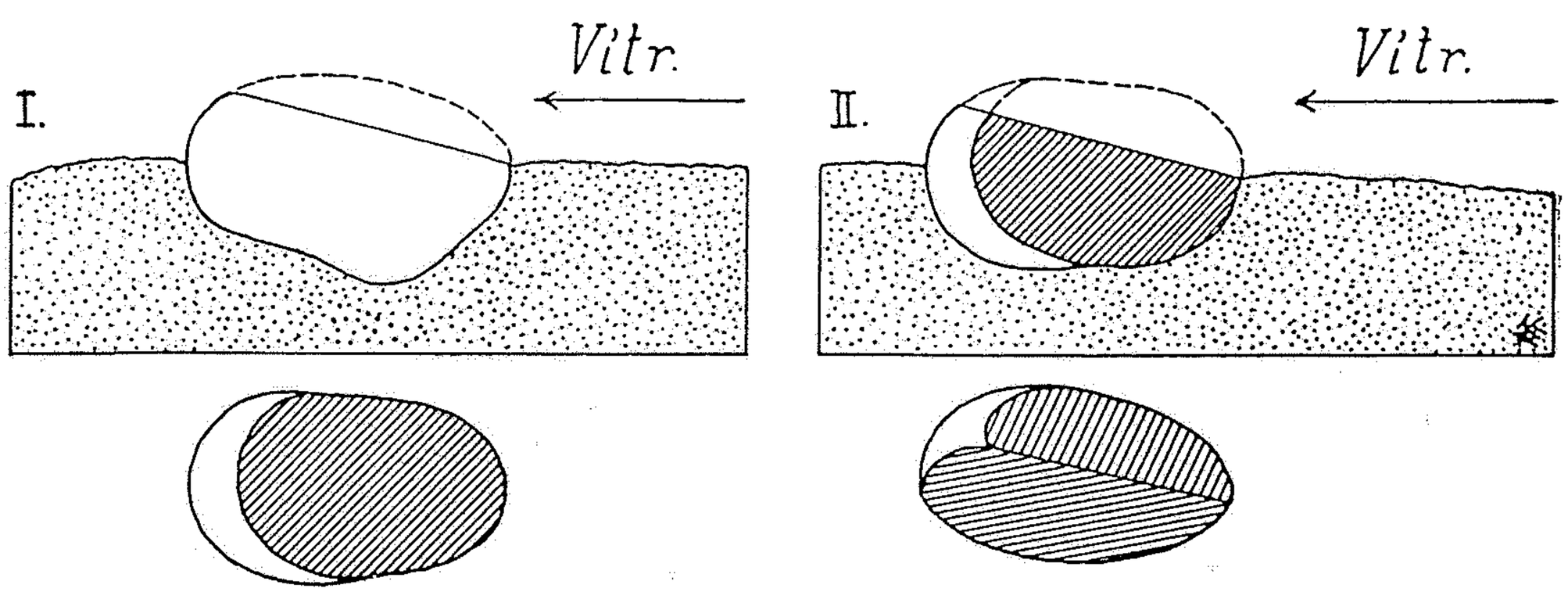

Obr. 94. *Vznik hranců.* I. *Písek hnaný větrem přes valoun vyčnívající z povrchu pískových uloženin obrušuje valoun a vytváří na něm sbroušenou plochu (facetu).* II. *Změní-li takto sbroušený valoun svou polohu, vytváří na něm vátý písek další facetu, která se s facetou první stýká v ostré hraně.*
(Podle G. WAGNERA.)

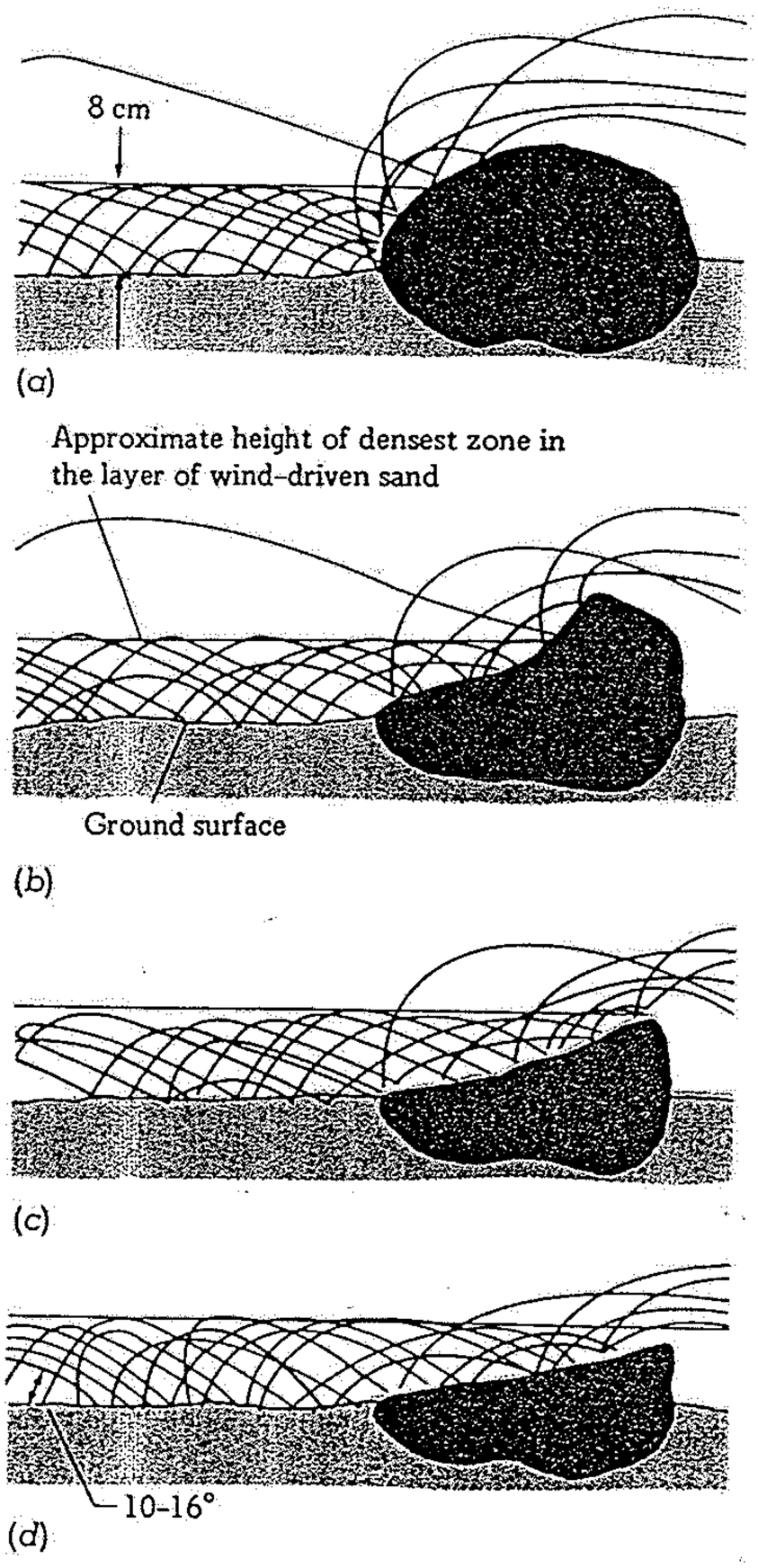

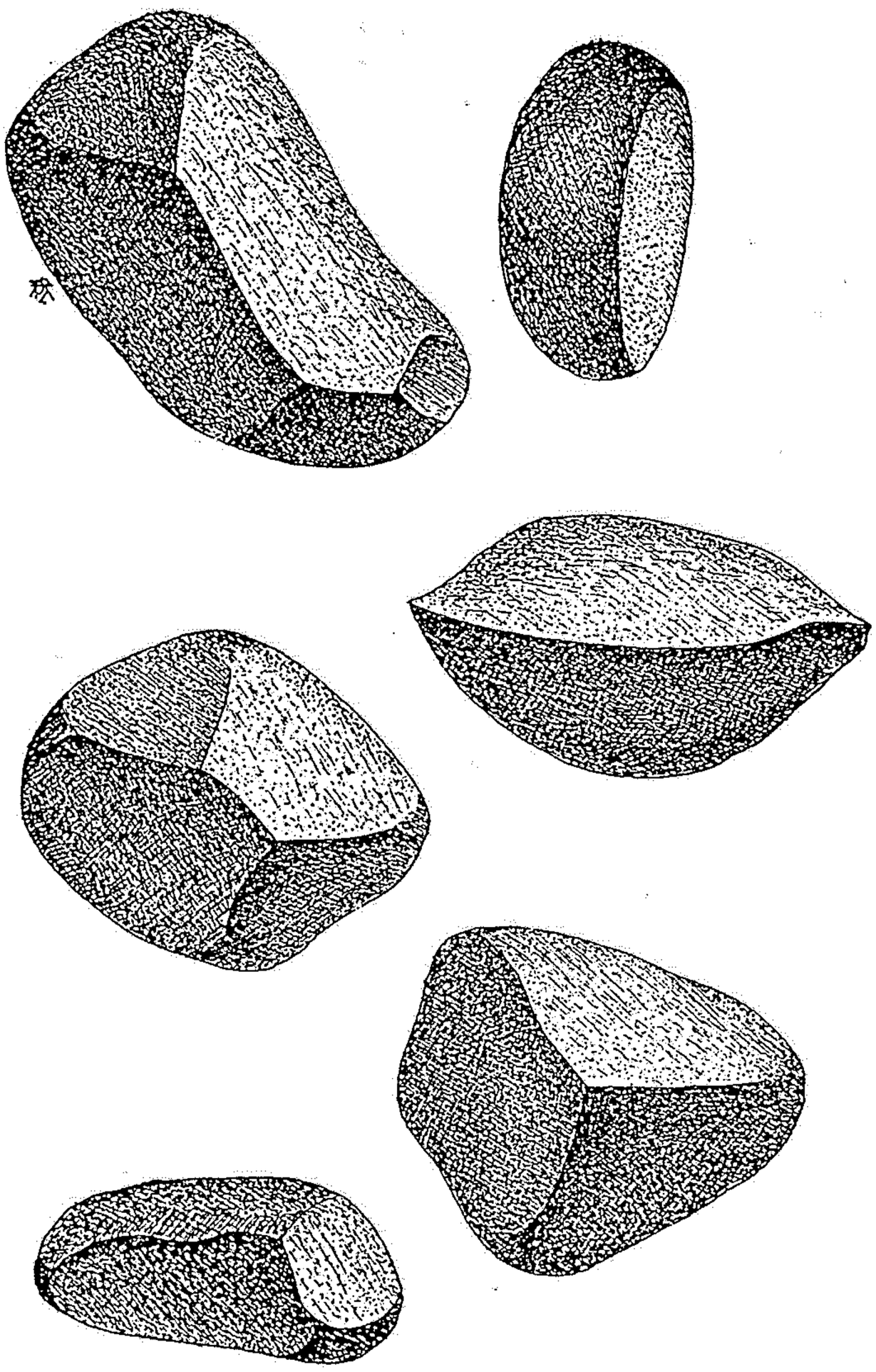

17.7 A facet on a ventifact is cut by the impact of grains of wind-driven sand. [After Robert P. Sharp, "Pleistocene Ventifacts East of the Big Horn Mountains, Wyoming," *J. Geol.*, vol. 57, p. 182, 1949.]

Snow-blasted boulder, Taylor Dry Valley, Antarctica. (Photo by Warren Hamilton, U.S. Geological Survey.)

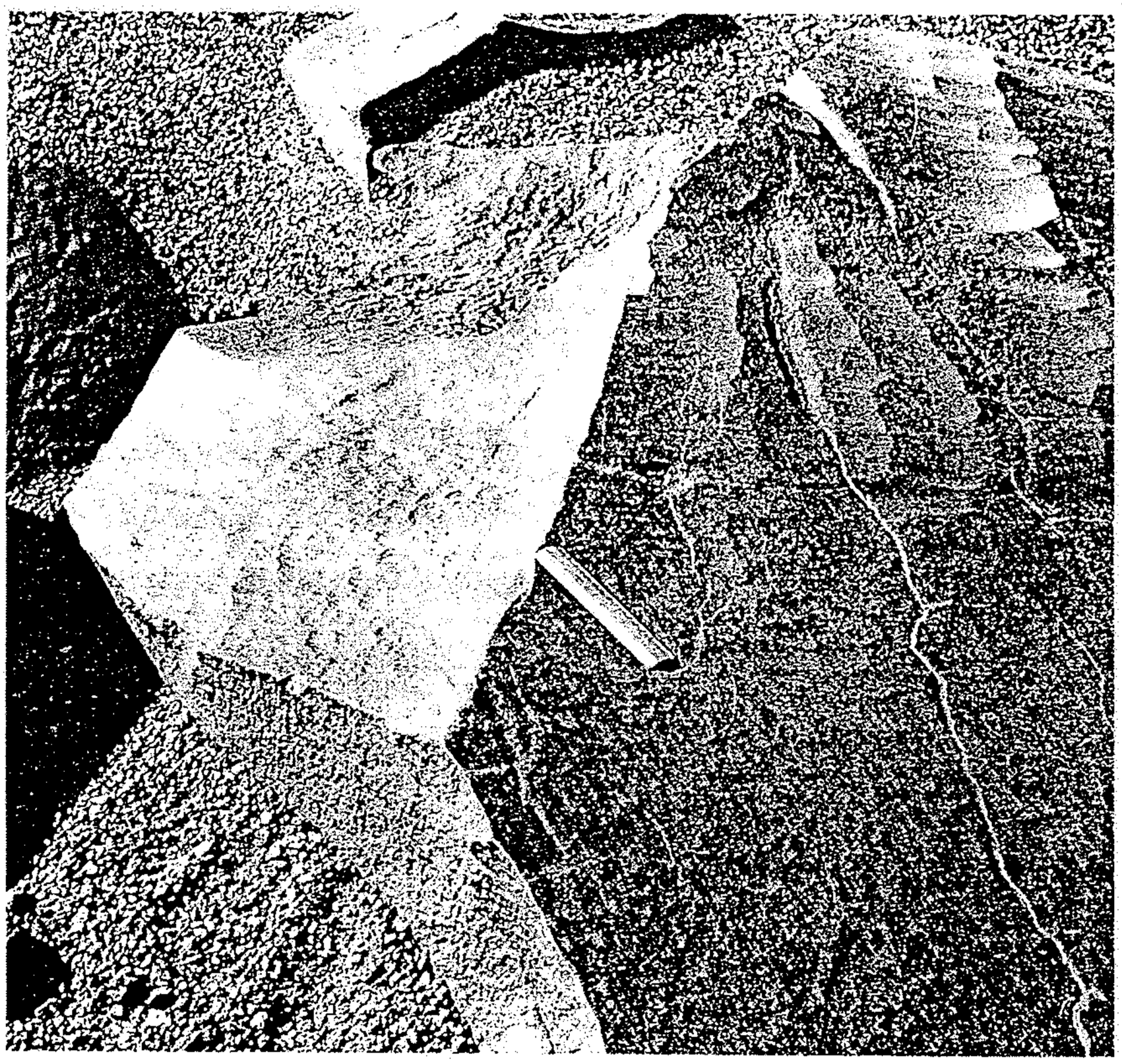

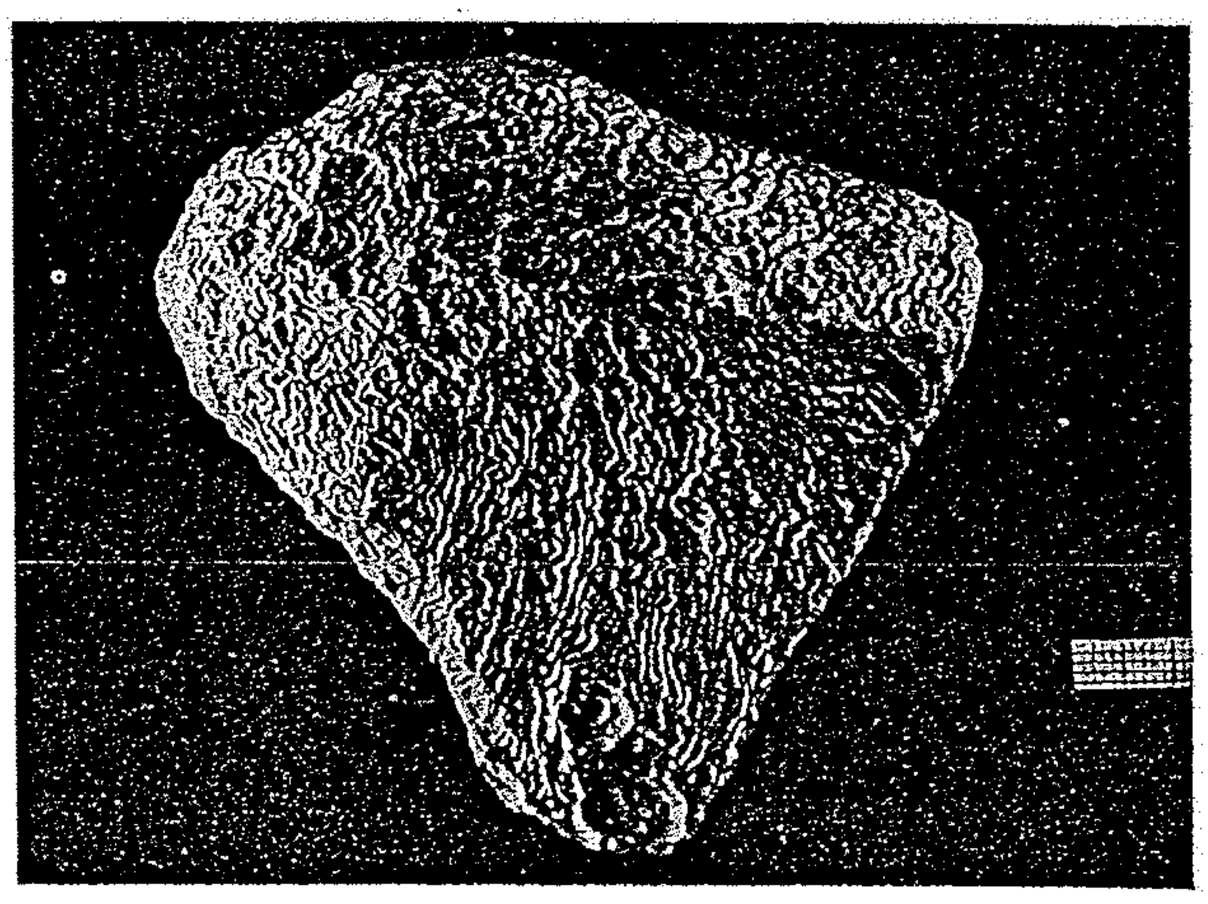

Fig. 5. Minikarst phenomena caused by dew on terrace gravels (scale, on the right: mm graph paper). Photo: Wolfermann, Labor, FU Berlin.

Fig. 6. Basalt hamada in Jabal as Sawdā' at approximately 550 m a.s.l. In the foreground fresh heat cracks are clearly visible. The surface is very slightly undulated. Oct. 1977.

Fig. 7. Woolsack forms in basalt at approximately 500 m a.s.l. The material is covered by numerous hairline cracks. Oct. 1977.

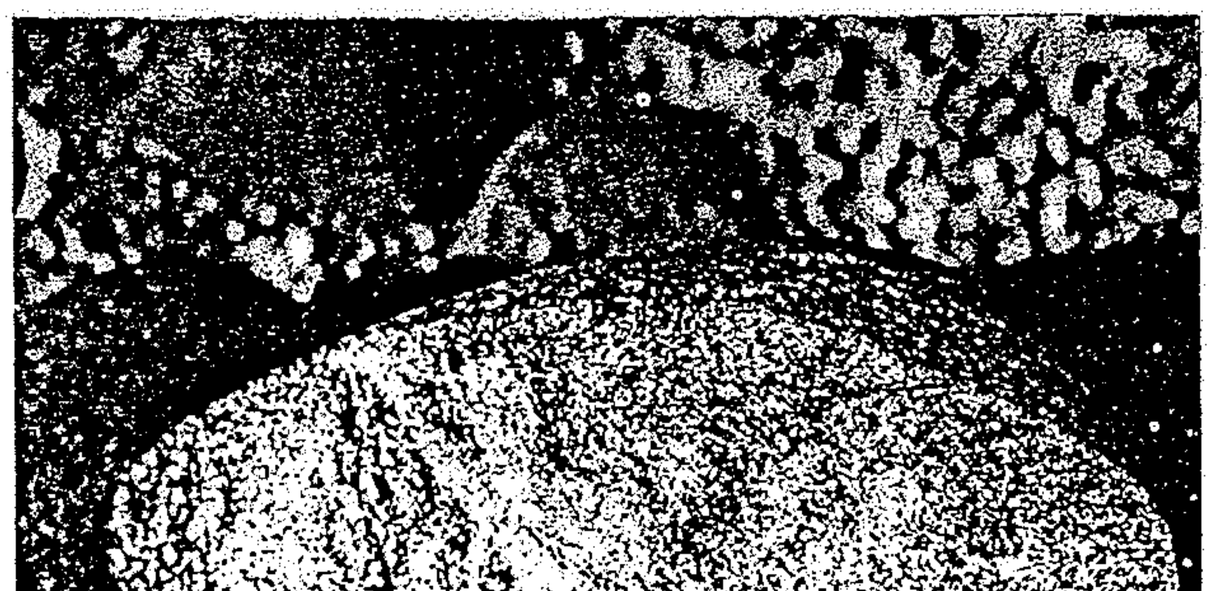

Fig. 8. Basalt detritus rounded by weathering, with 2–3 mm weathering crust. Oct. 1977.

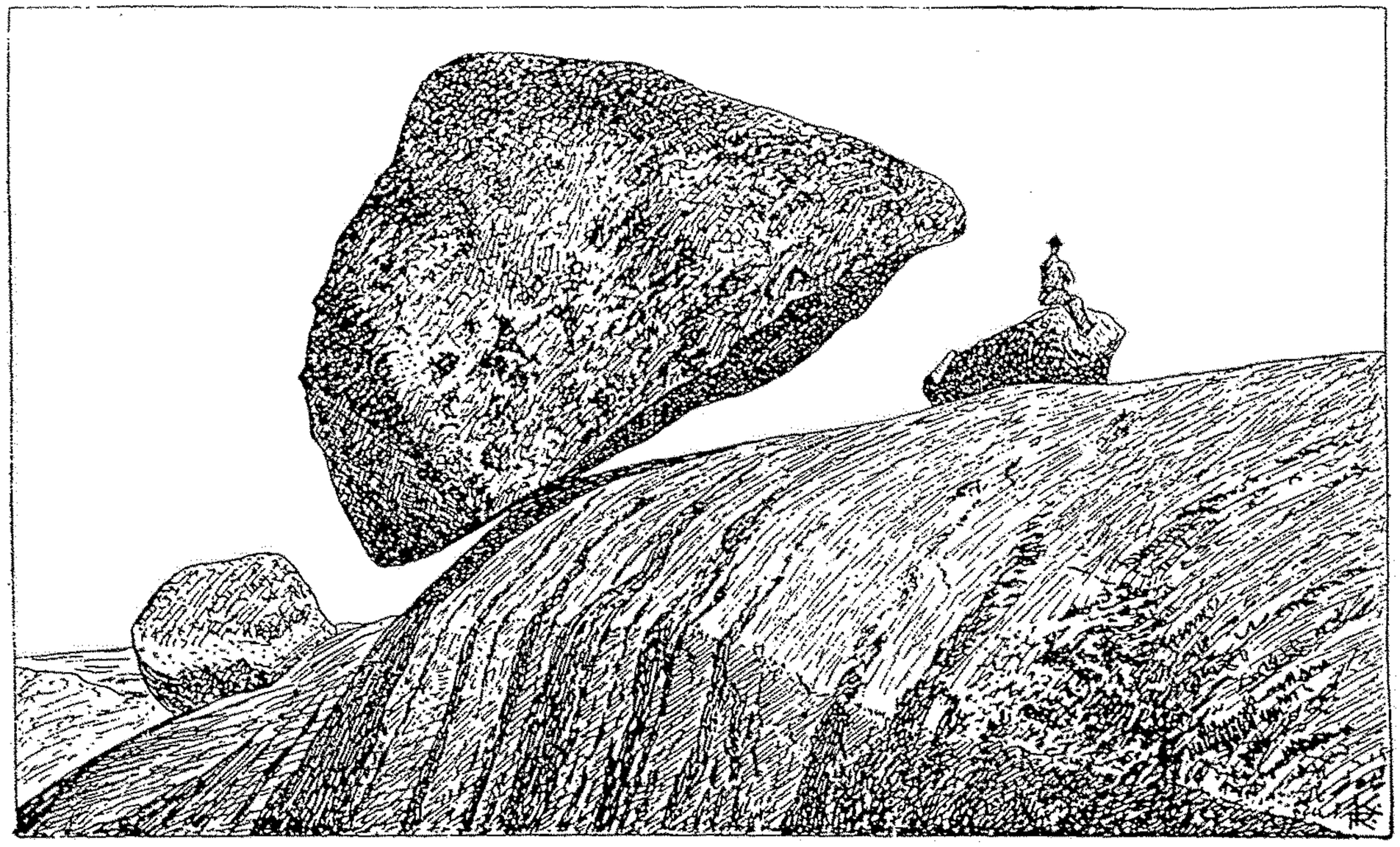

Obr. 91. *Viklan u Tandilu nedaleko Buenos Aires.* (Podle vyobrazení z díla JOH. WALTHERA Das Gesetz der Wüstenbildung kreslil autor.)

Ryc. 127. Piaskowiec trzeciorzędowy na wyspie Rab wygładzony przez fale; u dołu gładko, u góry selekcyjnie (komórkowo), gdzie piaskowiec zawierał spoiwo wapienne
Fot. J. Kunsky

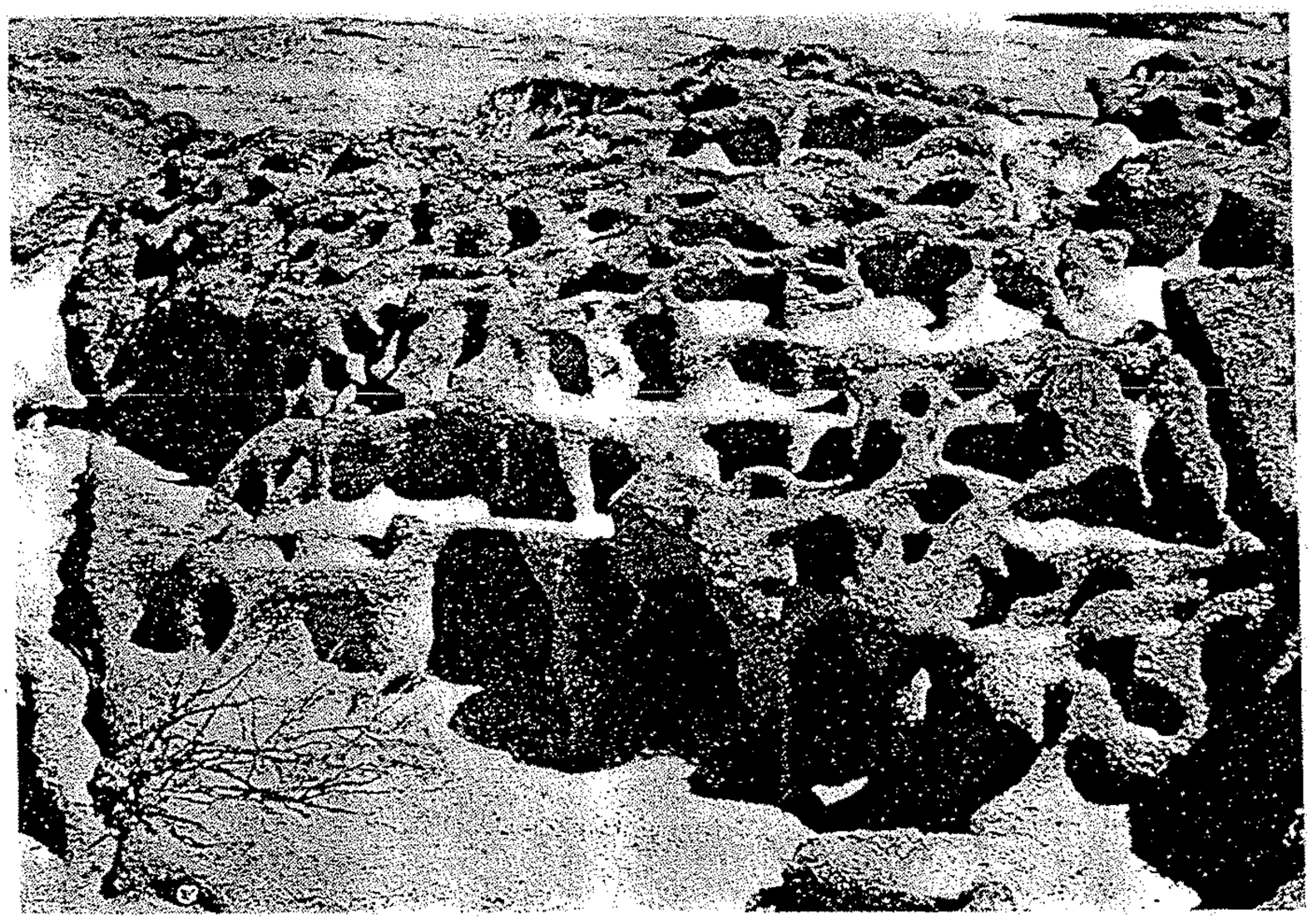

Abb. 50 Korrasionswirkung an Granit („Bienenwaben"). Namib, SW-Afrika (Foto *Uebel)*

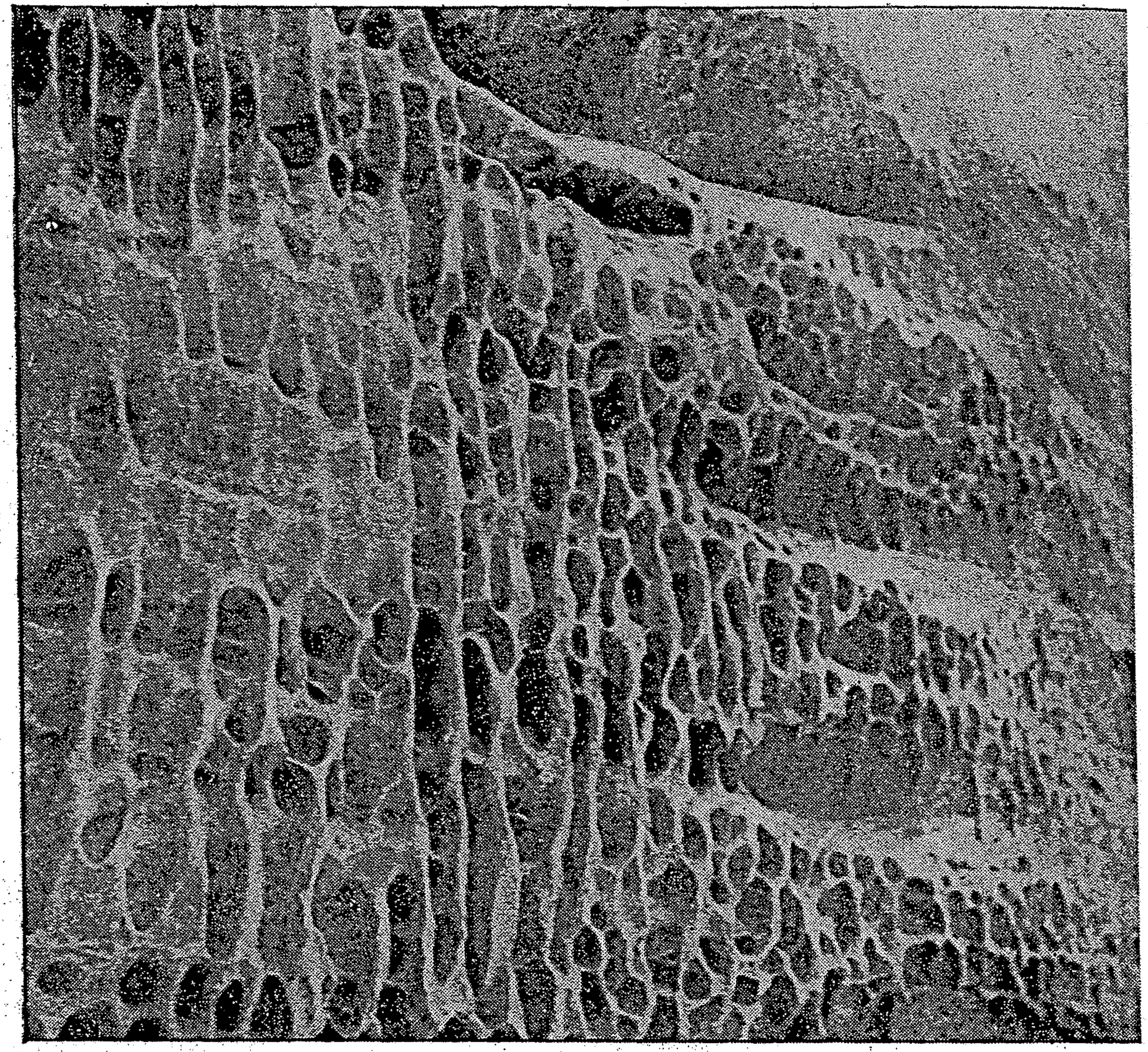

Obr. 174. *Voštinovité zvětrávání kvádrových pískovců křídového útvaru v Prachovských skalách u Jičína.* (Fot. B. Bouček.)

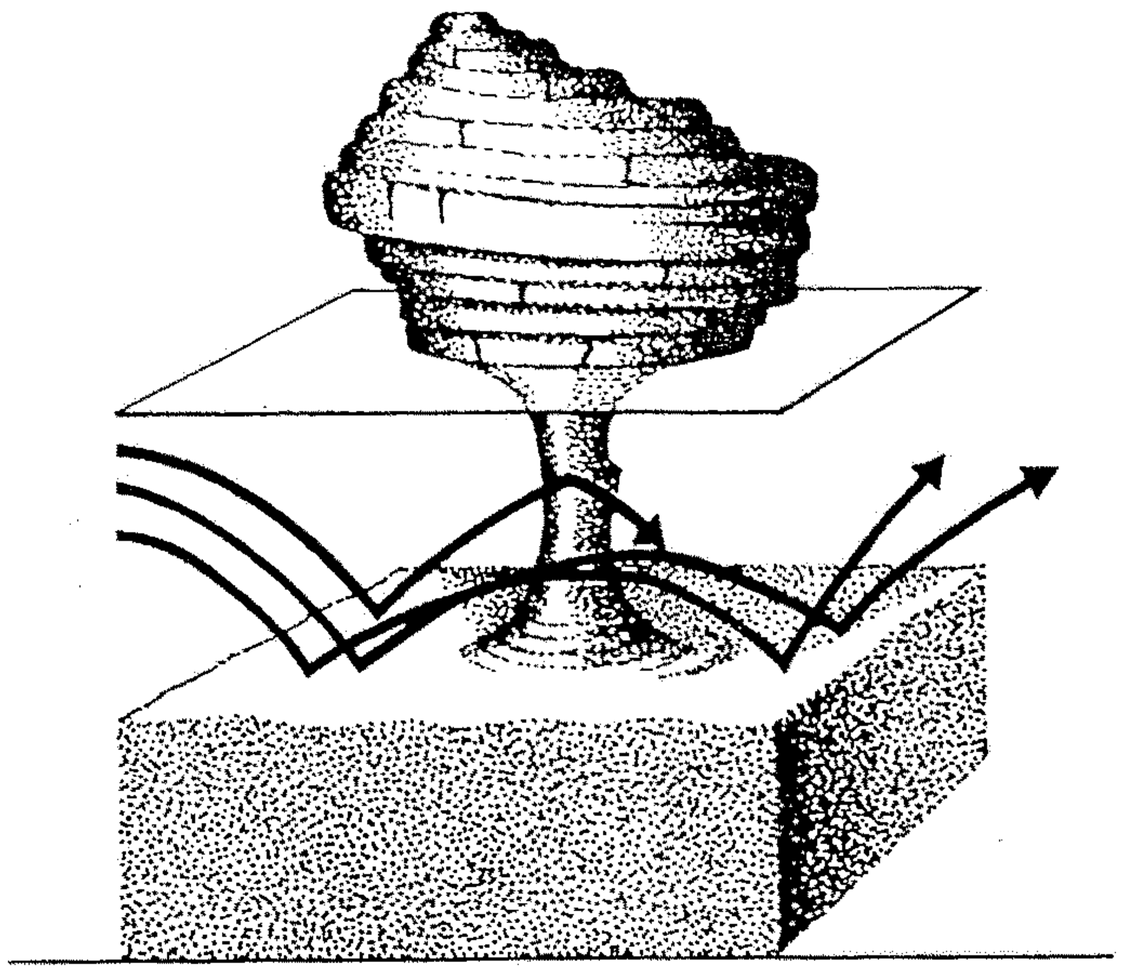

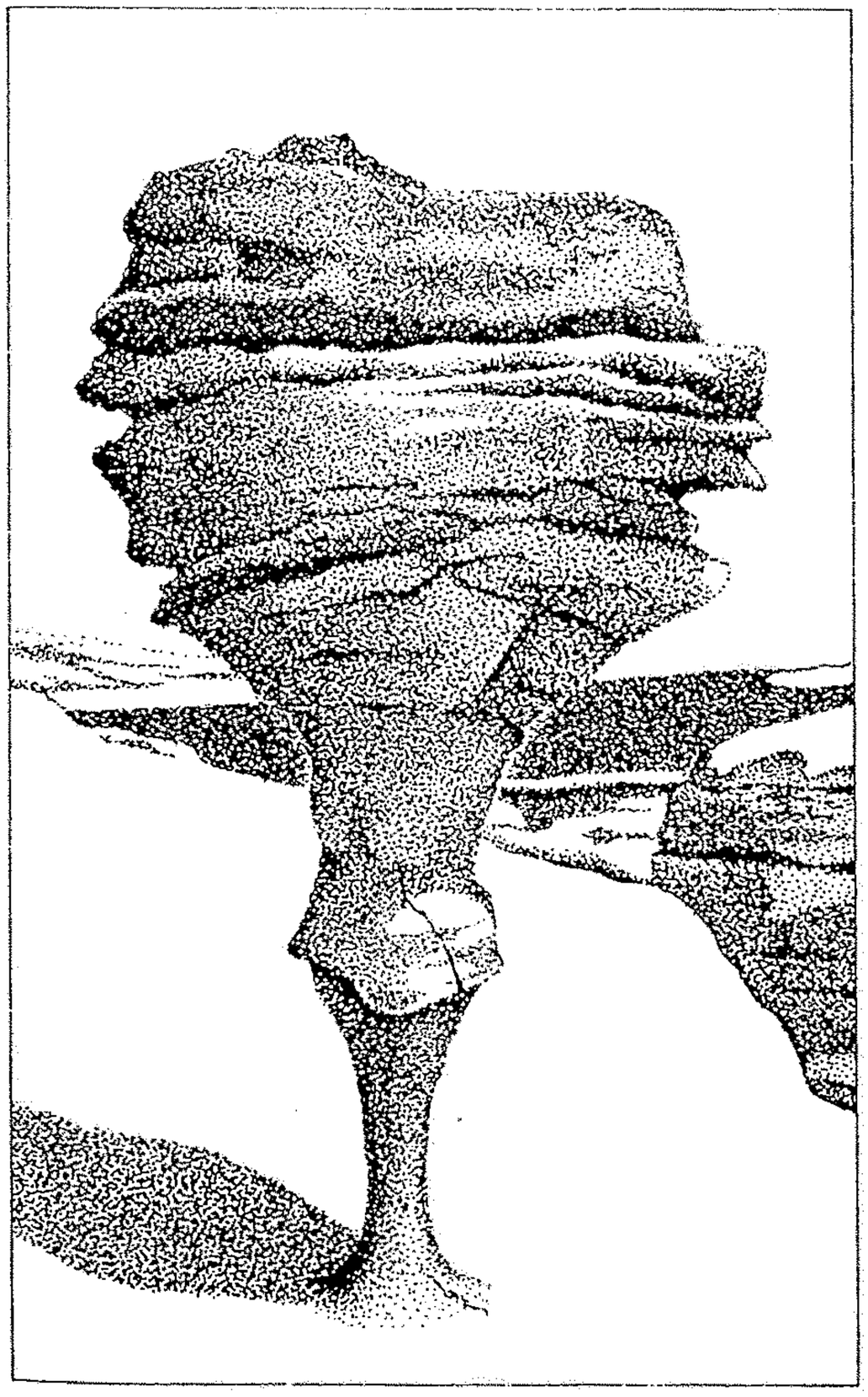

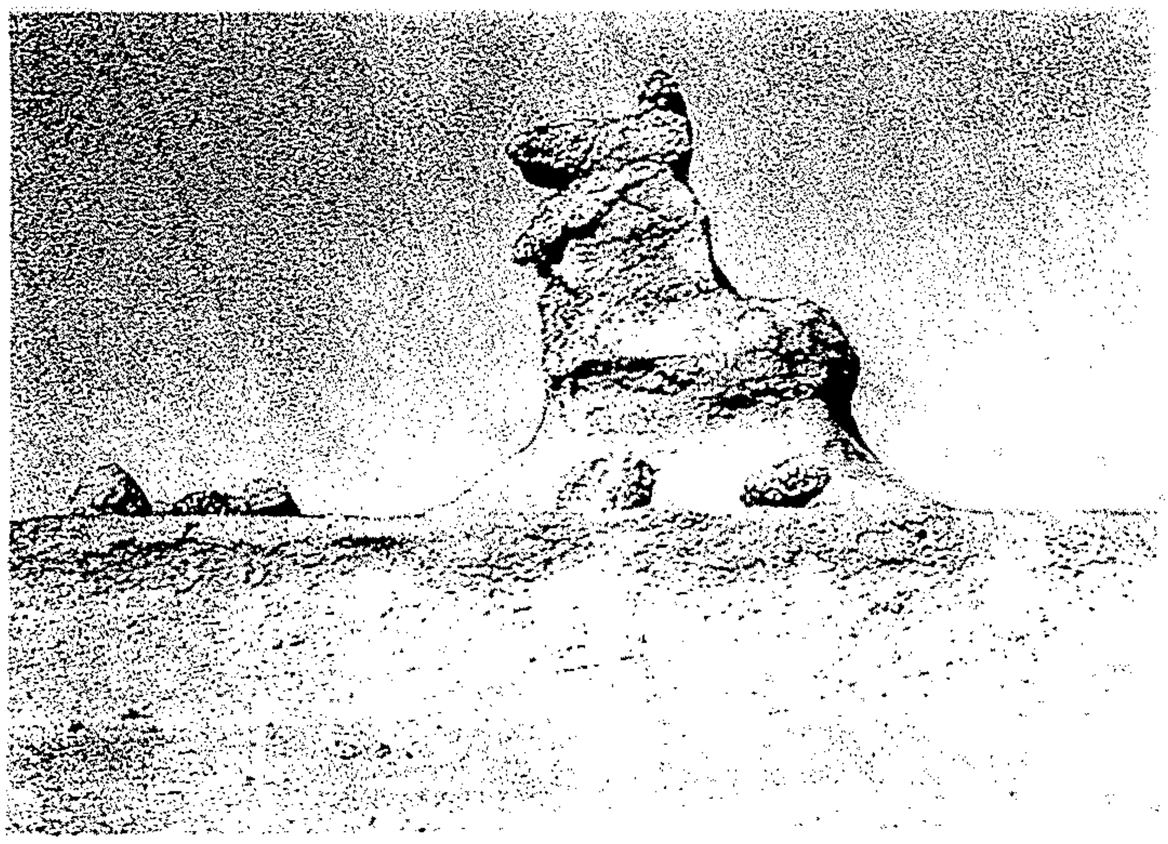

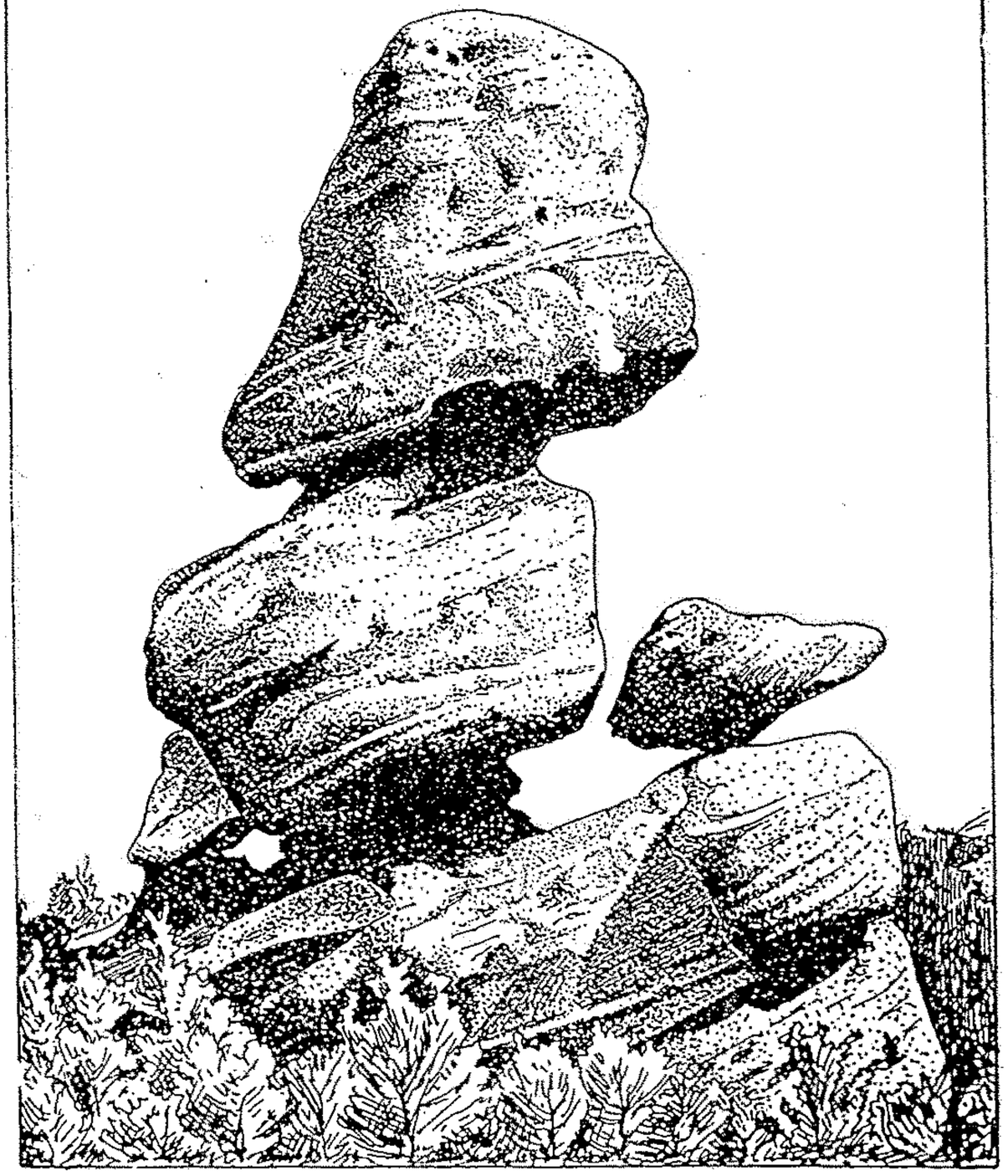

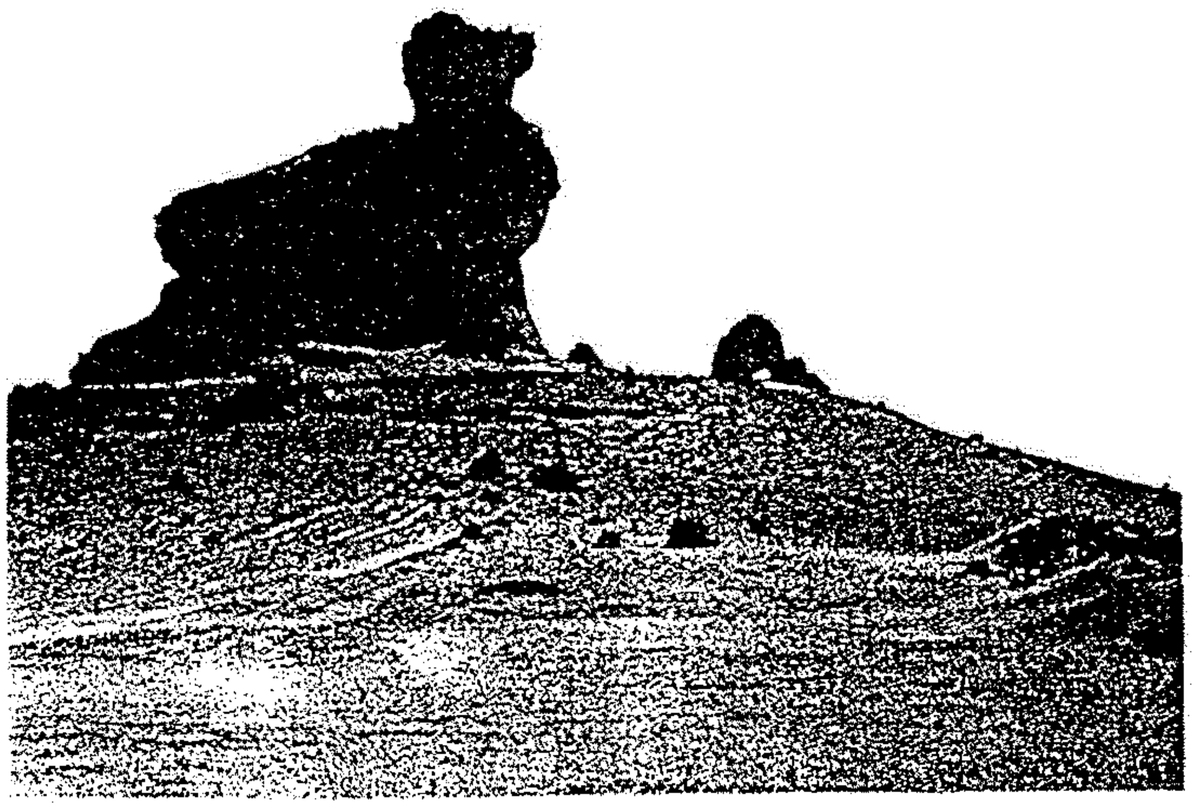

Obr. 92. *Vznik viklanů v Coloradu* (*USA*). (Autorova kresba podle vyobrazení z díla Joh. Walthera.)

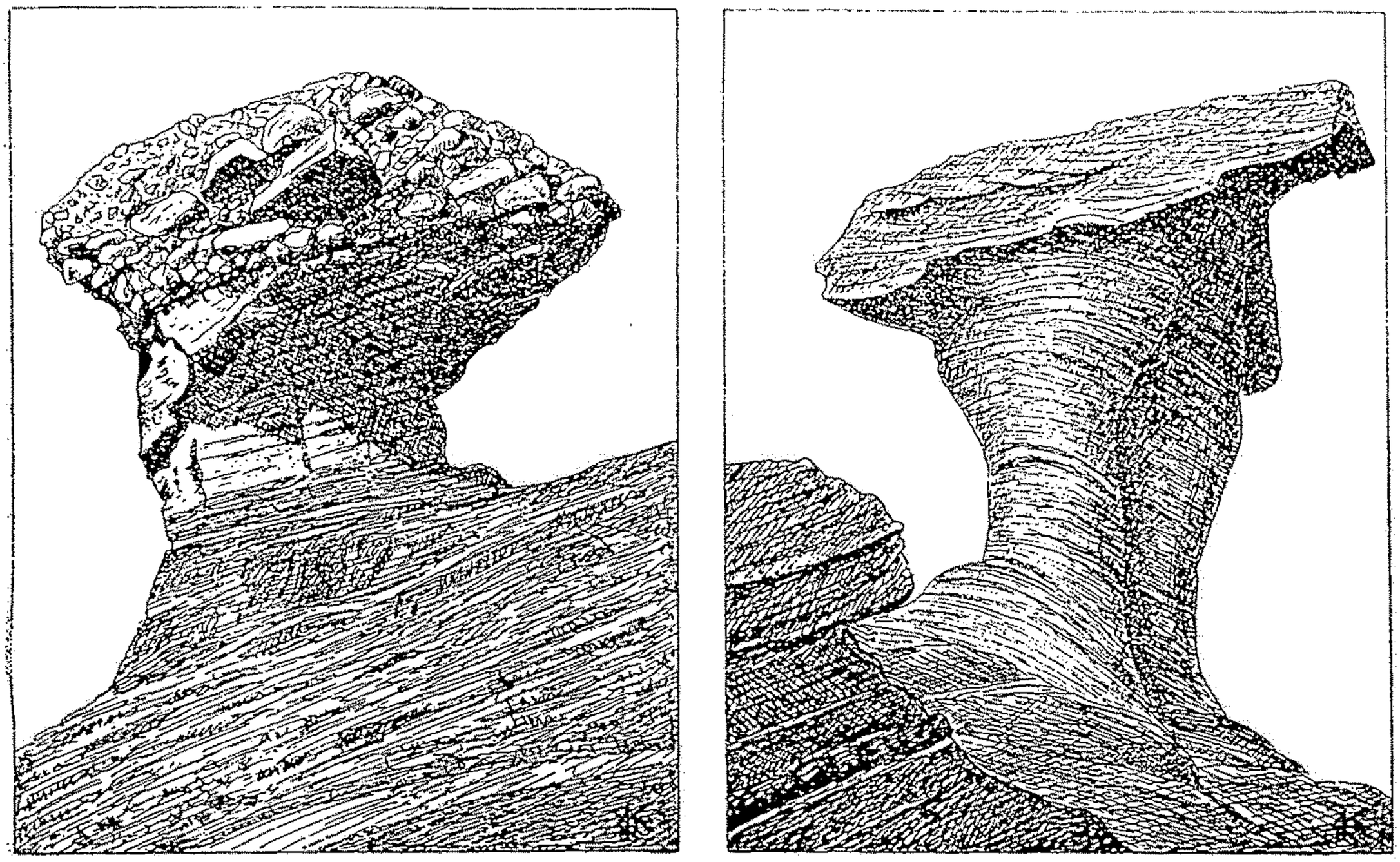

Obr. 89. *Hřibovité skalní útvary vzniklé větrnou korasí. Nalevo skála Ras el Kadi u Chargeha v Horním Egyptě* (podle Joh. Walthera), *napravo skála ve státě Montana v USA* (podle J. S. Allisona.) (Kresby autorovy.)

Hřibovité útvary vzniklé větrnou korasí; Monument-Park v Coloradu (USA).

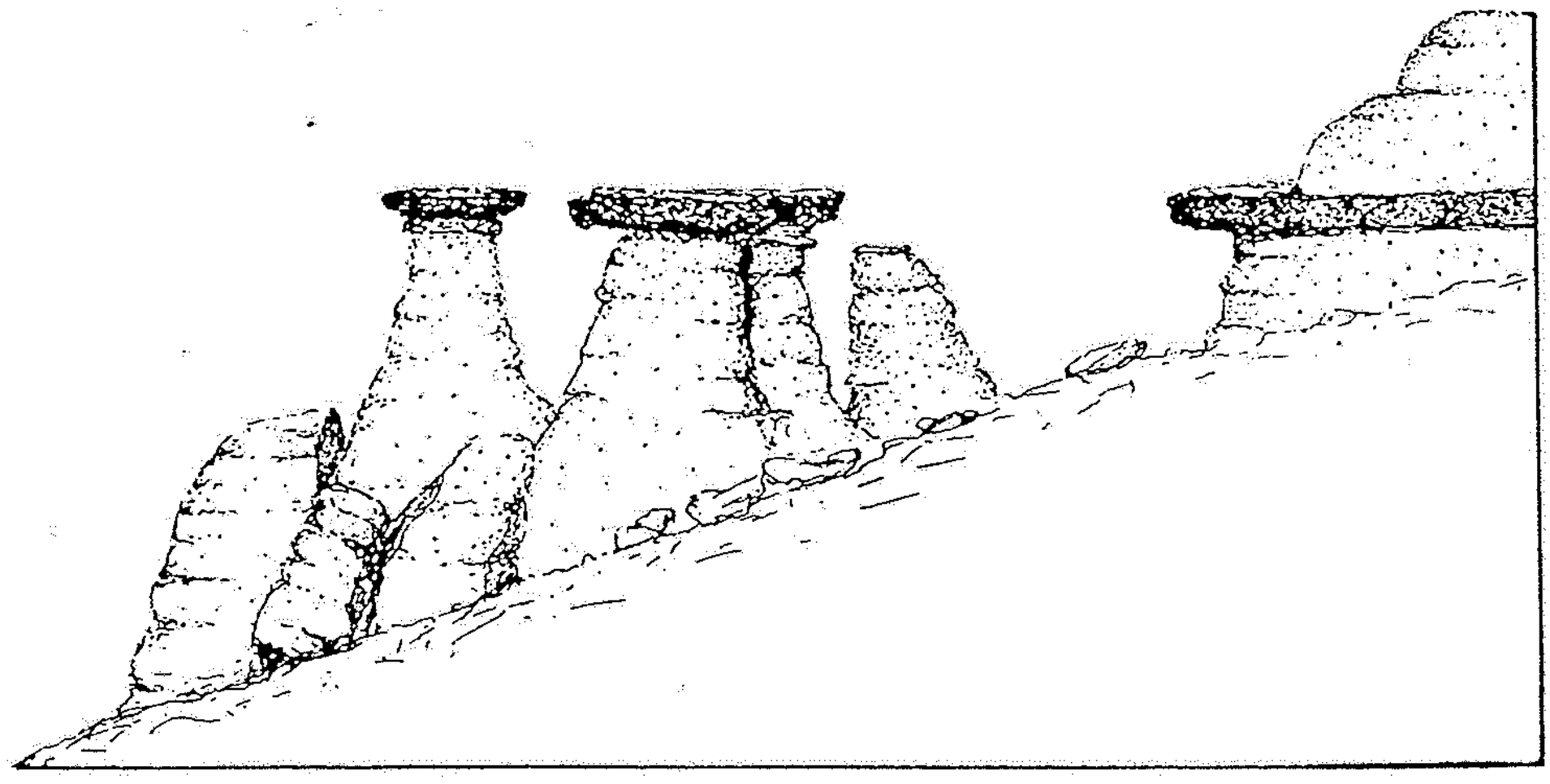

73. Pokličky, typ zemních pyramid v křídových svrchnoturonských kvádrových pískovcích v Kokořínském údolí blízko Mšena. Krycí desku na vrcholu pokliček tvoří vrstevní deskovité polohy tvrdých železitých slepenců v měkkých rozpadavých pískovcích; na údolním svahu (vpravo) vyčnívají železité desky jako římsy denudačních teras. (Upraveno podle Q. Záruby.)

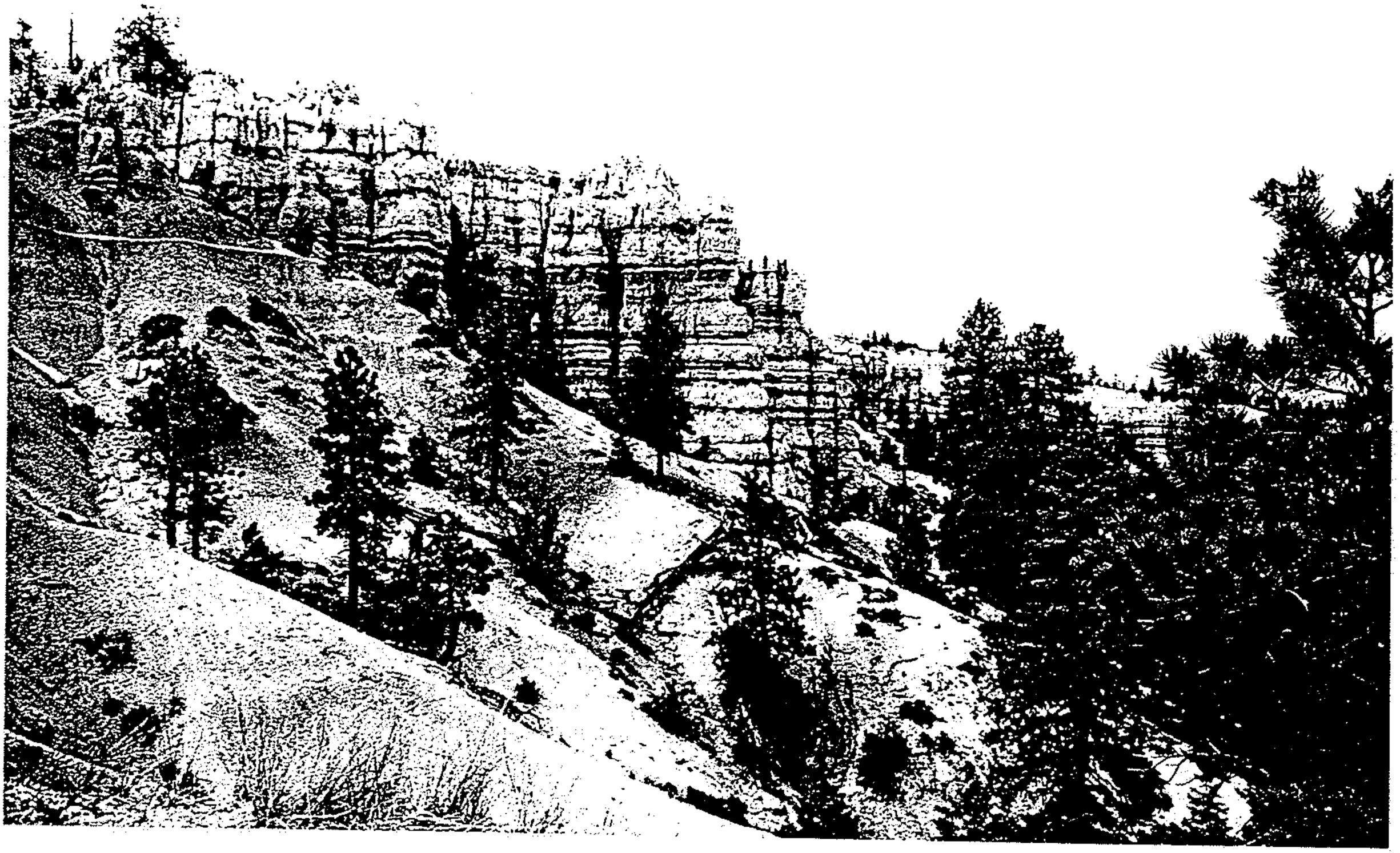

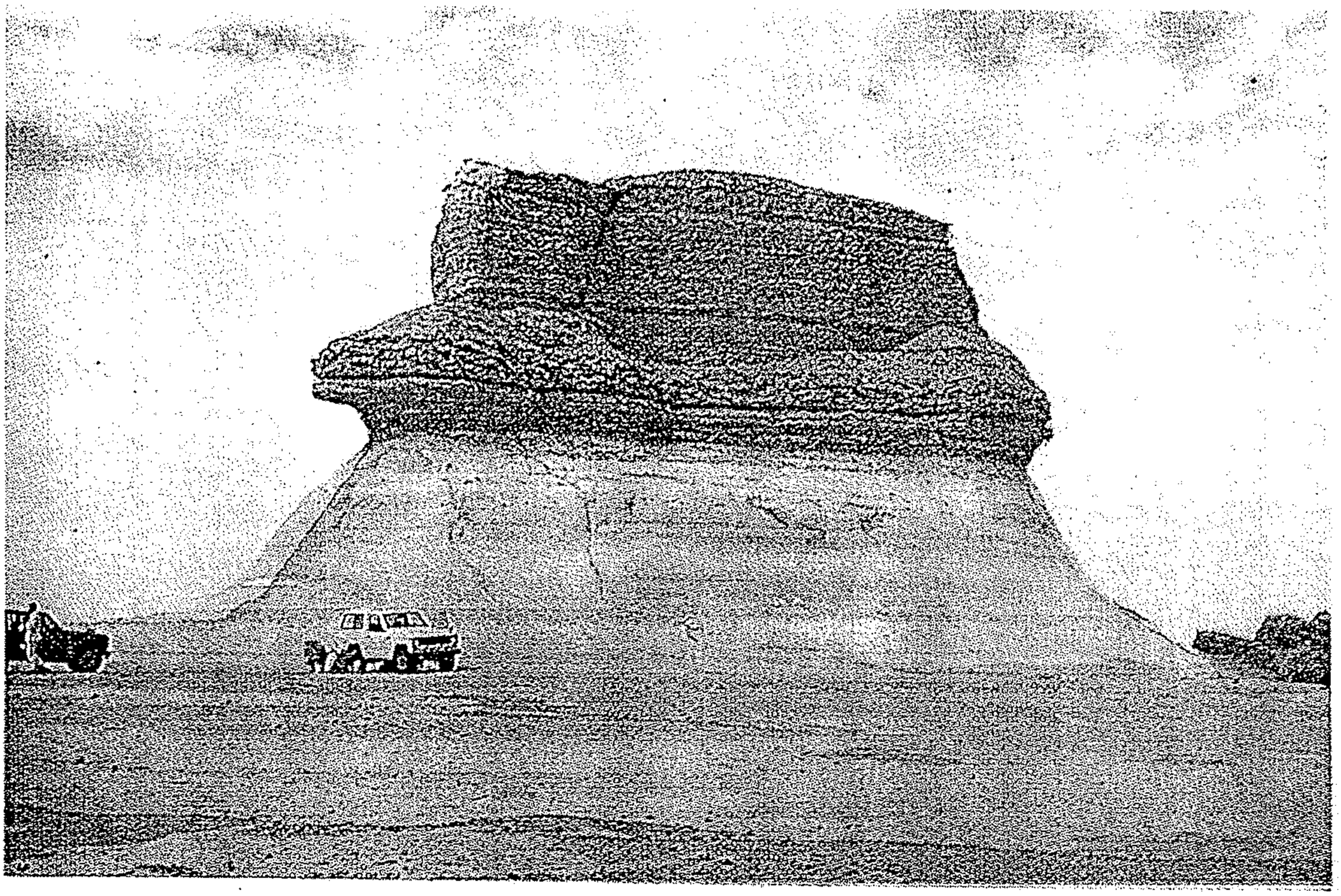

19. View of lithostratigraphic boundary between the Thmed al Qusúr Member below and the Qrárat al Jifah Member above. 5 km S of Abú Na'ím. Photo J. Zikmund.

15. Oyster bank in the basal part of the Al Gata Member. 5 km NE of Qárat al Qalbah. Photo J. Zikmund.

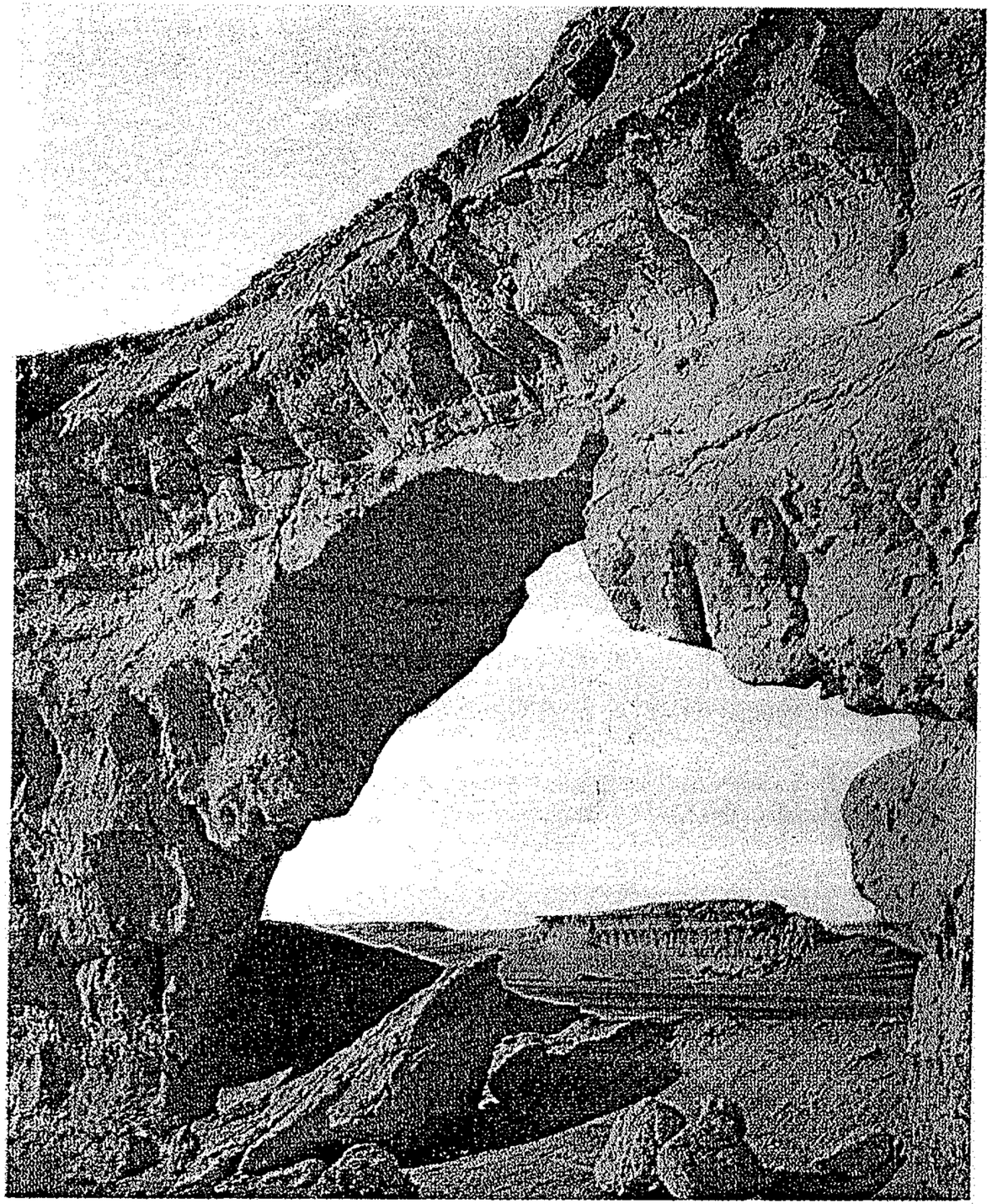

23. Rock gate in the dolomitic limestone in the Al Gata Member. Qarárat al Hufrah, 27 km SE of Hufrah. Photo J. Otava.

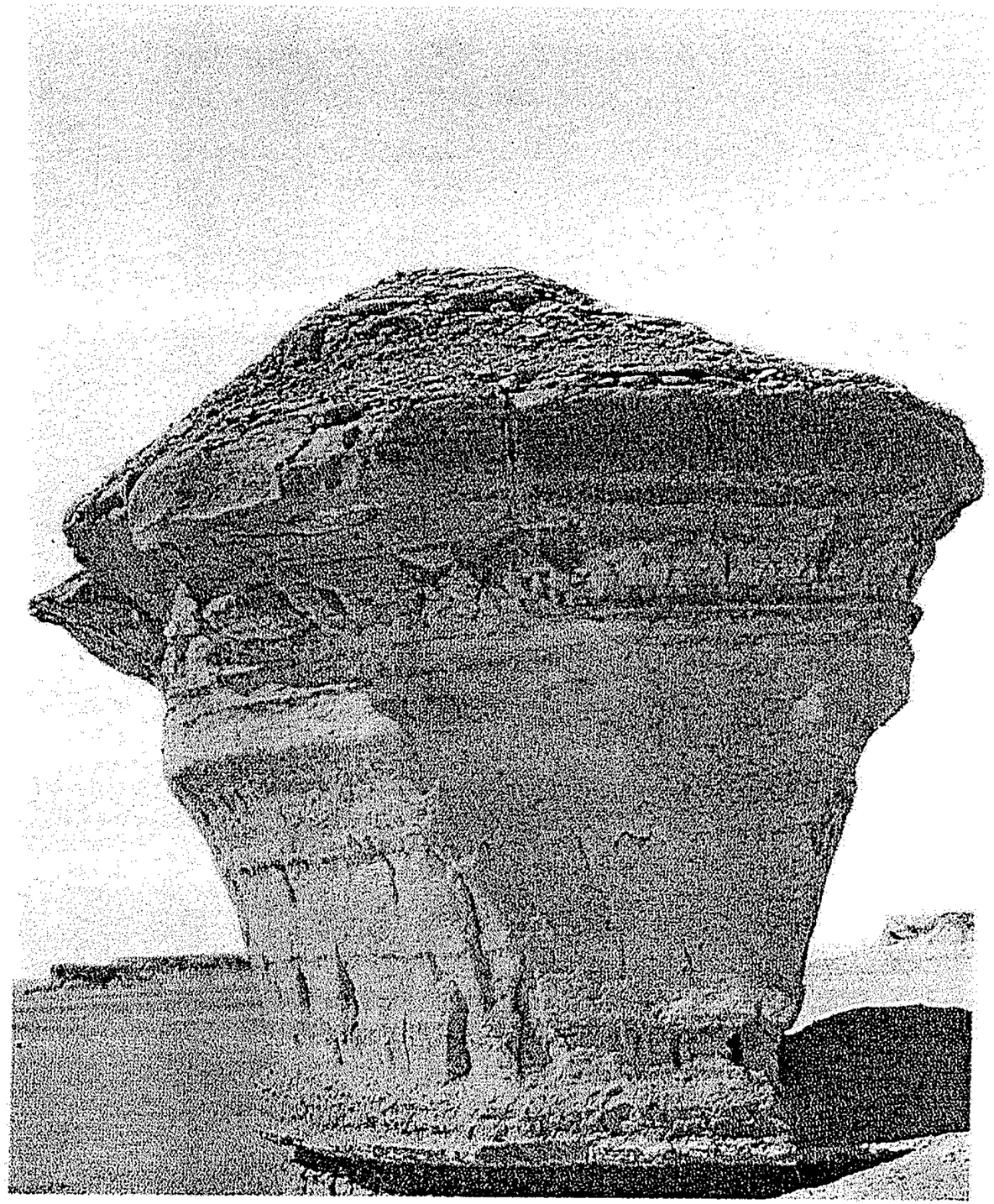

24. Tower formed by dolomitic limestone of the Al Gata Member. The top is built up to crustified chalky dolomitic limestone of the Thmed al Qusúr Member. Wádí Dakákín Bú Haqf. Photo J. Otava.

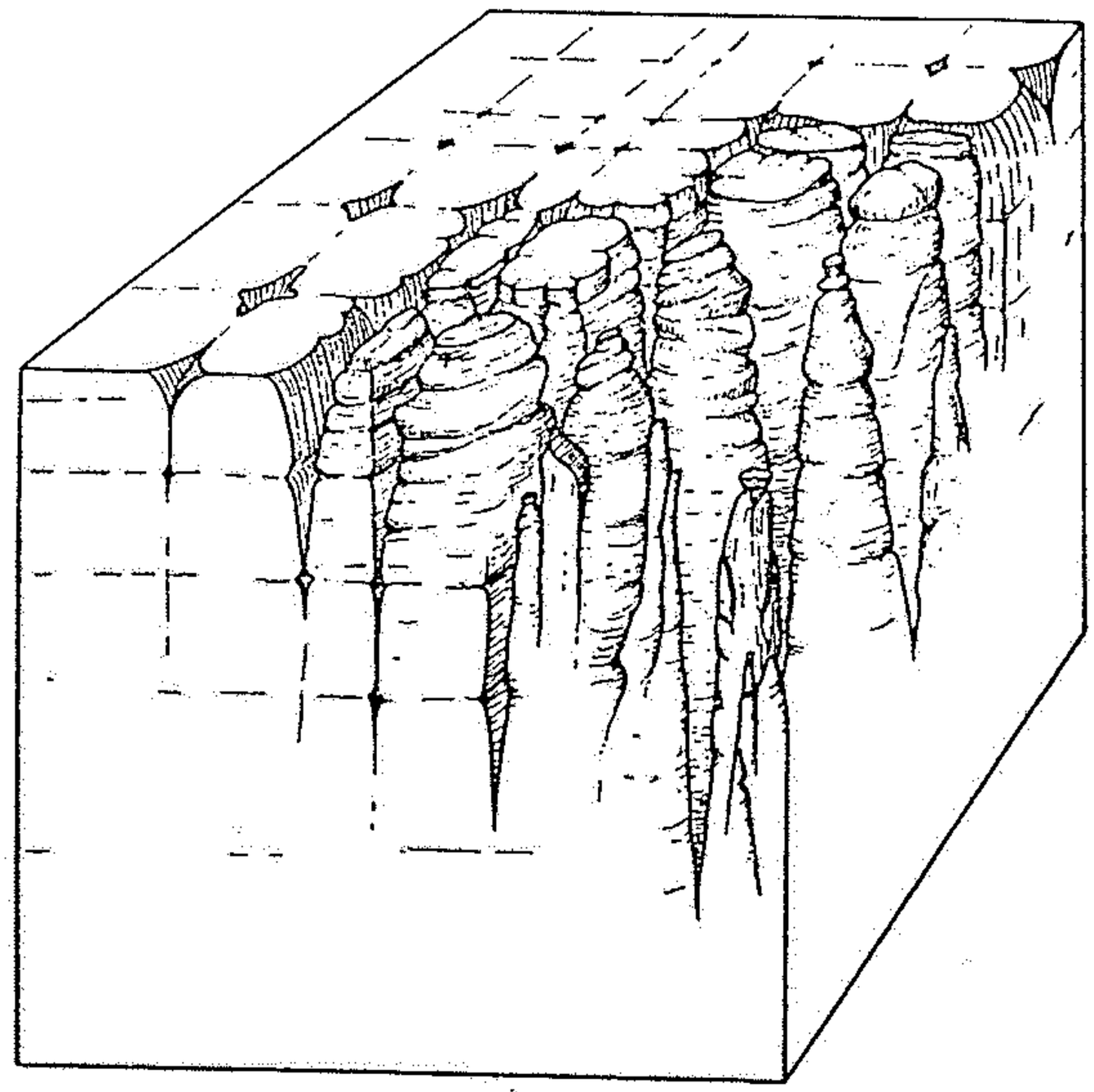

20. Vznik a vývoj pískovcového skalního města. Souvrství kvádrových pískovců České křídové tabule je proniknuto svislými, navzájem kolmými puklinami a vodorovnými vrstevními spárami. Na křižovatkách puklin vznikají závrty, jež se spojují a prohlubují ve žleby. Ty rozdělují hmotu pískovců ve svislé kvádry, dále modelované podél vrstevních spár a puklin podle různé tvrdosti pískovce, ronem a větrem v detailní tvary. (Podle autora.)

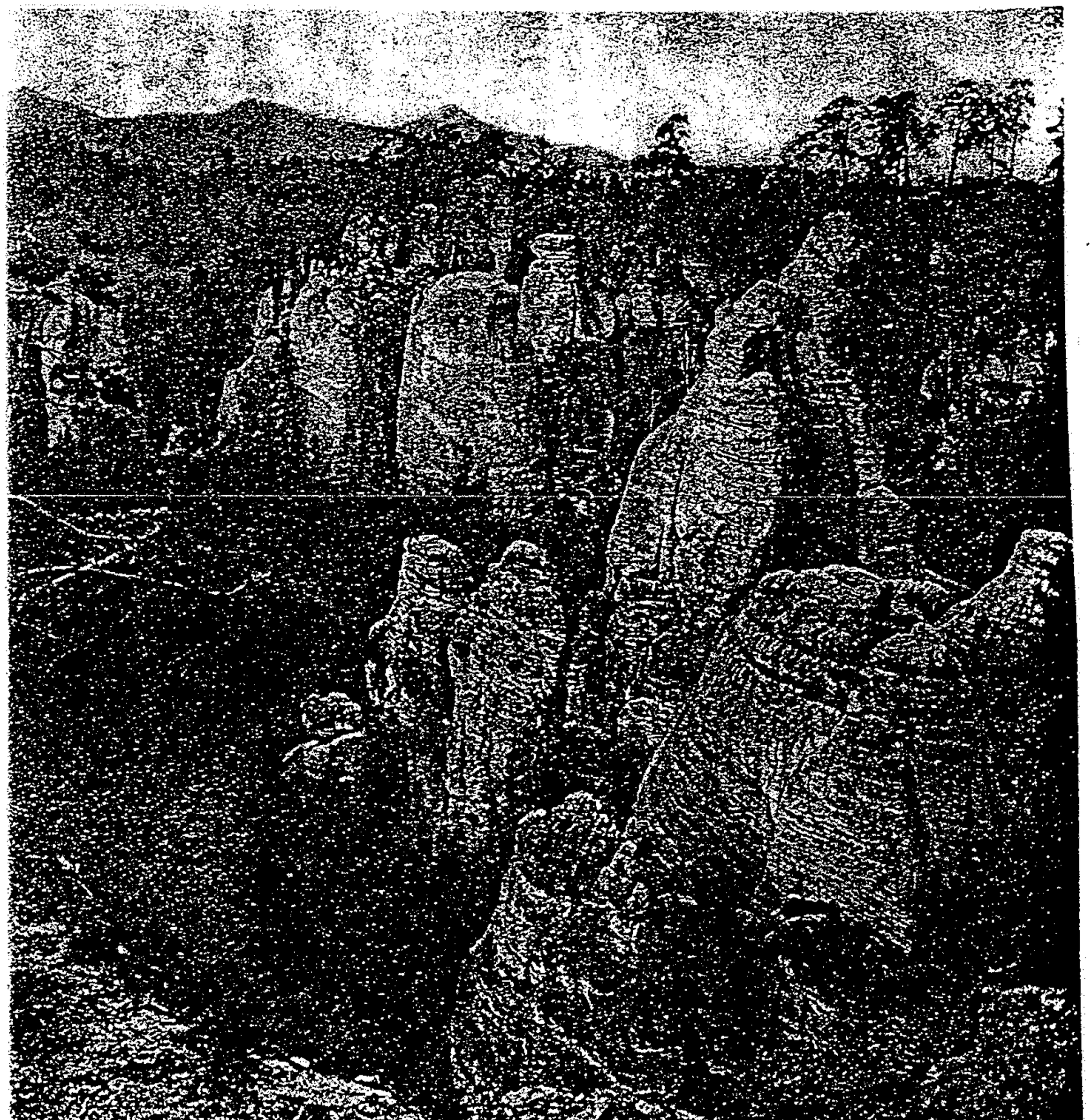

72. Velká část severních Čech a severní Moravy je pokryta usazeninami křídového stáří. Z nich kvádrové pískovce mají příznačný, hrubě sloupovitý rozpad a tvoří porůznu „skalní města". Prachovské skály u Jičína; v pozadí čedičové suky Vyskeř, Velká hora a Trosky.

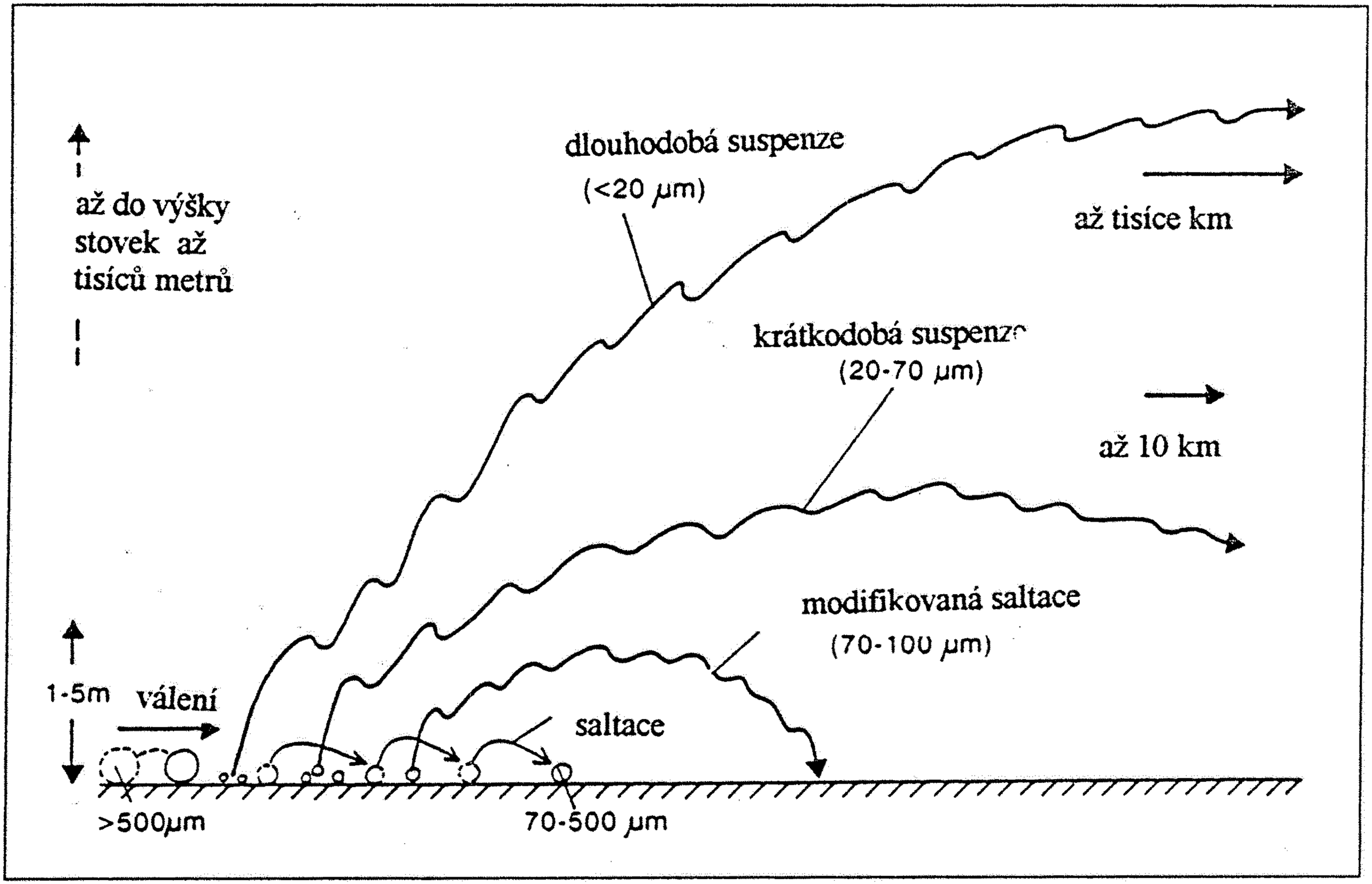

Obr. 12O: Různé způsoby eolického transportu siltu (jemného písku), písku, a štěrku. během větrné bouře (rychlost větru od 10 do 2O cm /s (podle Pye 1987 in Einselle 1992)

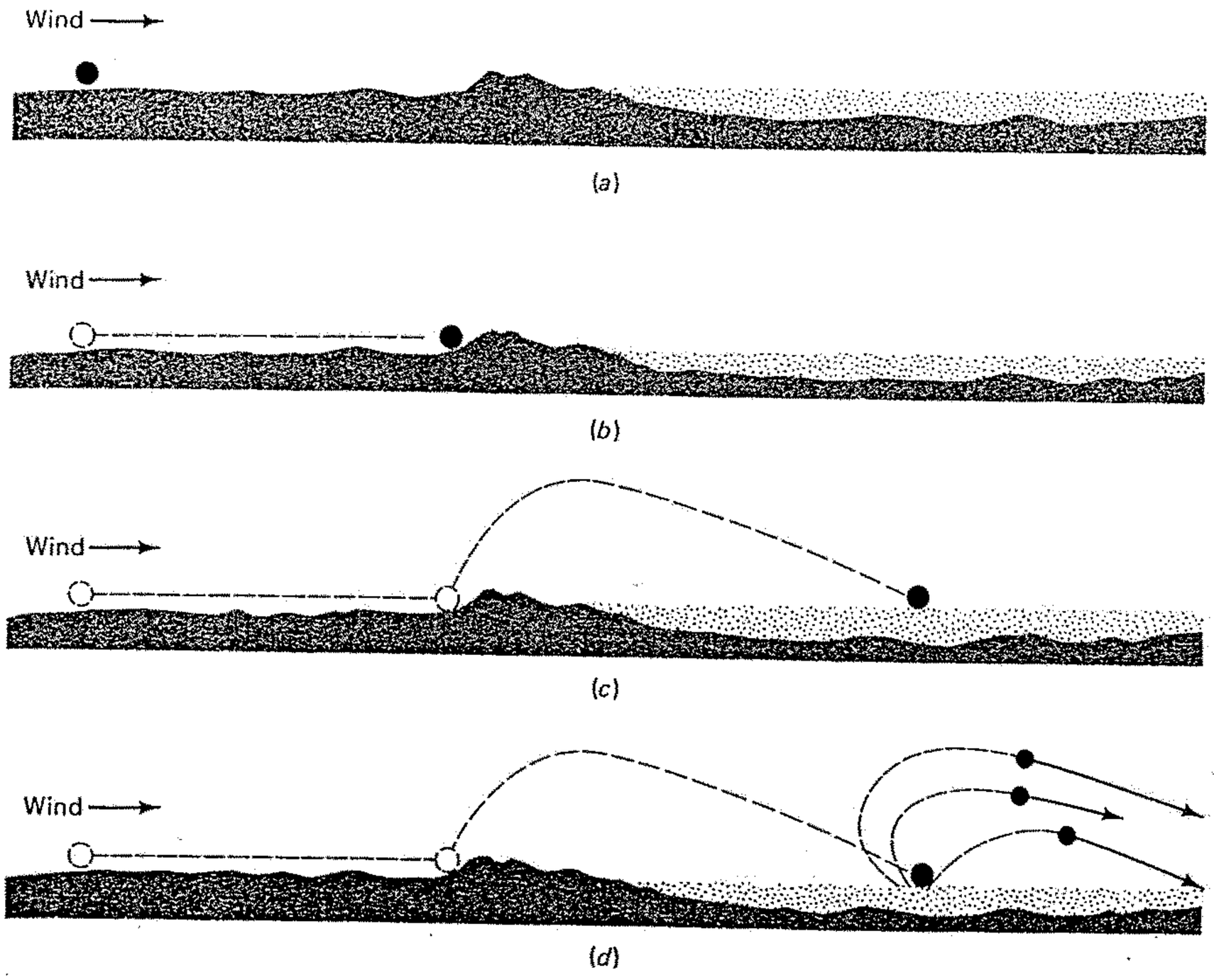

15.12

In this series a sand grain is first driven forward by the wind (a) *and then bounces off an obstruction on the surface* (b). *It next follows the path shown in* (c), *and strikes into a bed of other sand grains. Several of these are thrown into the air as a result and driven forward as shown in* (d). *See also Figure 15.13.*

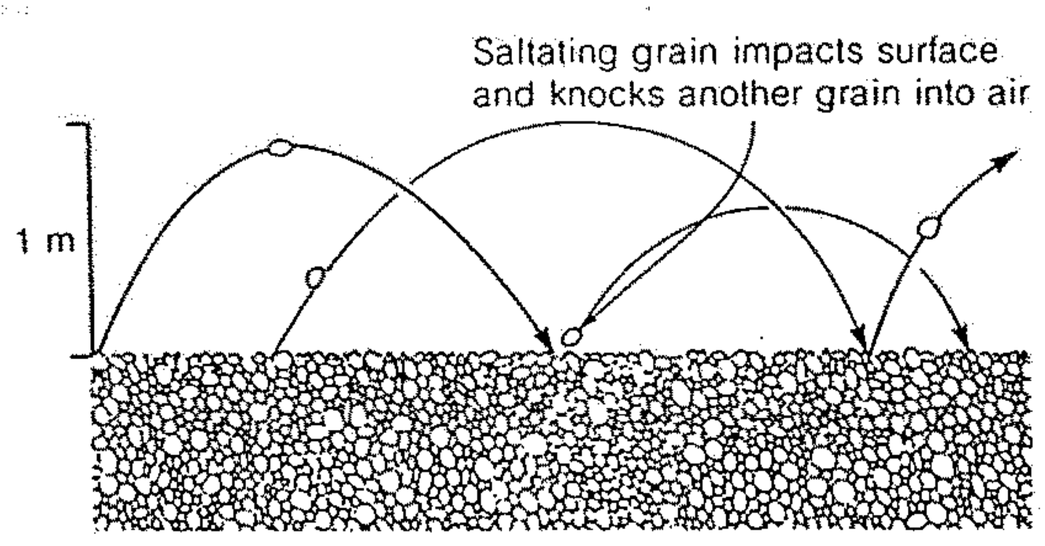

Figure 9-3

Saltation transport of sand grains in wind. As a saltating grain falls to the ground, it may strike another grain lying on the surface with sufficient force to throw the struck grain into a saltation trajectory.

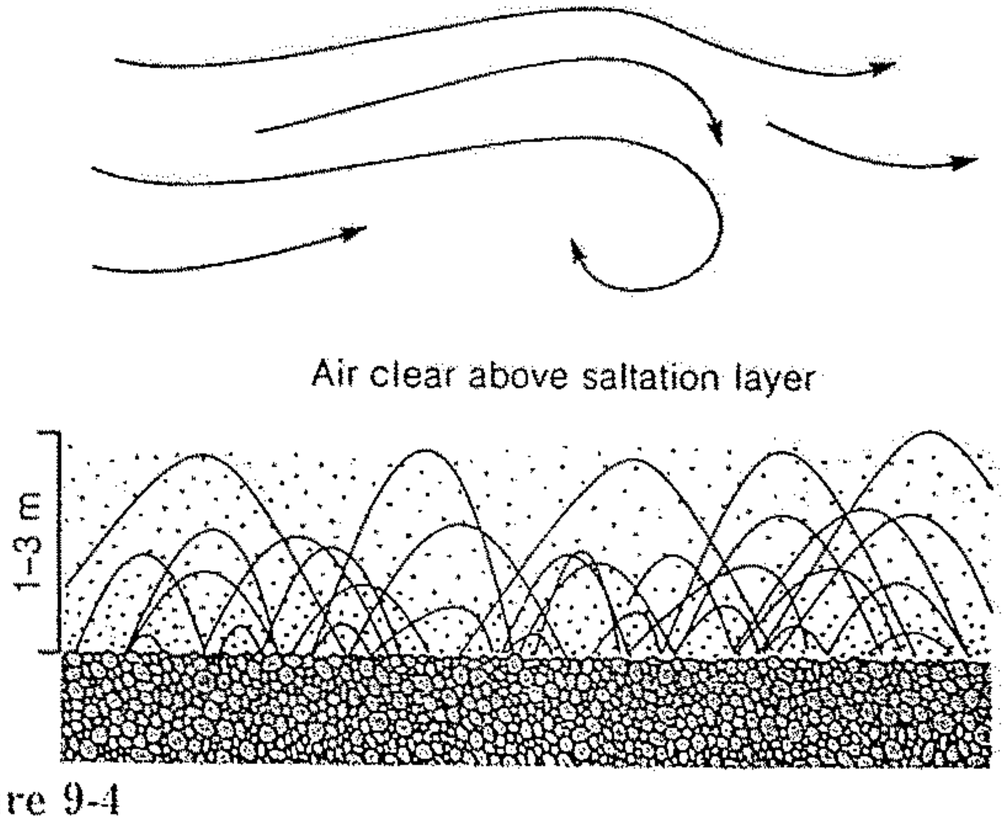

Figure 9-4

Saltation layers formed during many windstorms are so dense that the ground cannot be seen, yet the top of the layer may be sharp and the air above it clear.

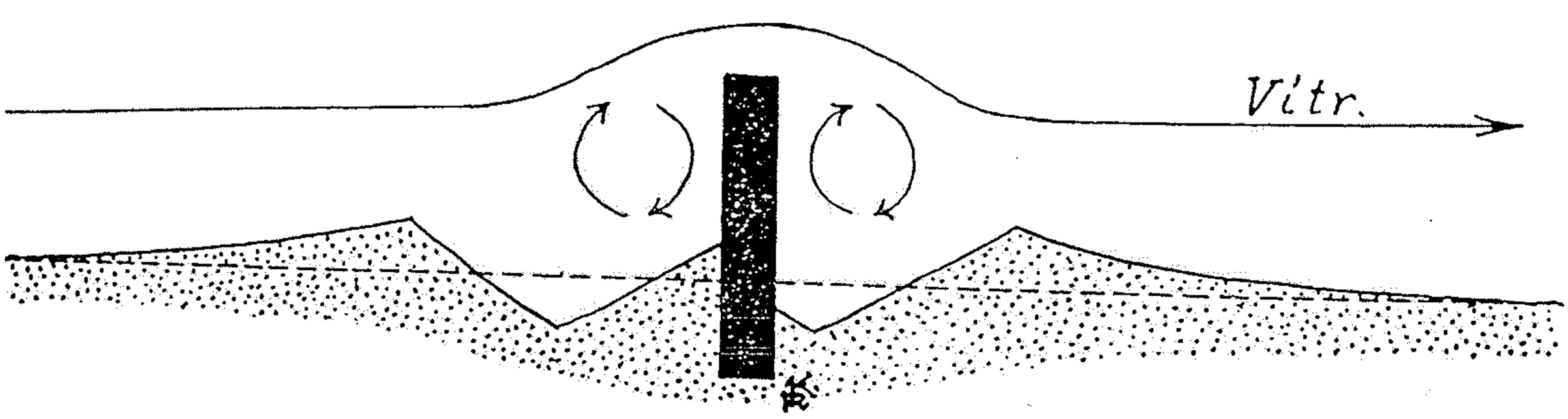

Obr. 97. *Diagram, znázorňující vznik větrných vírů a větrných brázd, které se tvoří před překážkou a za překážkou. Tečkovaně = uloženiny vátého písku.* (Podle V. CORNISHE.)

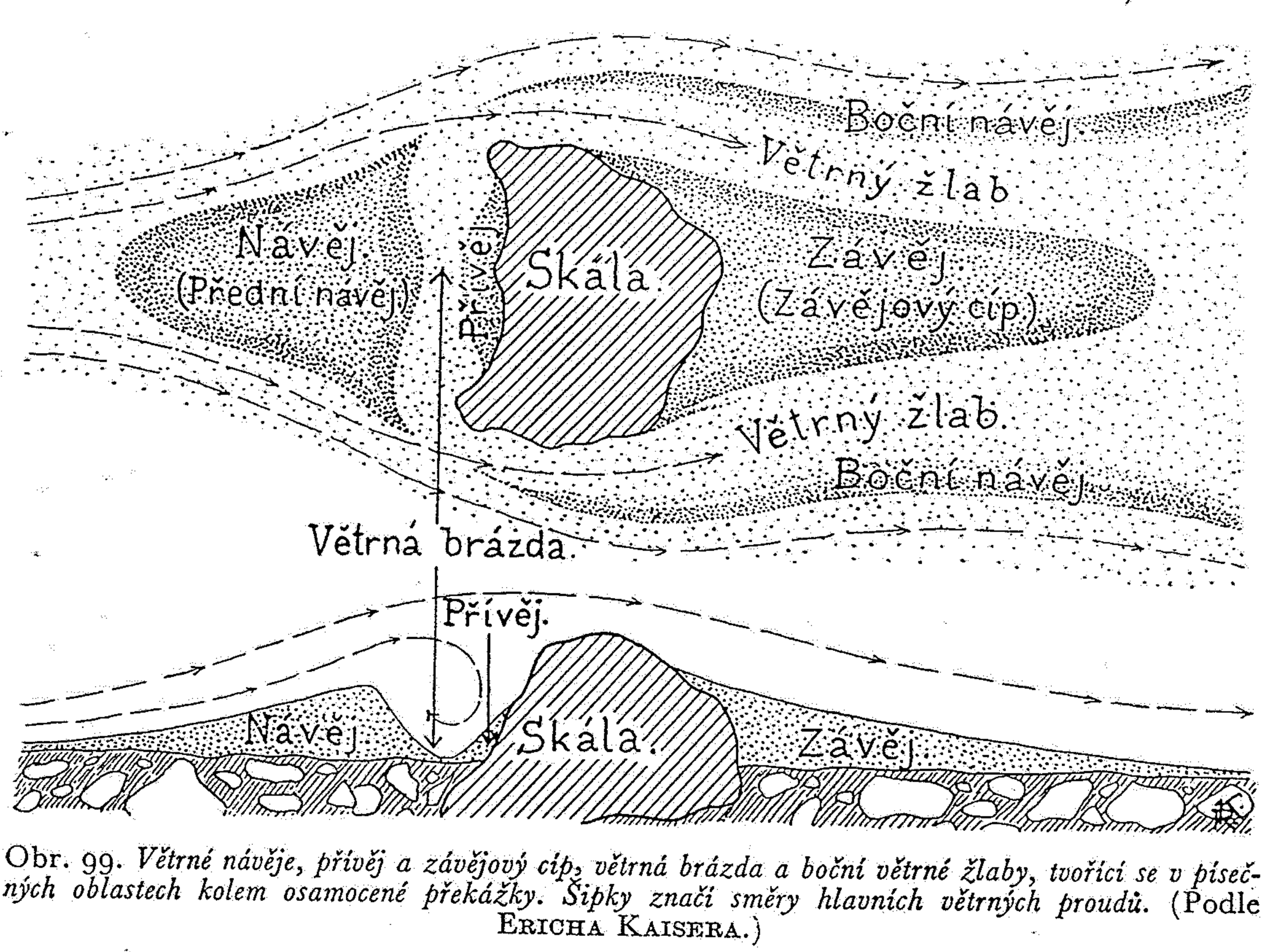

Obr. 99. *Větrné návěje, přívěj a závějový cíp, větrná brázda a boční větrné žlaby, tvořící se v písečných oblastech kolem osamocené překážky. Šipky značí směry hlavních větrných proudů.* (Podle ERICHA KAISERA.)

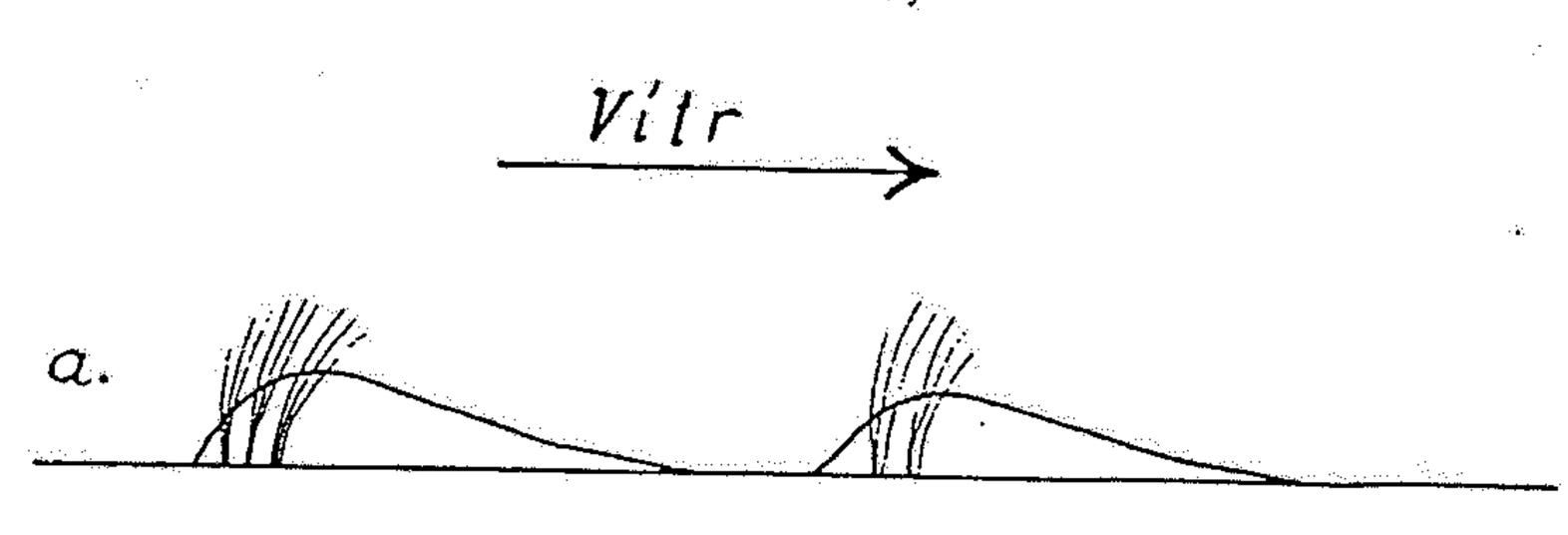

Obr. 108. *Zachycování dunového písku a zpevňování dun trsy a plazivými odenky t. zv. písečného ovsu — Ammophila arenaria na Kurské kose.* (Podle K. H. PAULA.)

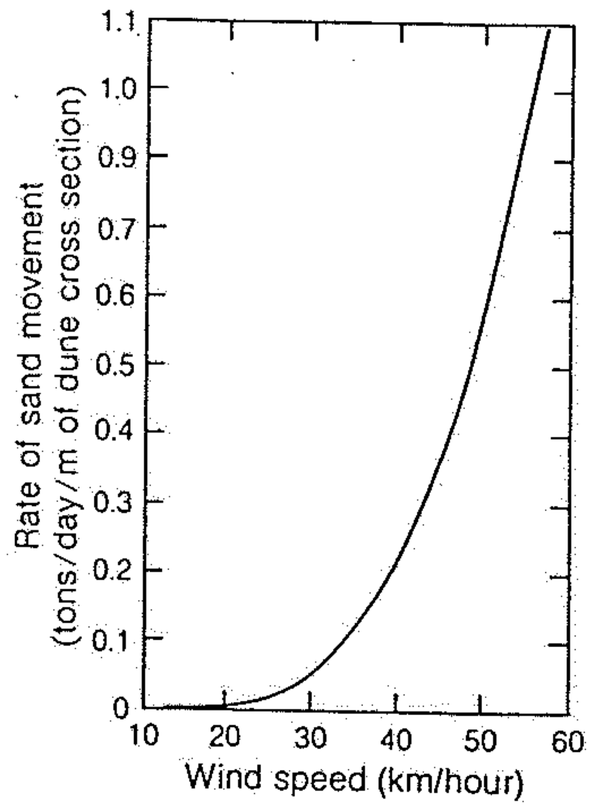

Figure 9-2

The amount of sand moved across each meter of width of a dune cross section in relation to wind speed. High-speed winds blowing for several days can move enormous quantities of sand and change dune positions markedly. [After *The Physics of Blown Sand and Desert Dunes* by R. A. Bagnold, London: Methuen, 1941.]

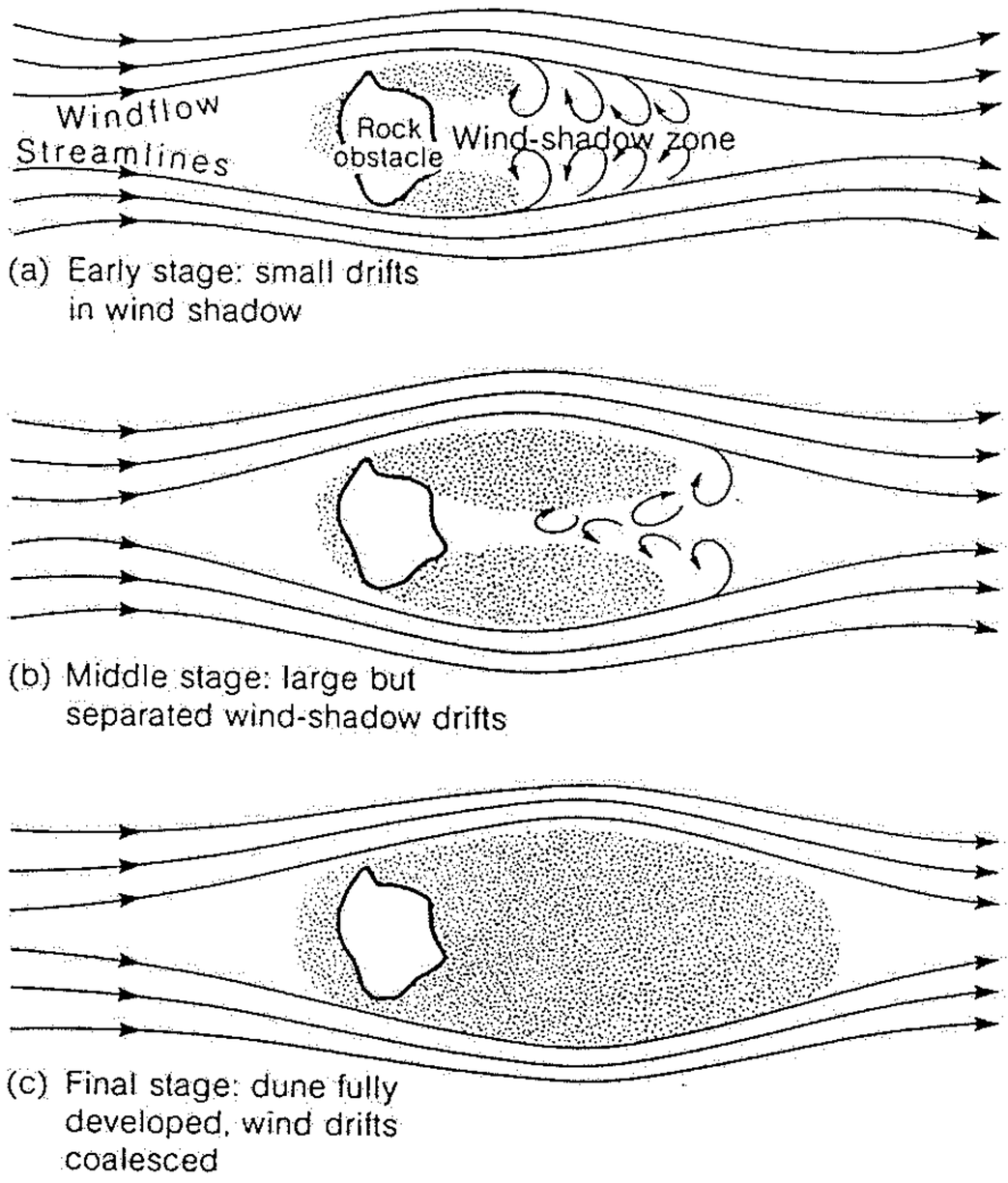

Figure 9-19

Formation of sand drift in the lee of an obstacle, such as a rock. The obstacle, by separating the flow streamlines, creates a wind shadow in which the eddies are weaker than the main windflow, thus allowing saltating grains to settle and build up a drift. The drift is a streamlined body built in response to the nonstreamlined obstacle. [After *The Physics of Blown Sand and Desert Dunes* by R. A. Bagnold. London: Metheun, 1941.]

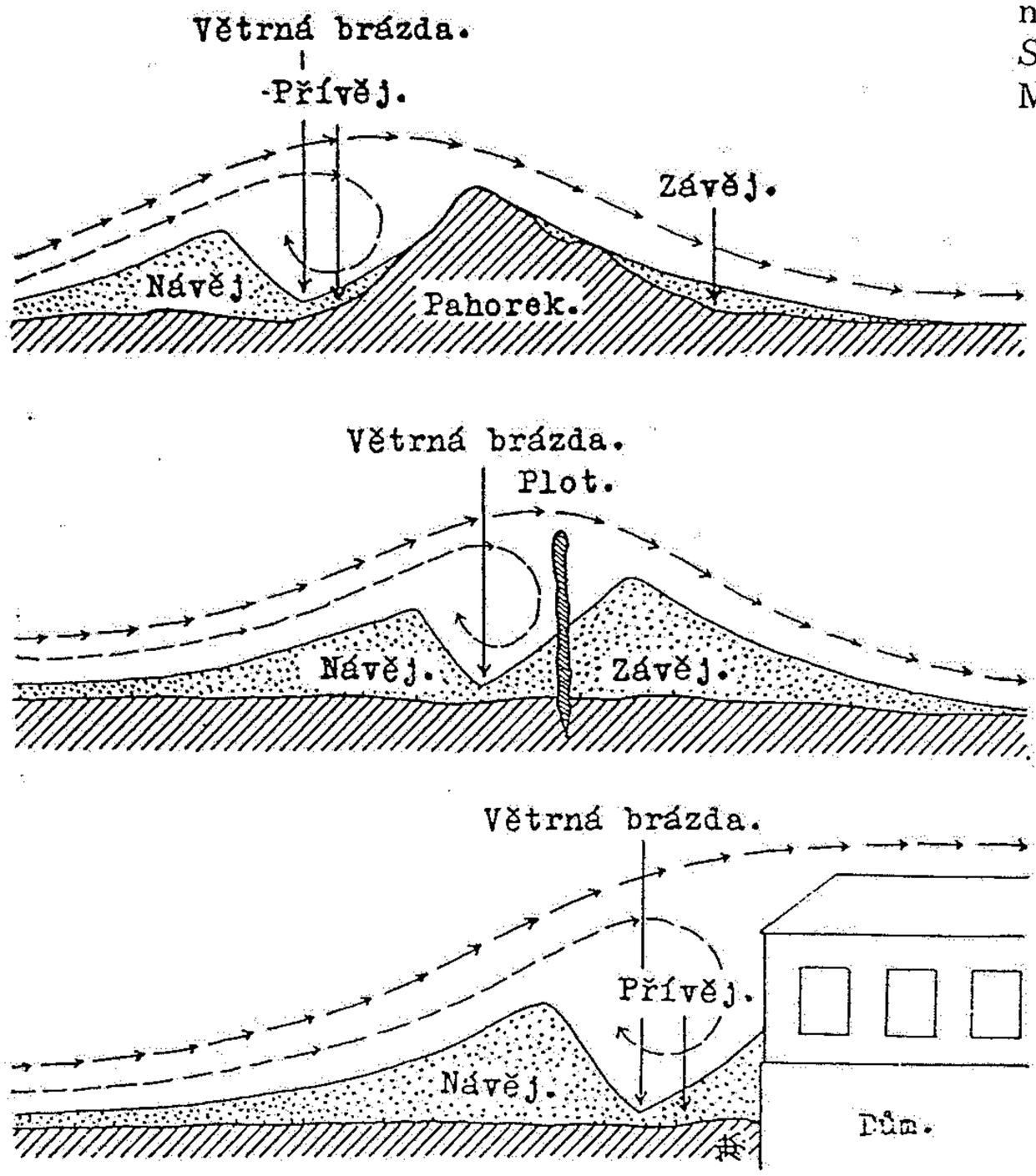

Obr. 98. *Vznik větrné brázdy v navátém písku před překážkou (pahorkem, plotem, budovou). Písek nahromaděný před překážkou dělí se touto brázdou v návěj a přívěj.* (Podle ERICHA KAISERA.)

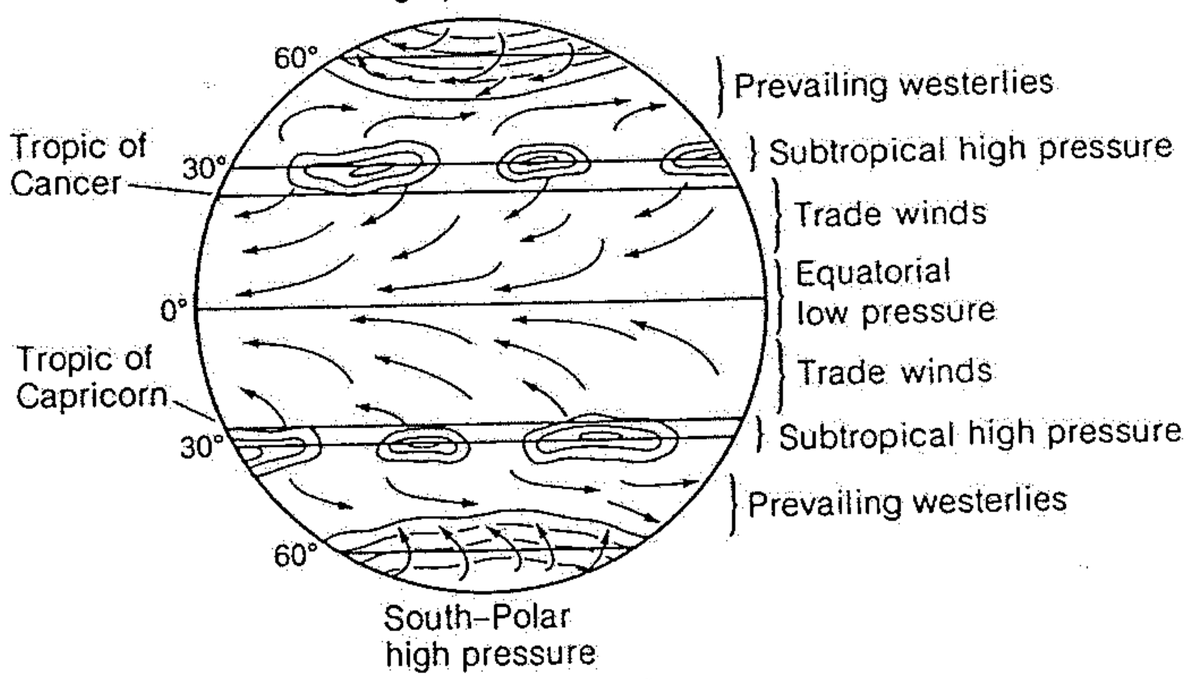

Figure 9-1

The global pattern of belts of surface winds and barometric-pressure cells. The subtropical high-pressure cells move somewhat and change size from summer to winter. Arrows show generalized wind directions.

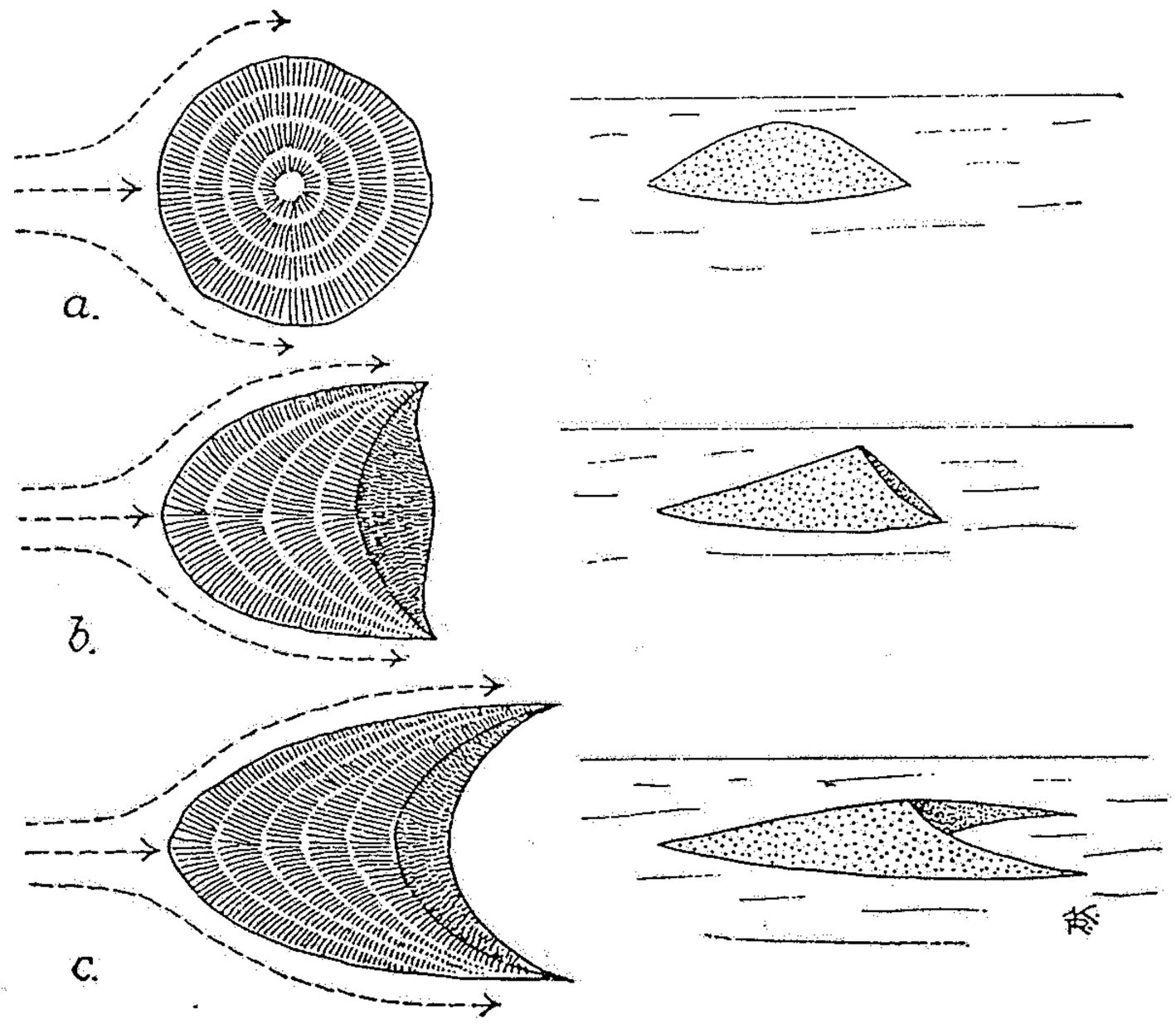

Obr. 100. *Přetvoření hromady písku jednostranným působením větru v srpovitou dunu* (*barchan*). (Orig.)

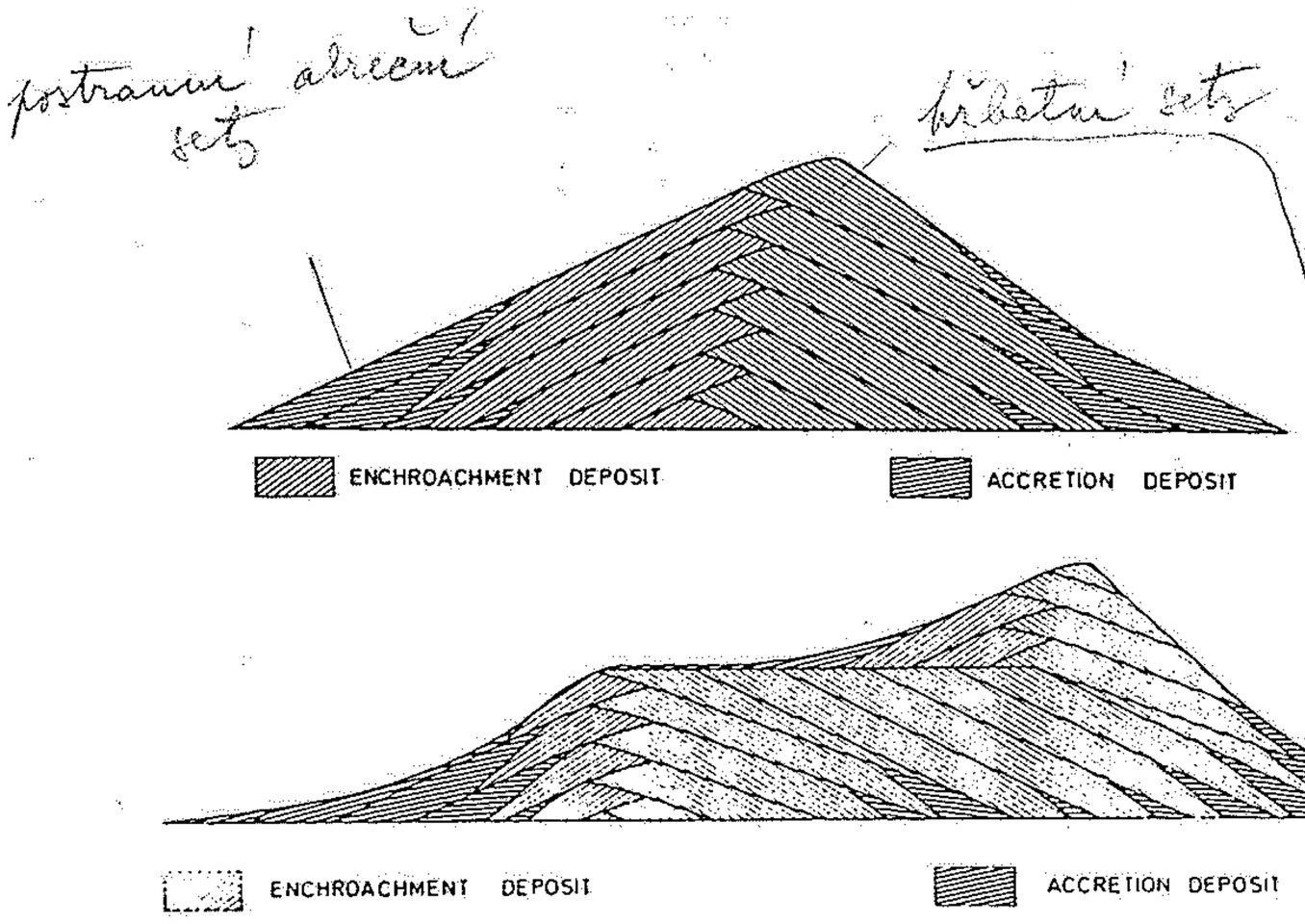

Fig. 338. Schematic internal structure of a seif dune. The central part is made up of opposed dipping high-angled cross-bedded units (encroachment deposit), and the lower parts (i. e., flanks) are made up of low-angled to horizontal-bedded accretion deposits. (Redrawn after Bagnold 1954a)

Fig. 339. Hypothetical internal structure of whalebacks associated with seif dunes. Note the arrangement of low-angled accretion deposits and high-angled encroachment deposits. (Redrawn after Bagnold 1954a)

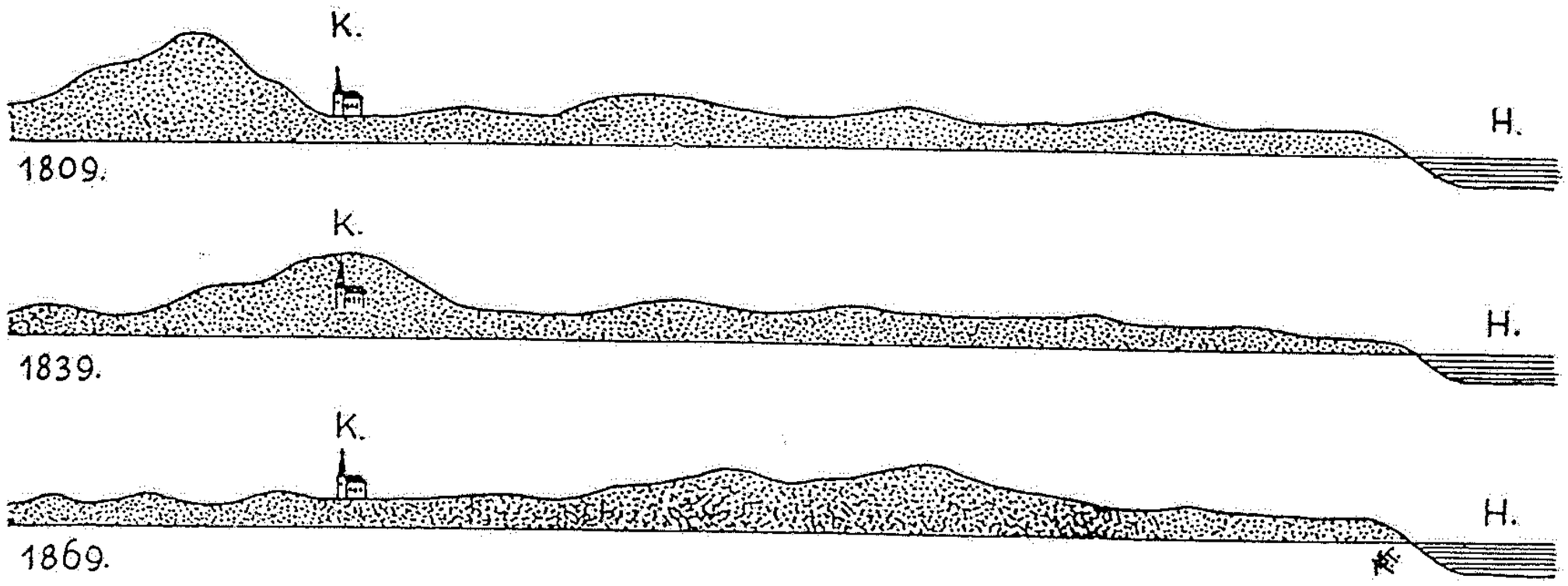

Obr. 107. *Stěhování přímořských dun na Kurské kose ve Vých. Prusku. Na počátku 19. století sahaly duny k okraji kostela a obce Kunzen* (*K.*). *V r. 1839 byly kostel a obec zcela zaváty pískem. V r. 1869 byly zříceniny kostela a obce po odvátí písku směrem ke Kurské zátoce* (*H.*) *opět obnaženy.* (Podle Behrenda.)

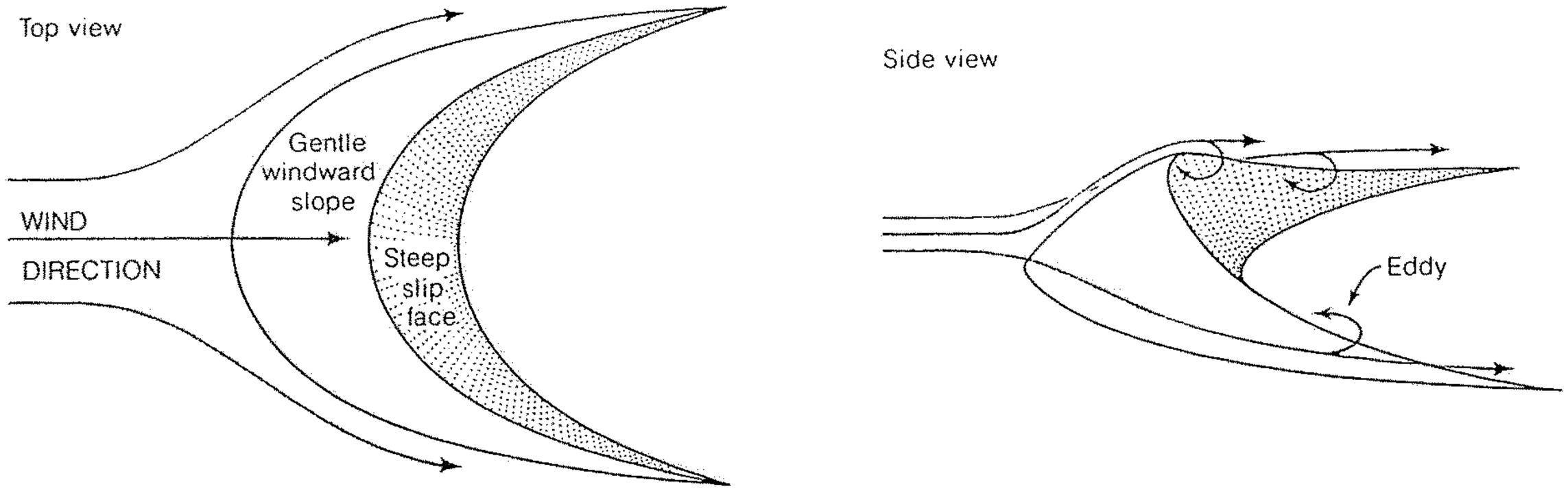

Figure 9-26

Barchans are solitary dunes whose horn shapes point downwind. One horn may elongate as the dune moves downwind; sometimes one barchan may overtake and coalesce with another.

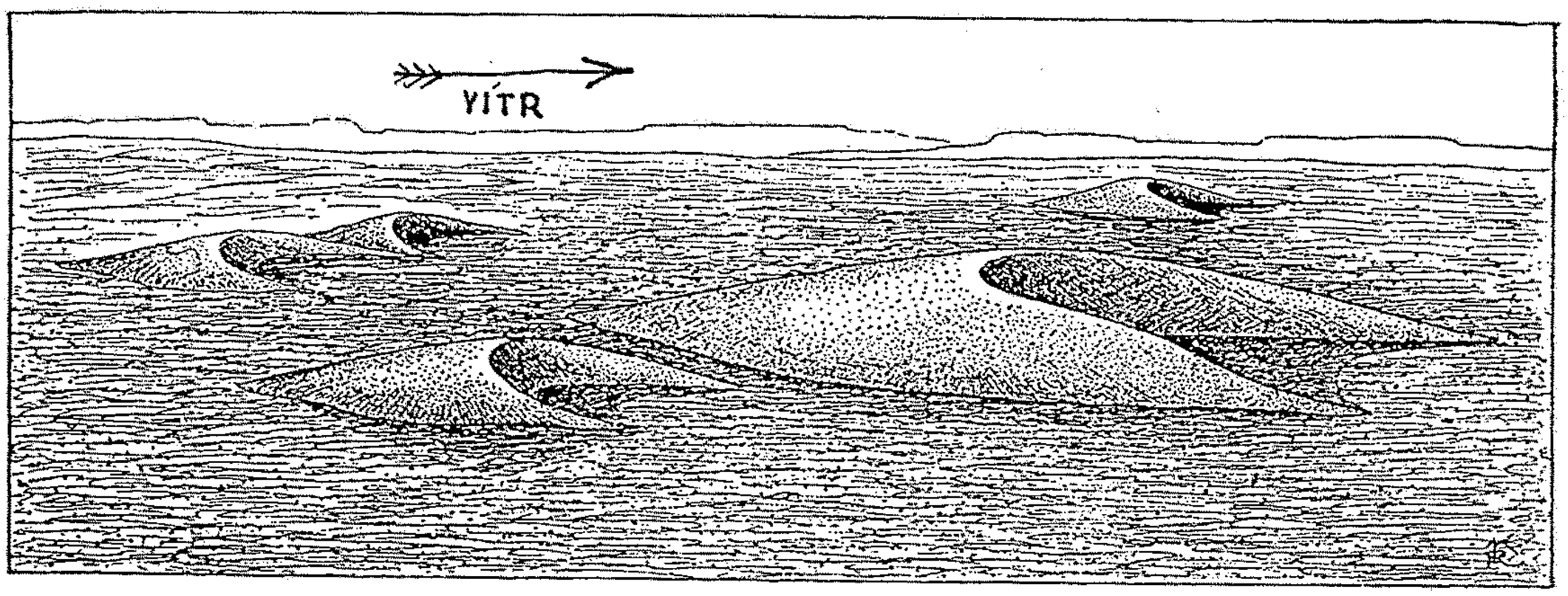

Obr. 101. *Srpovité duny — barchany.* (Kresba autorova.)

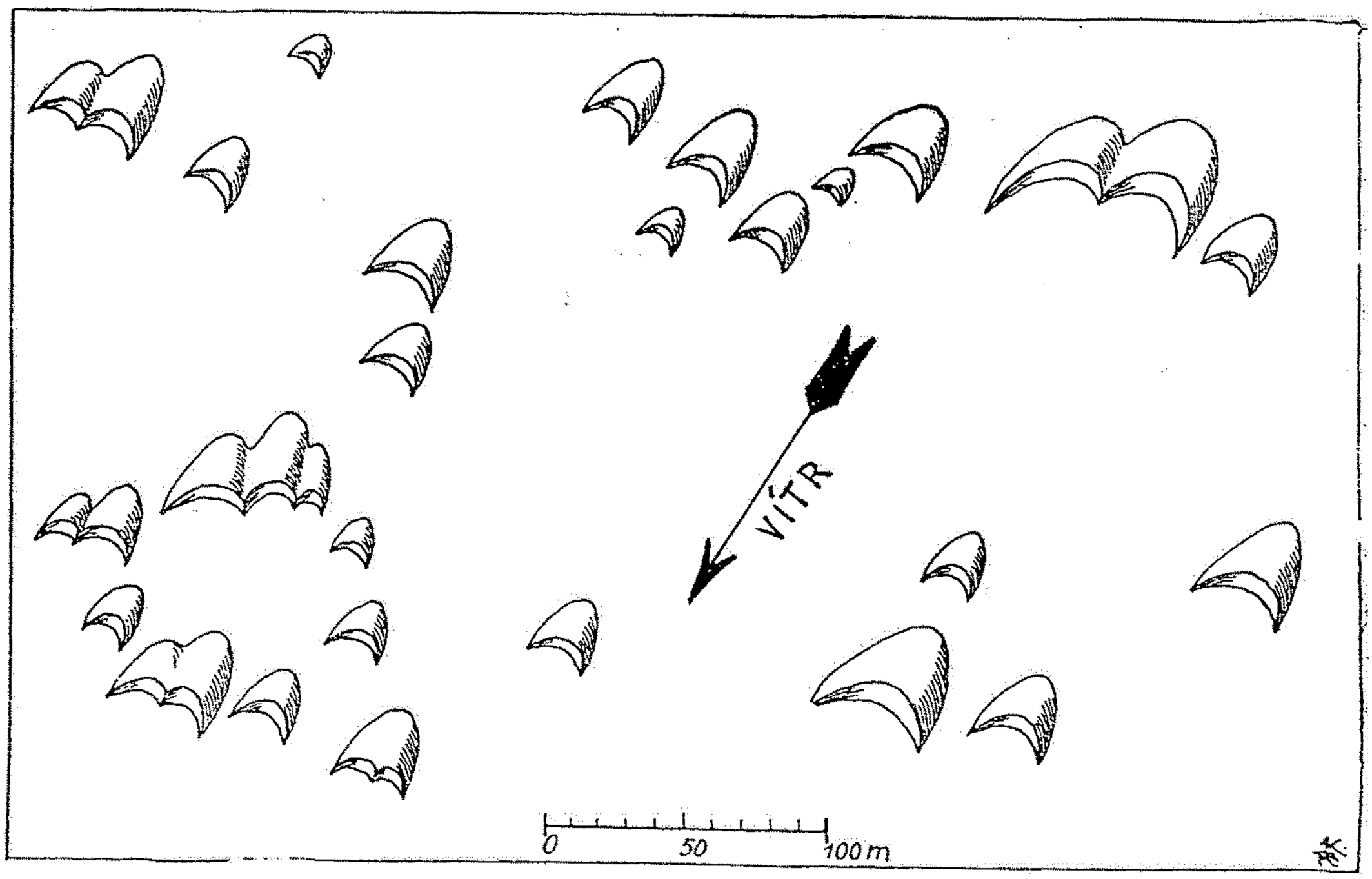

Obr. 102. *Půdorys srpovitých dun (barchanů) v Buchaře v Turkestanu.* (Podle JOH. WALTHERA.)

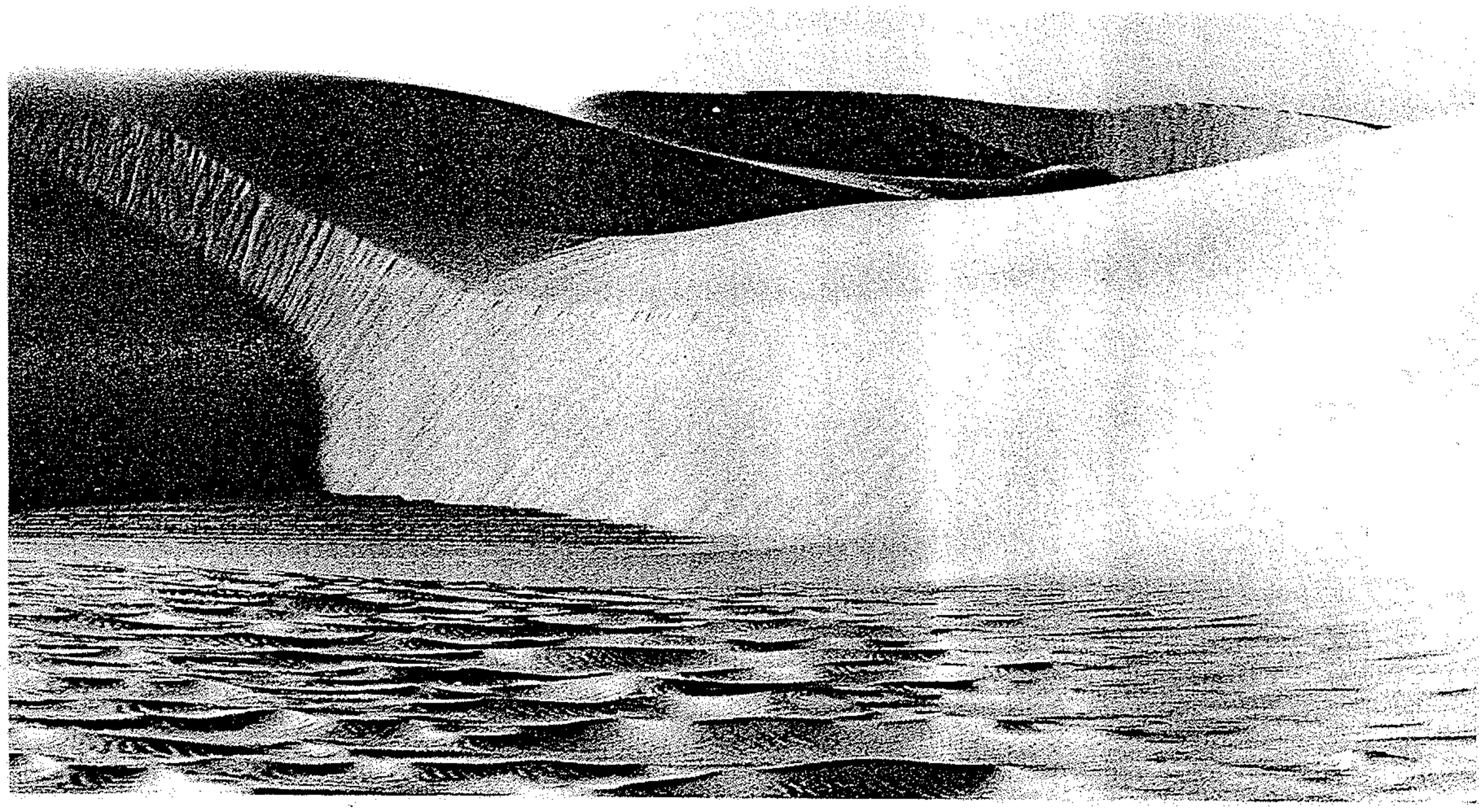

Figure 9-22

Dunes in the Arabian desert, showing the slip face of a large dune advancing on a sand-rippled surface. The grooved appearance of the slip face is formed by cascades of sand grains assuming the stable angle of repose. [From Arabian American Oil Co.]

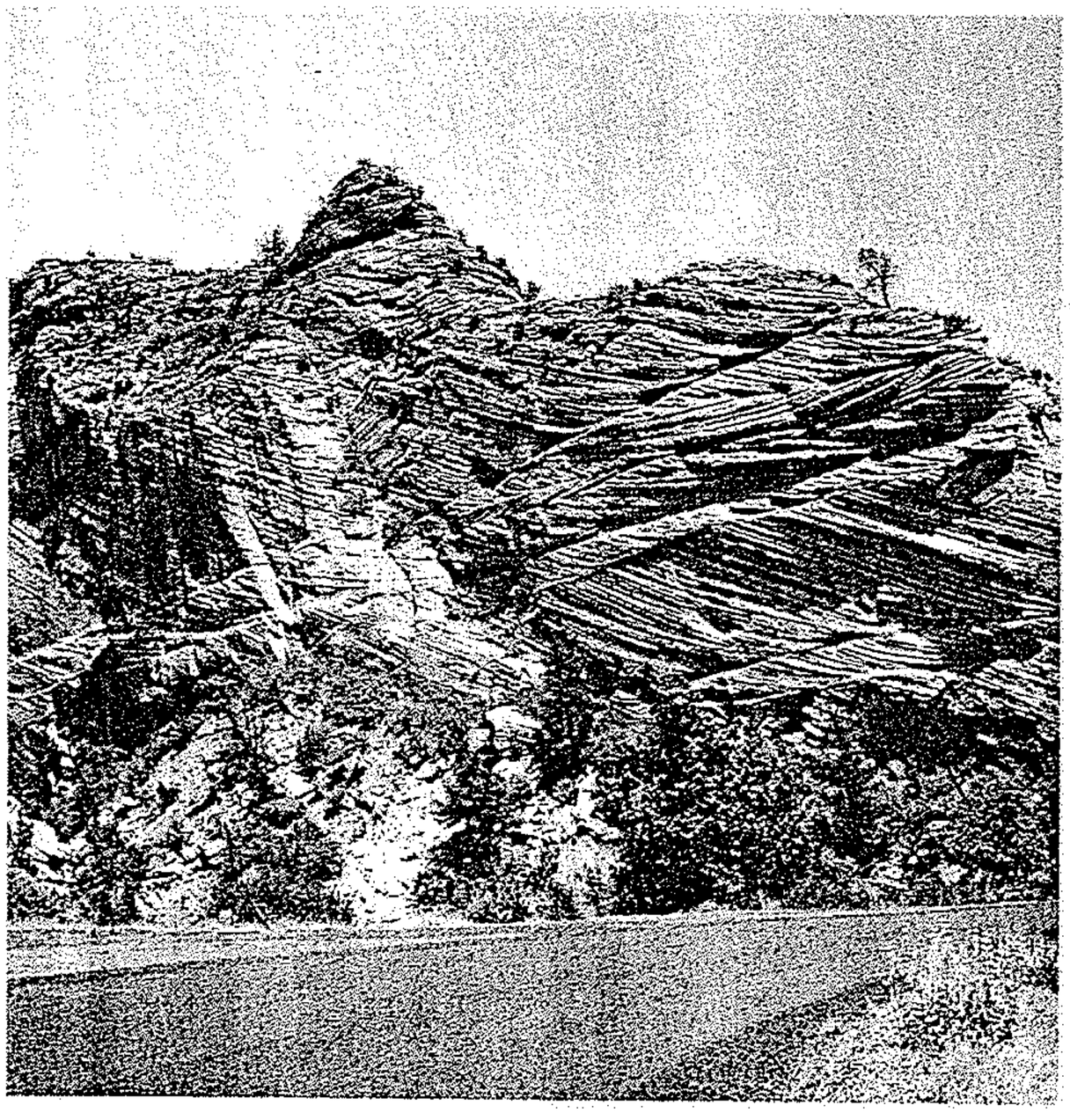

Figure 9-23

Interfering sets of cross-beds in an ancient eolian sandstone. The complex pattern is a response to variable wind directions. The appearance can be similar to the interfering trough cross-bedding of Figure 8-11. [Photo by R. Siever.]

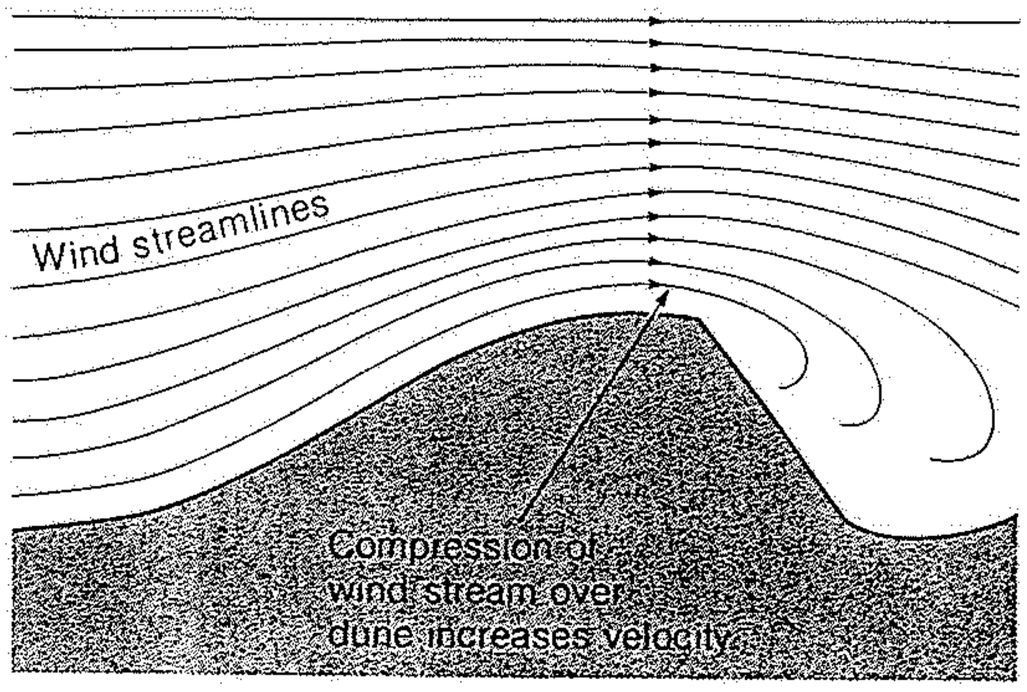

Figure 9-24

Limitation of the height of a sand dune by a compressed wind stream. As the dune grows higher, the wind stream (shown by streamlines) becomes more compressed and thus travels at a great velocity, which makes it more competent to transport sand grains. Eventually, a height is reached at which the wind speed is so great that all of the sand is transported, and the dune stops growing vertically.

Figure 9-25
Desert sand "mountains," draas, in the Saudi Arabian desert may reach heights of as much as 250 m (820 ft). [From Arabian American Oil Co.]

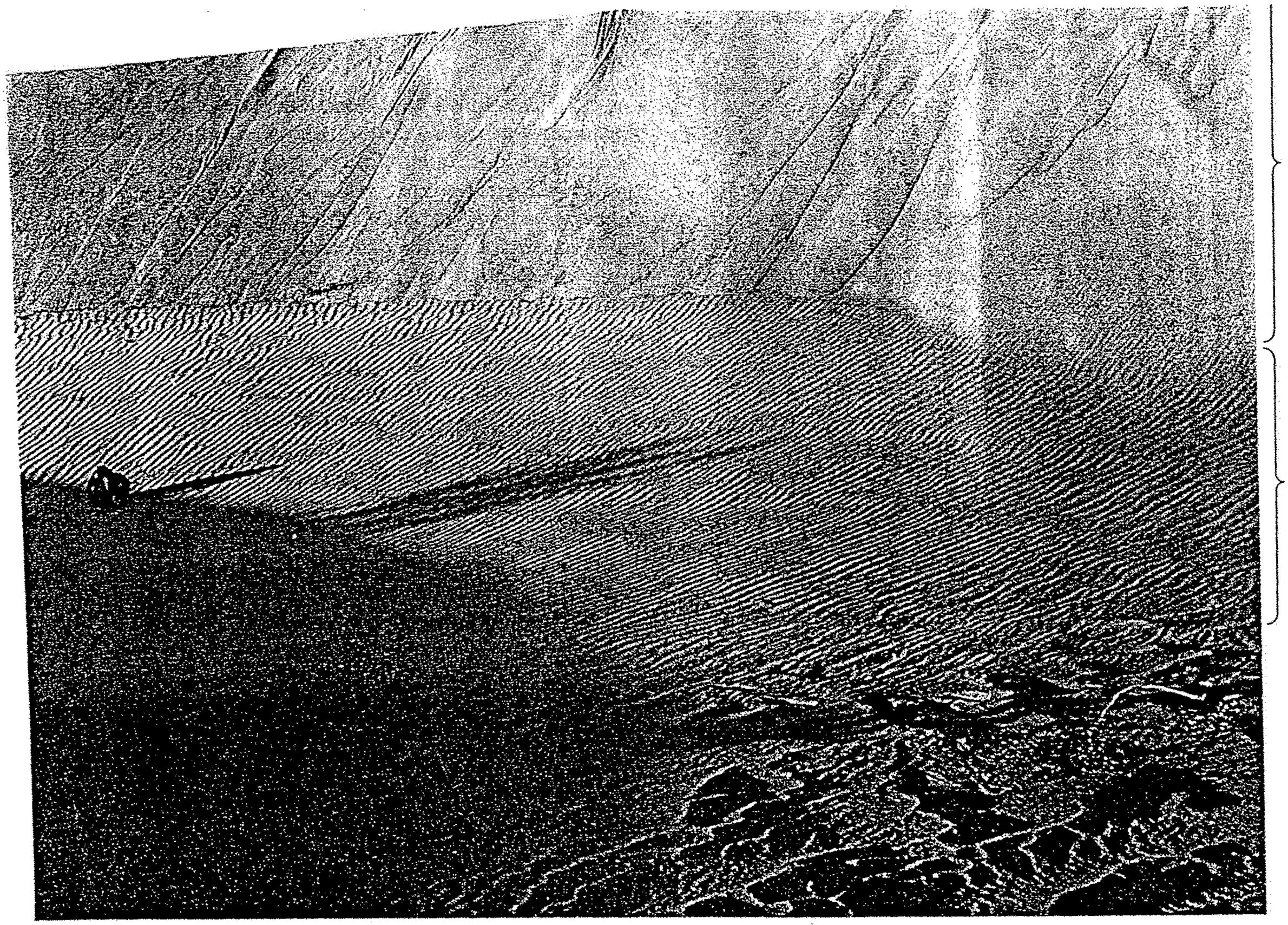

17.17 The steep slope facing the viewer is the slip face on the lee side of a New Mexican dune. The dune moves forward toward the viewer as sand is pushed up its windward side and is deposited on the lee side. Continuing small slips of loose sand keep the slip face steep. [Franklyn B. Van Houten.]

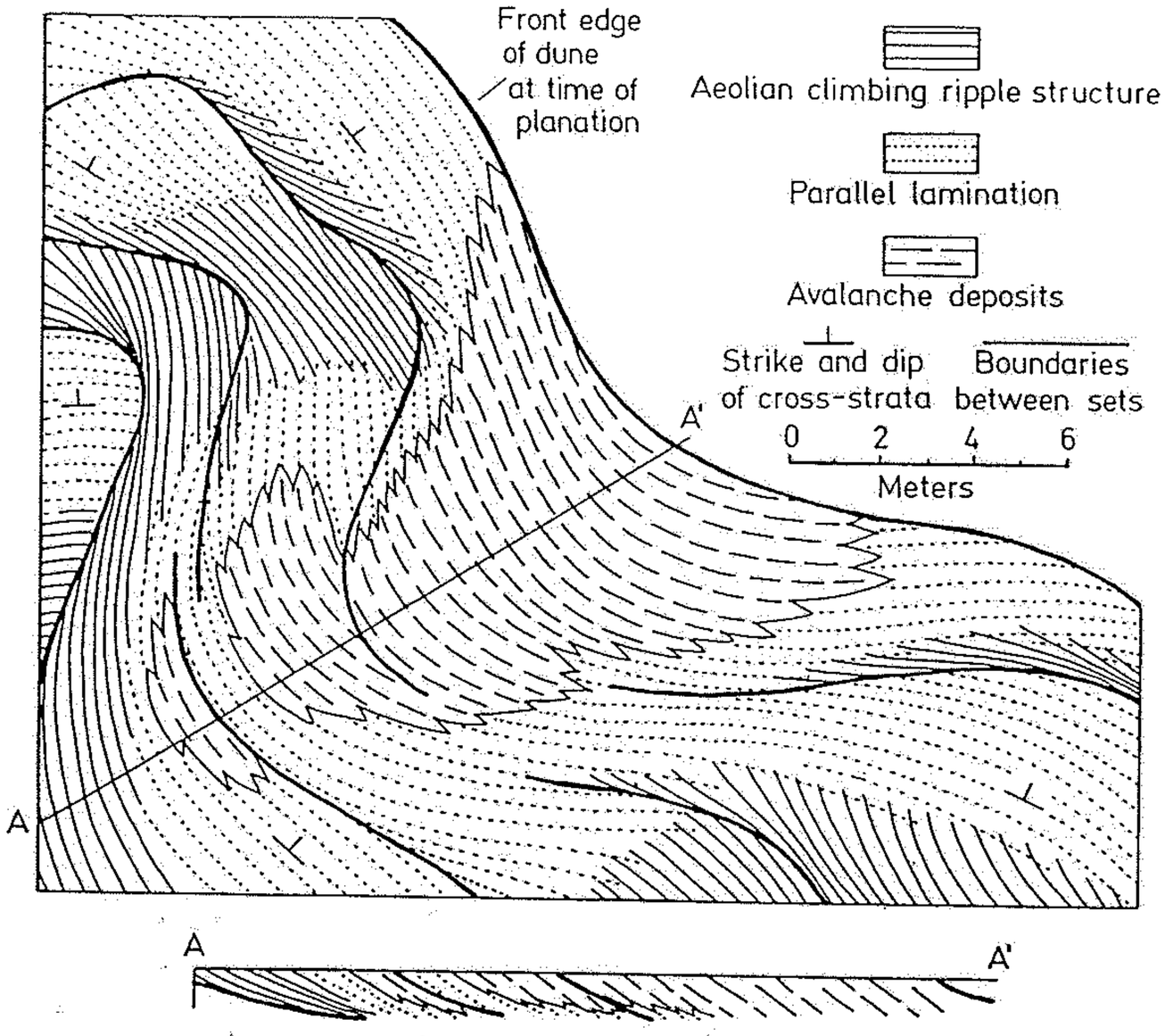

Fig. 325. Schematic diagram showing distribution of various types of bedding in an aeolian dune. Based on exposure on Padre Island, Texas. (After Hunter 1977)

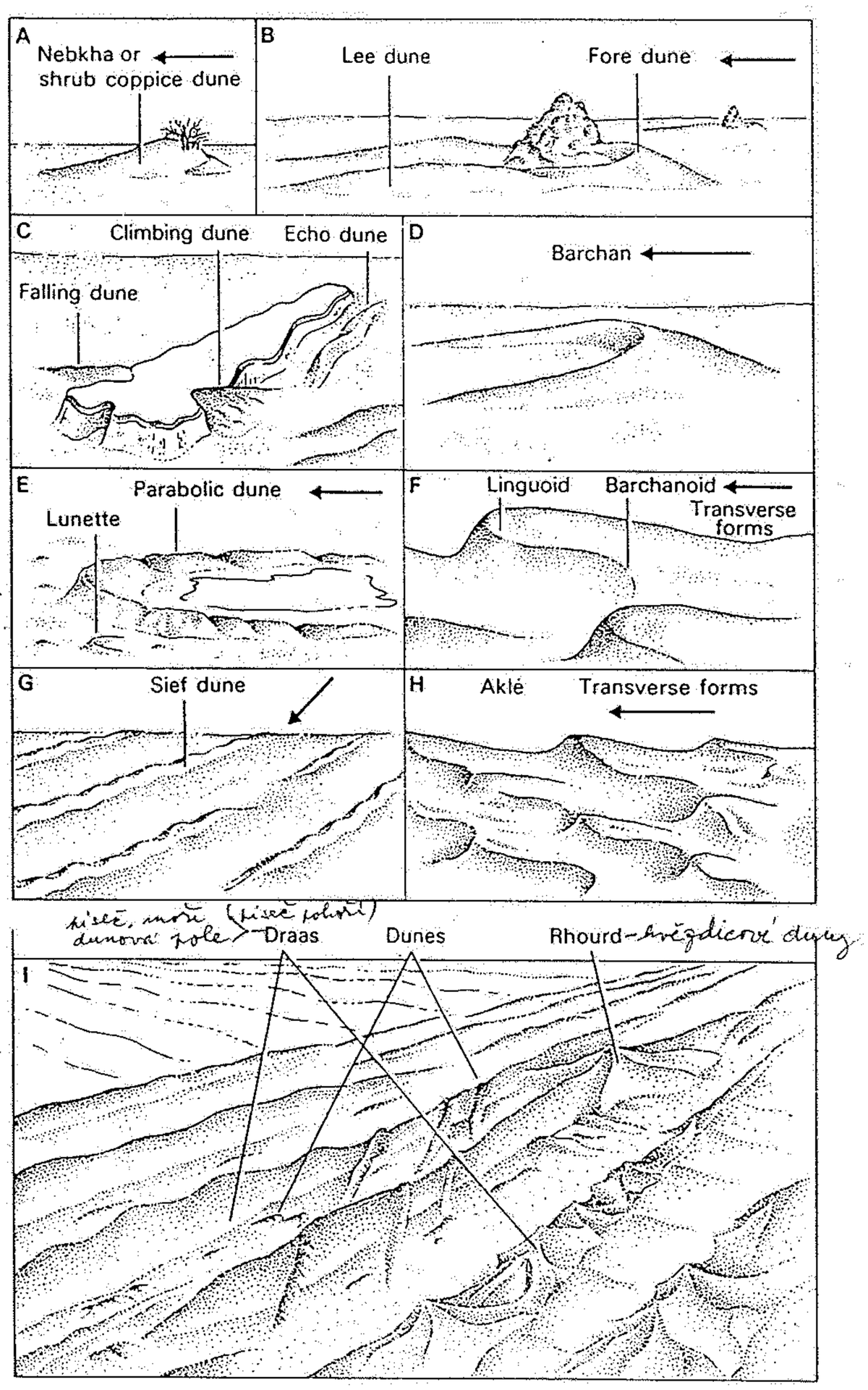

Fig. 5.4. Main types of aeolian dune and draa. The terms used in Figs. D–H may be applied to dunes as well as draas. Effective wind direction is indicated where appropriate. In Figs. C and I no one direction dominates. Figure I shows the size relationship between dunes and draas (after Cooke and Warren, 1973).

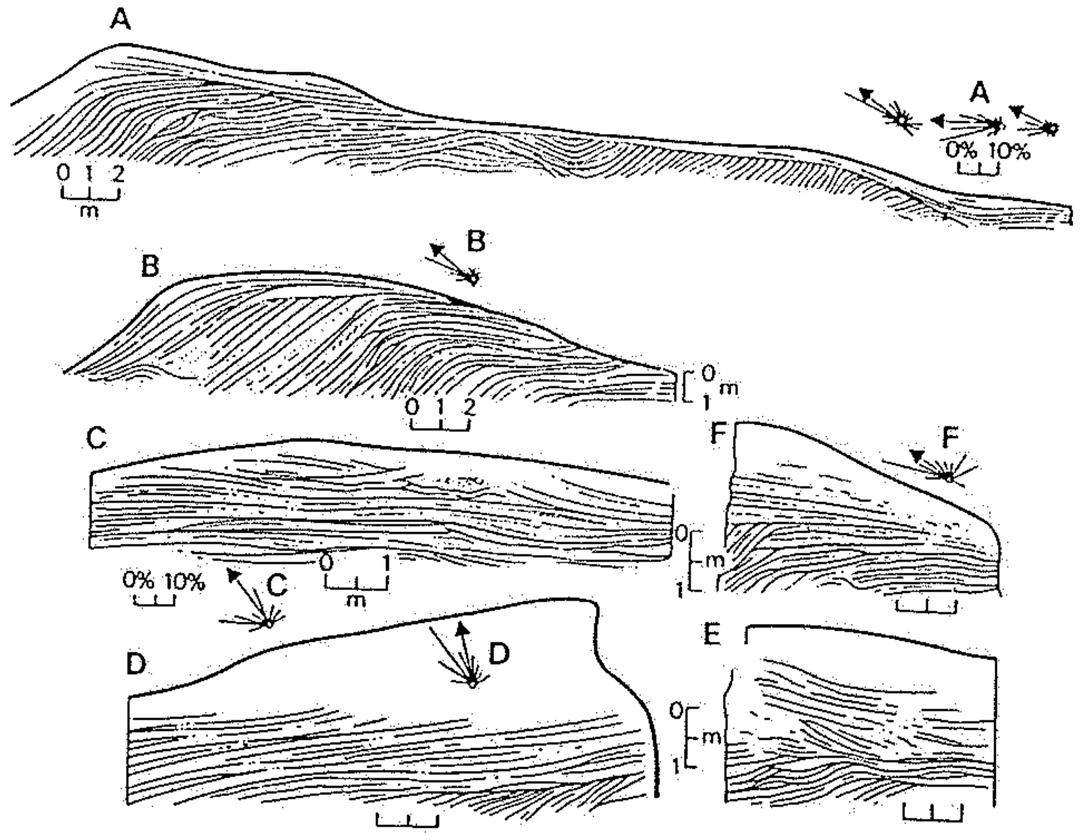

Fig. 5.7. Internal structures of coastal dunes, Parana, Brazil, with rose diagrams of foreset orientation. Note the similarity with the transverse dune from White Sands, New Mexico (Fig. 5.6, B(1)) (after Bigarella, Becker and Duarte, 1969).

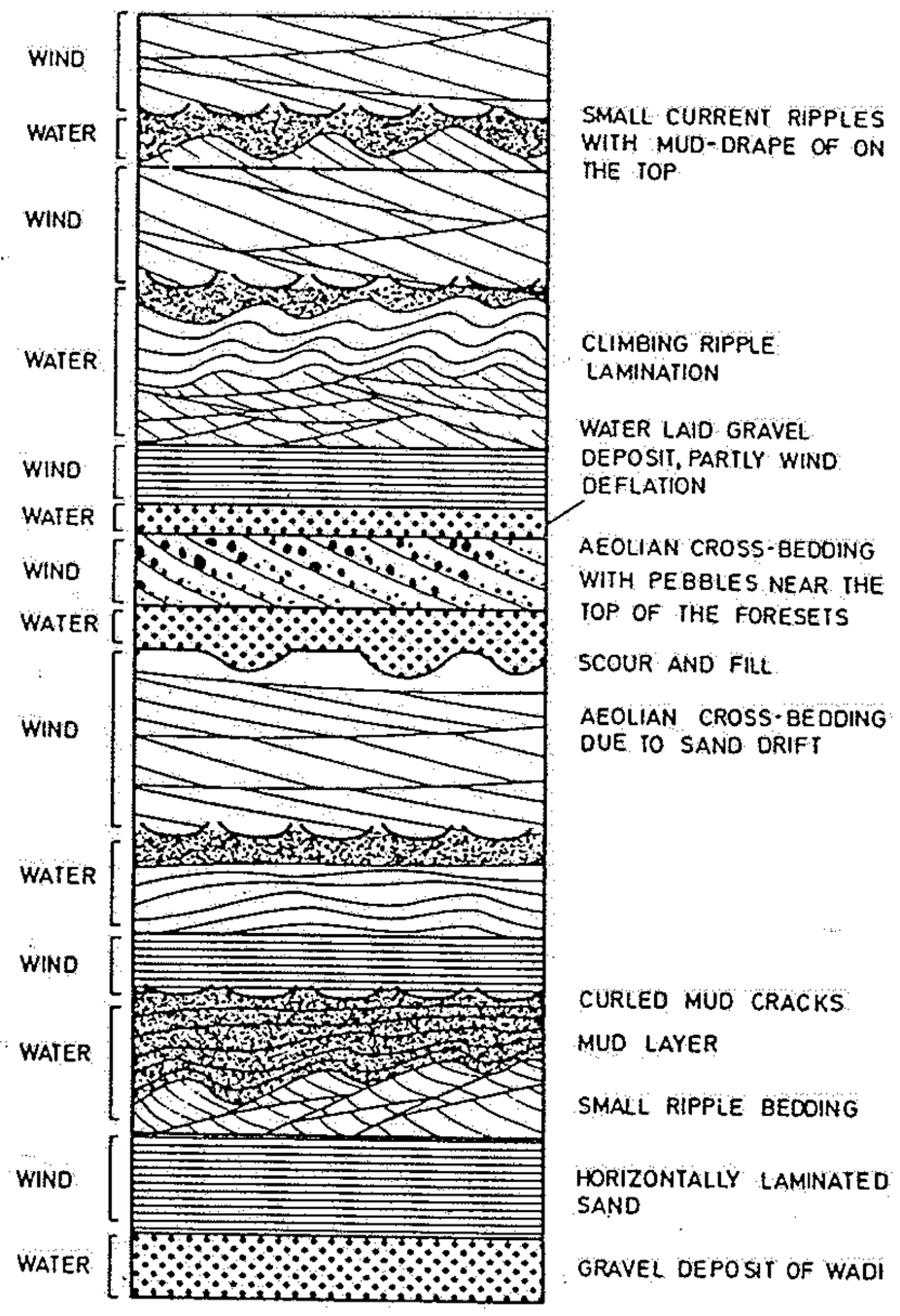

Fig. 317. Schematic diagram showing a sequence of wadi deposits with alternating wind-and water-laid sediments. Based mainly on data of Glennie (1970)

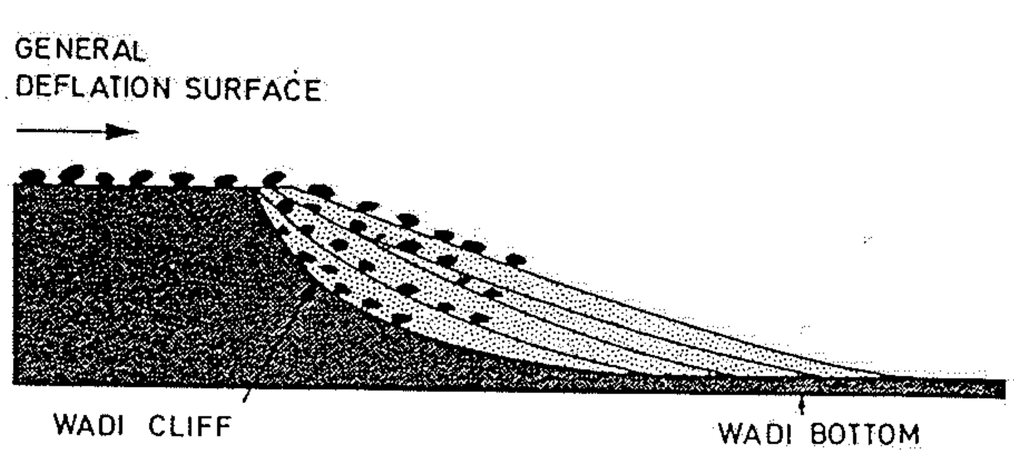

Fig. 318. Scheme showing the deposition of inclined foresets along a wadi bank in the form of sand drift. Larger pebbles are more common near the upper part of the foresets

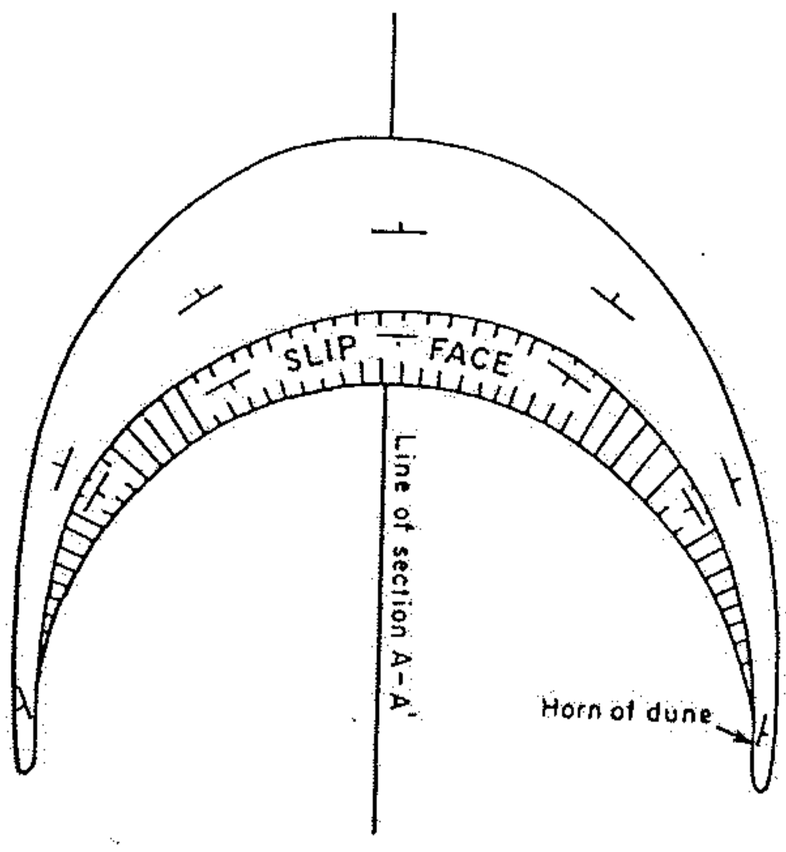

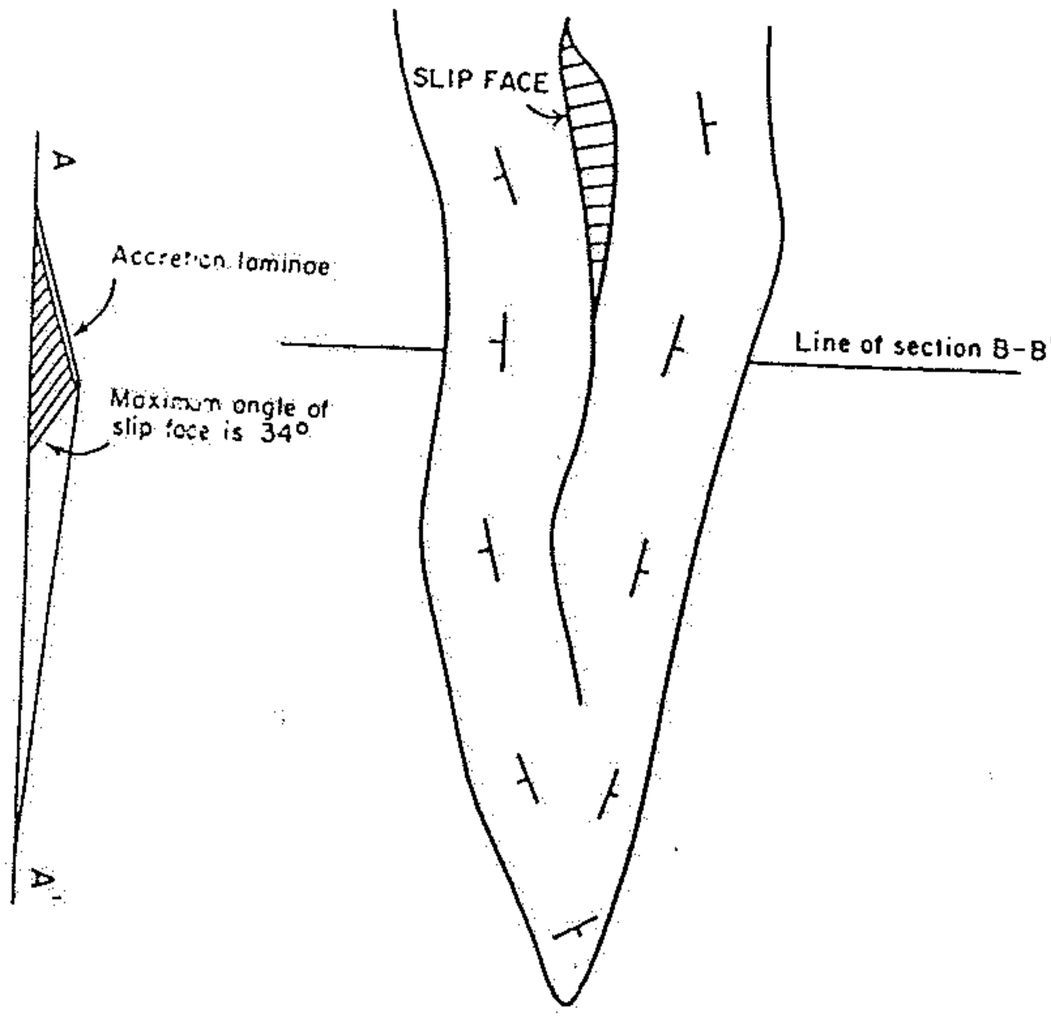

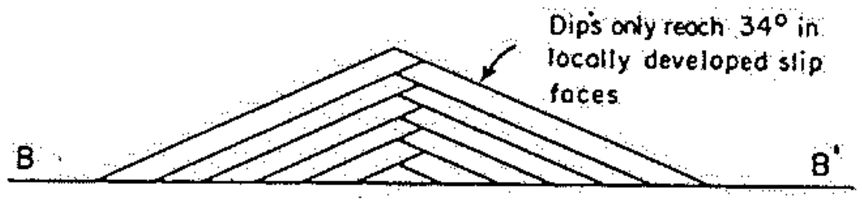

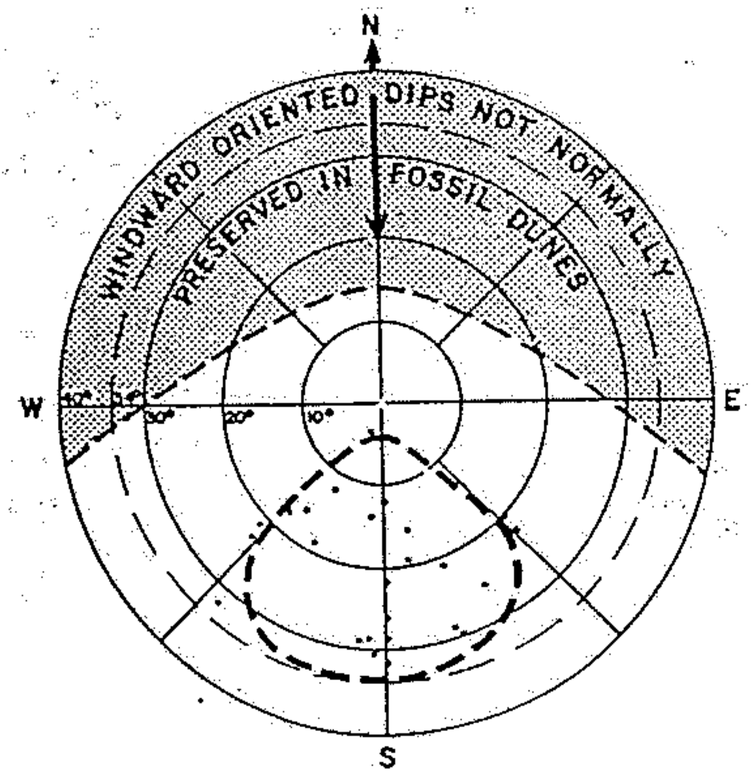

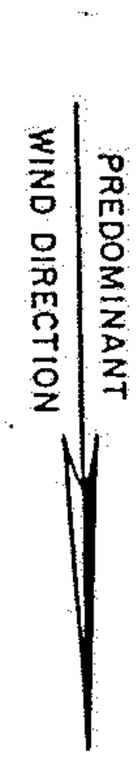

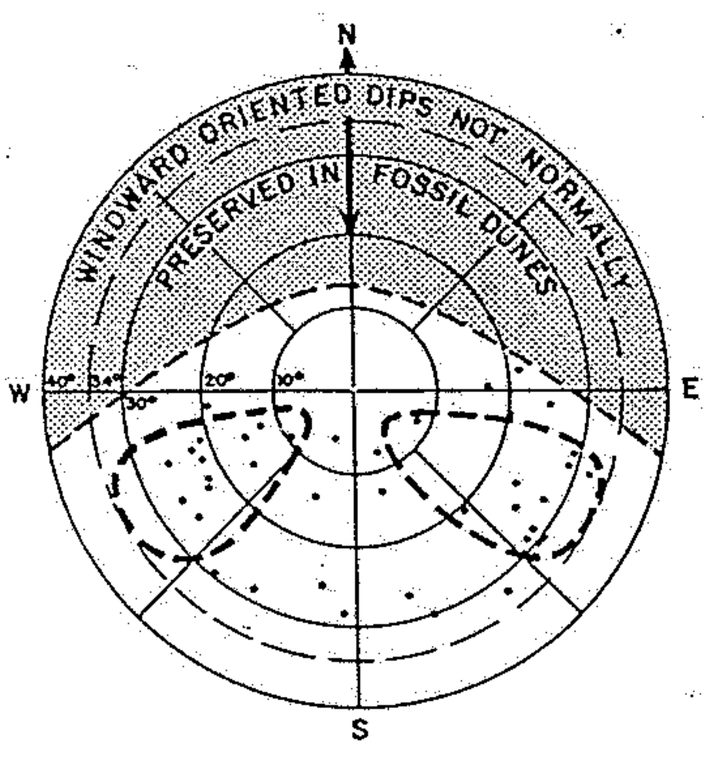

Barchan dunes

1. "Horns" of dune directed down-wind.
2. Bulk of dune foresets dip down-wind at angles of up to 34°.
3. A small proportion of low-angle dips will be oriented at almost 90° to the predominant wind direction but with a component in the direction of the wind. They represent the bedding on the horns of the dune and are very similar to that seen in a seif dune.
4. Low-angle dips oriented up-wind may be preserved when a barchan climbs onto the windward accretion slope of a more slowly moving dune of similar type.

Seif dunes

1. Axis of dune parallel to the dominant wind direction.
2. The bulk of the dune will have dips of up to 34° oriented almost at right angles to the predominant wind direction but with a component in the direction of the wind.
3. Seif dune bedding may be complicated by the migration of small local barchans over their surface.
4. The frictional effect of the bulk of a seif dune is thought to give the wind a 'corkscrew' rotational component directed towards the dune. Localised 34° laterally dipping slip-faces may result.
5. The slight sinuosity of the dune may result in the preservation of low-angle dips which have an up-wind component.

Fig. 335. Cross-bedding directions in a barchan dune and a seif dune in relation to wind direction. (After Glennie 1970)

These dunes in Peru are called barchans. The horns of the crescent point down wind (to the left) and the slip face is the concave side of the dune. They are migrating from right to left. (Photograph by Aerial Explorations, Inc.)

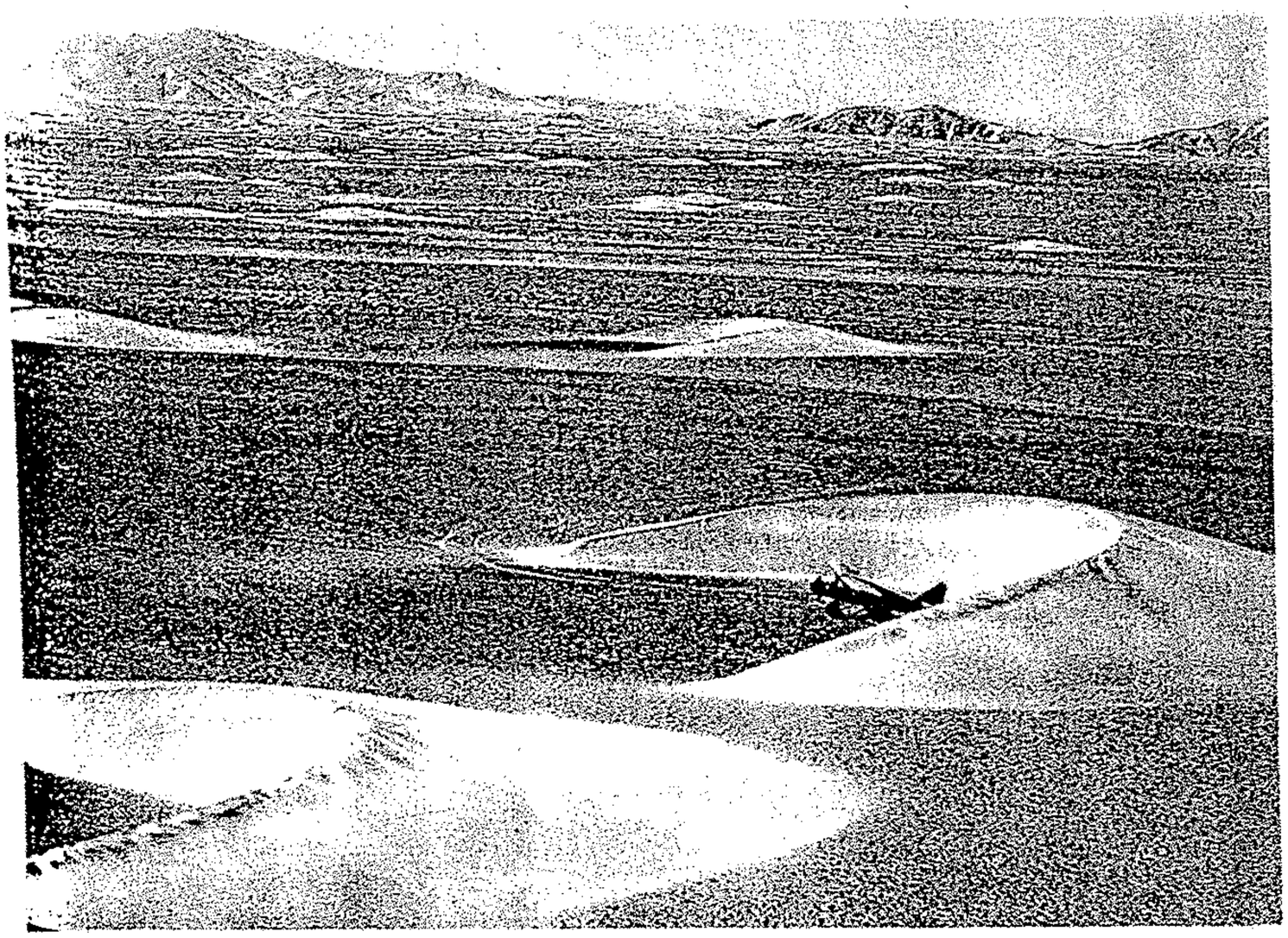

FIGURE 15–25
Cross-bedding in the Navajo sandstone, Zion Park, Utah. (Photo by Tad Nichols, Tucson, Arizona.)

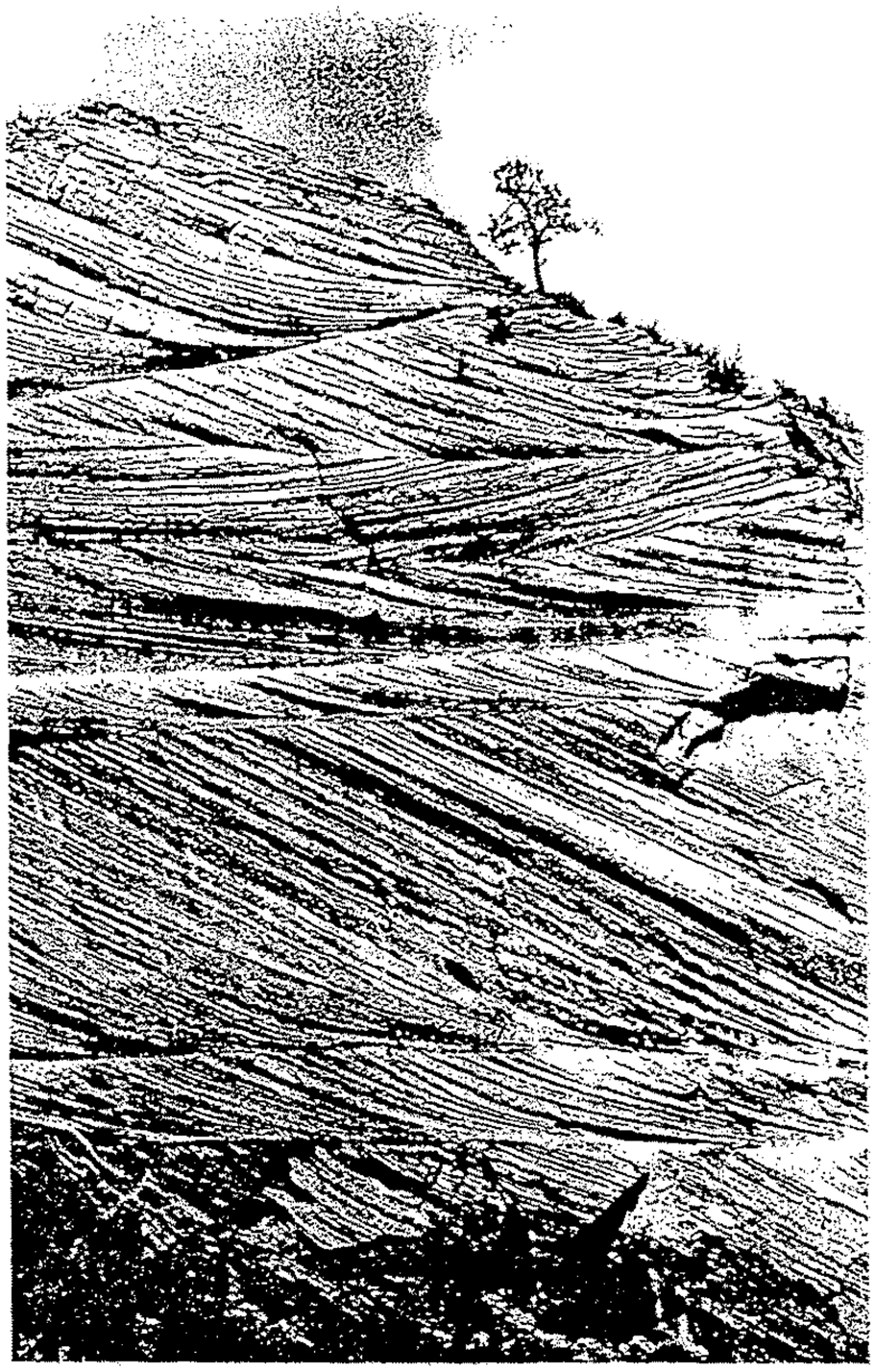

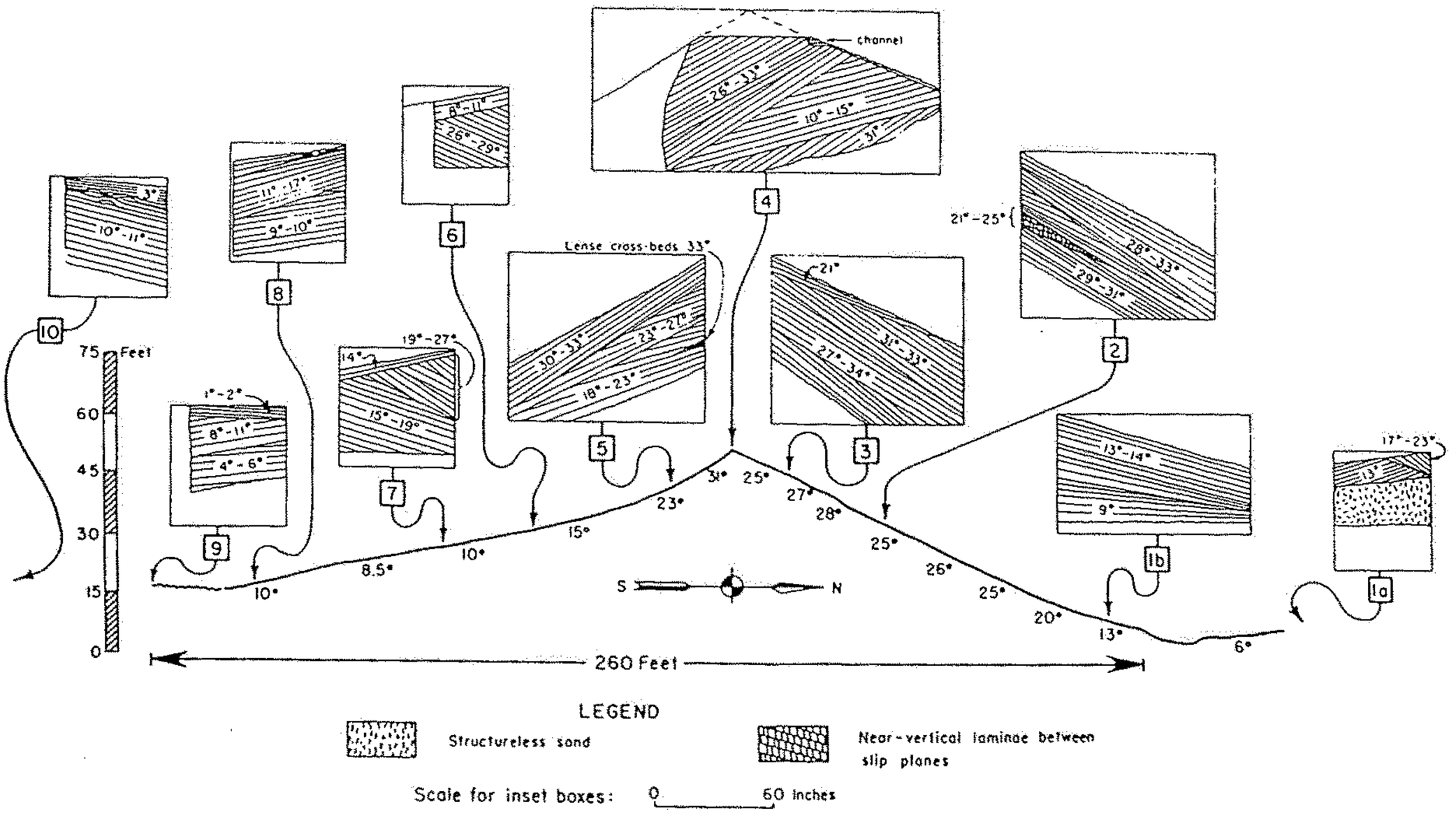

Fig. 337. Internal structure of a seif dune. (After McKee and Tibbitts 1964)

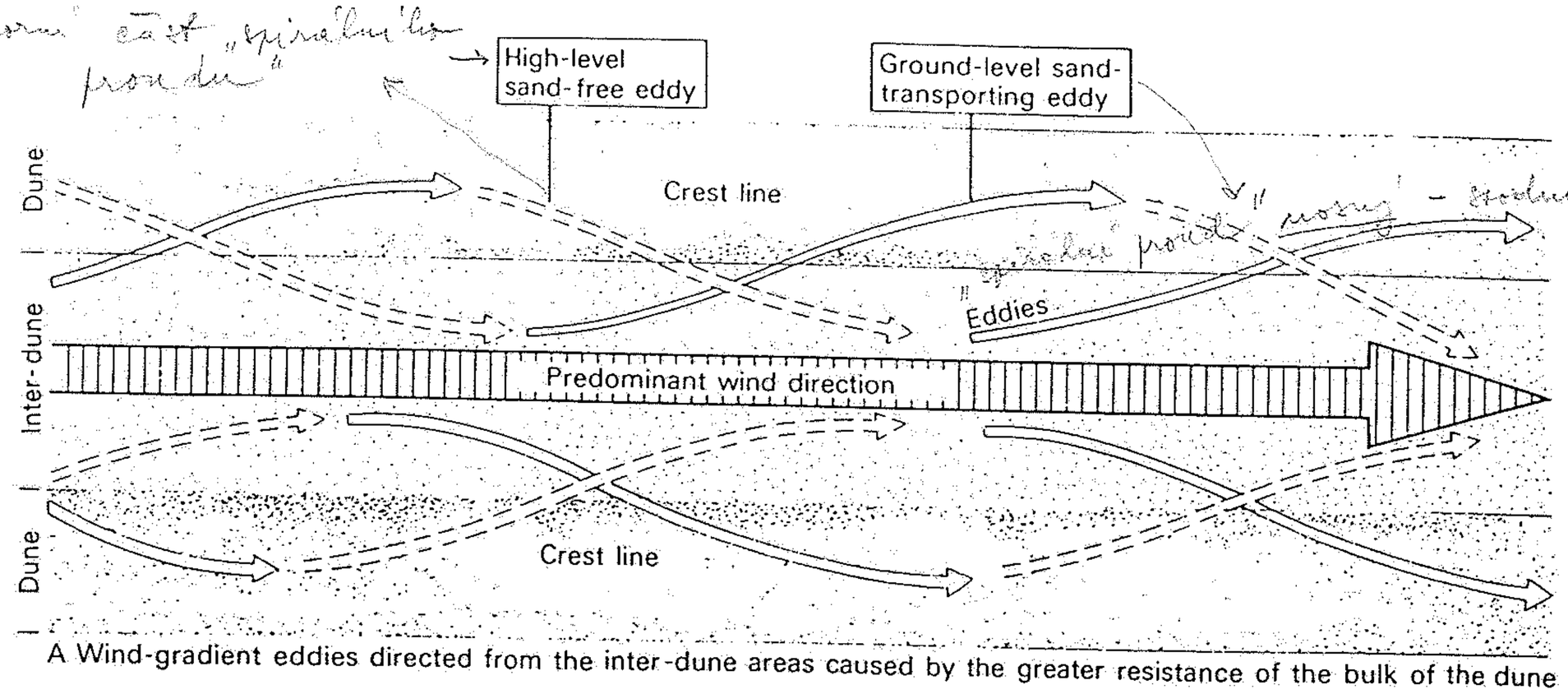

A Wind-gradient eddies directed from the inter-dune areas caused by the greater resistance of the bulk of the dune

Fig. 5.5. Suggested relationship between the form of seifs and the large-scale structure of the near surface wind (after Glennie, 1970).

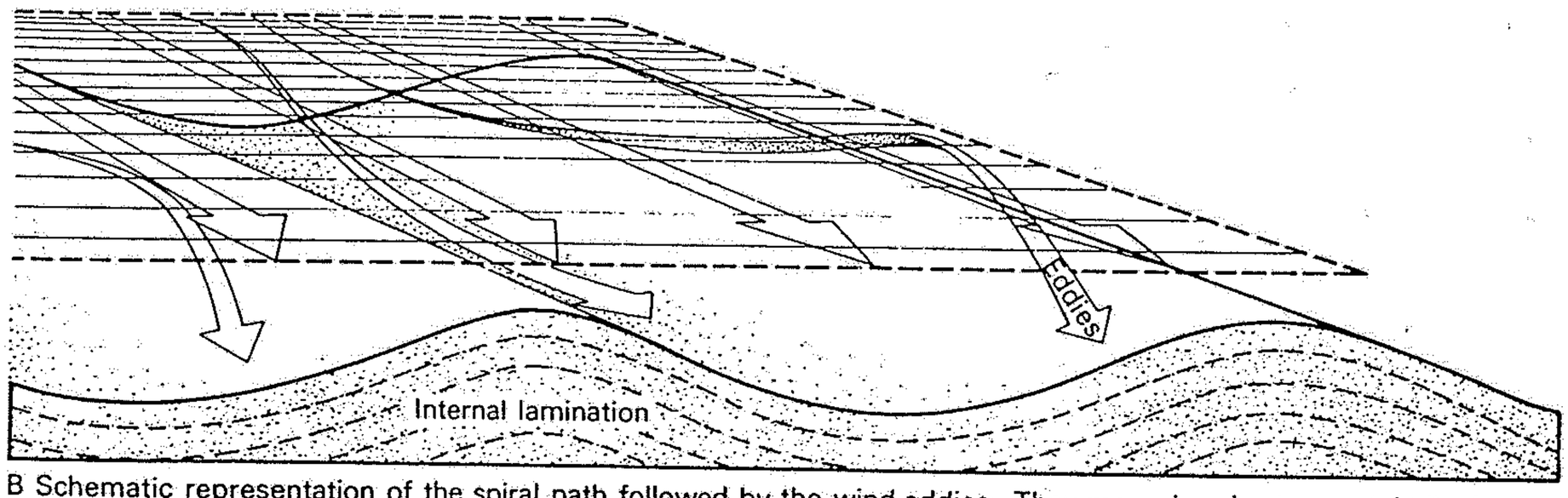

B Schematic representation of the spiral path followed by the wind eddies. They may give rise to crestal slip faces. A deviation of the wind from the predominant direction will accentuate the development of slip faces on one side of the dune

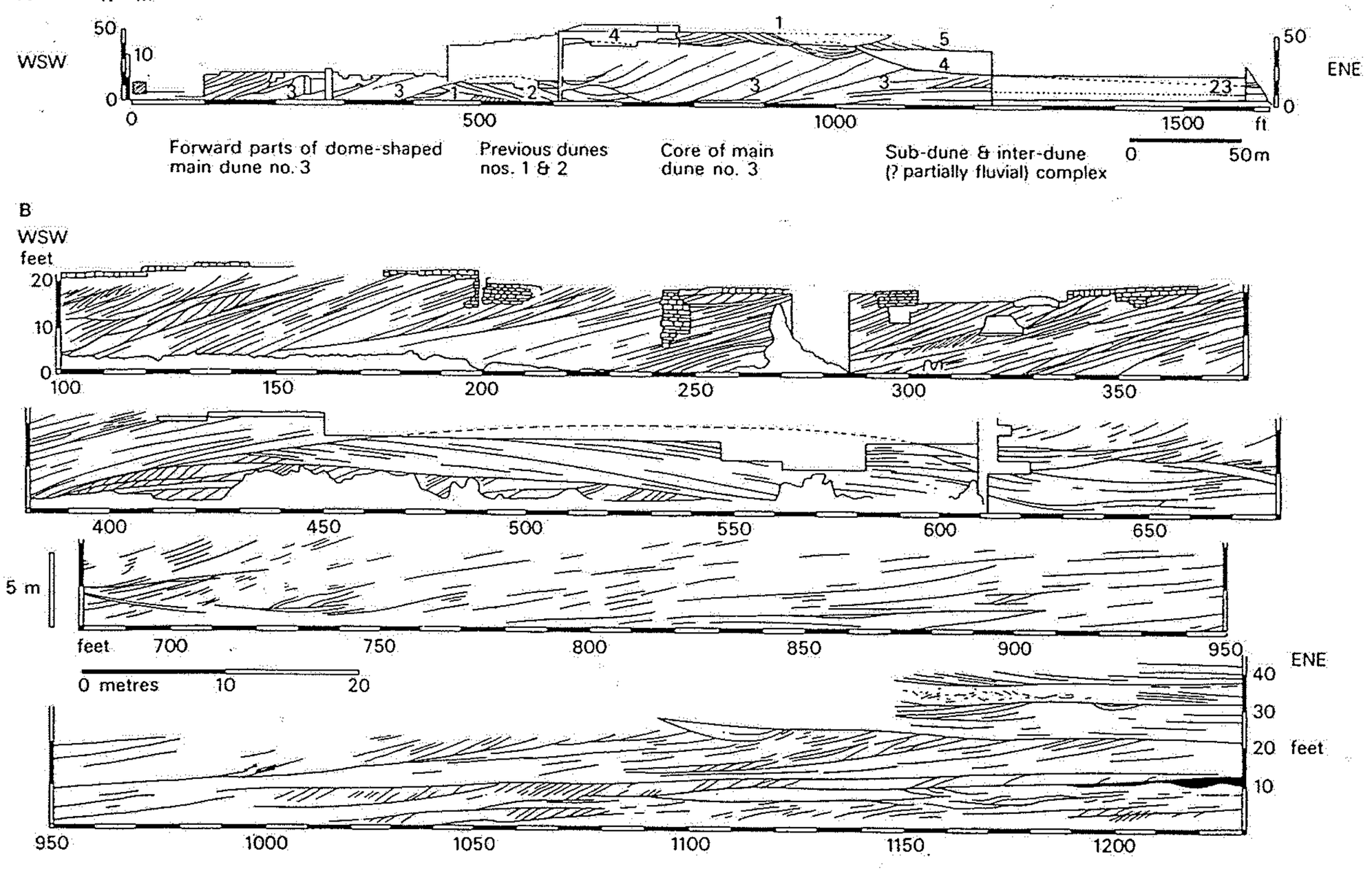

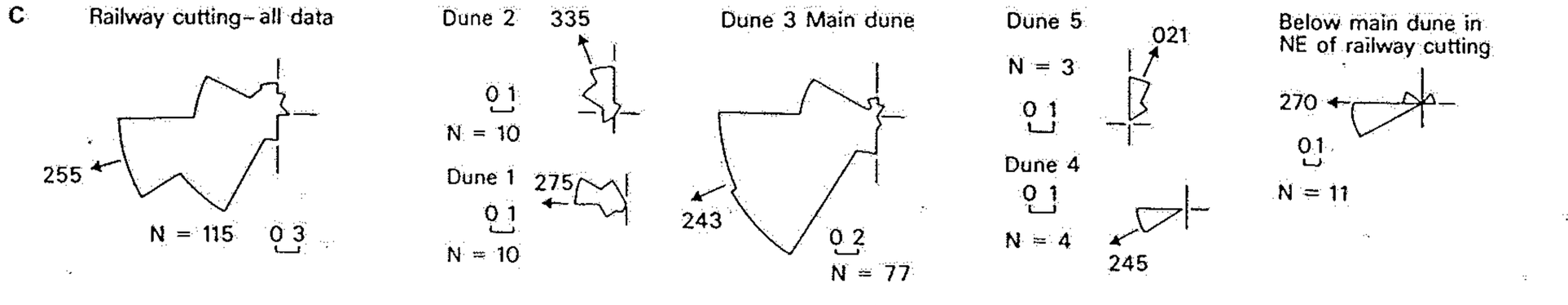

Fig. 5.13. Internal structures in the core of a supposed dome-shaped dune; Triassic, Cheshire, England. A. Shows the broad relationships of the main dune units; B. A more detailed section of the exposures in A; C. Foreset azimuth rose diagrams from each of the main units identified in A (after Thompson, 1969).

Internal Structure of Sand Dunes

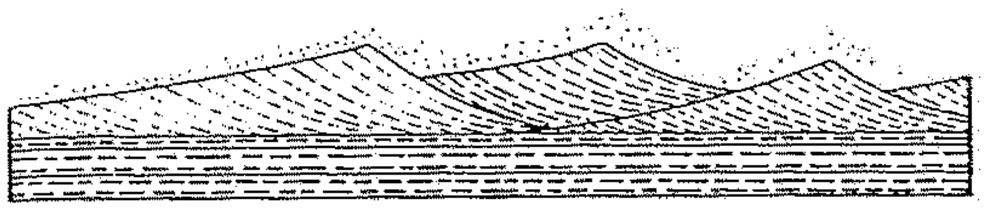

1. Dune sand accumulates on previous level substratum.

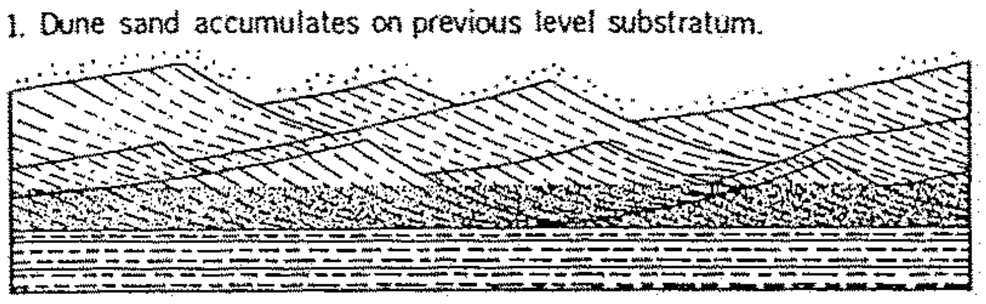

2. Sand accumulation continues, water table rises in sand.

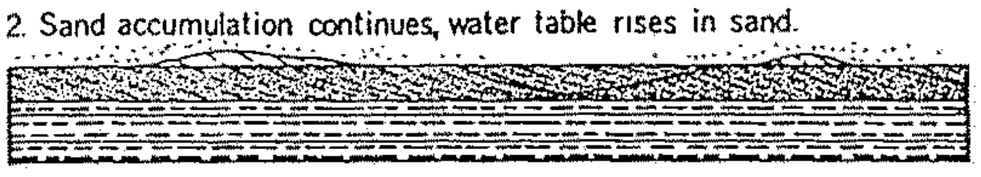

3. Wind action removes sand to water table.

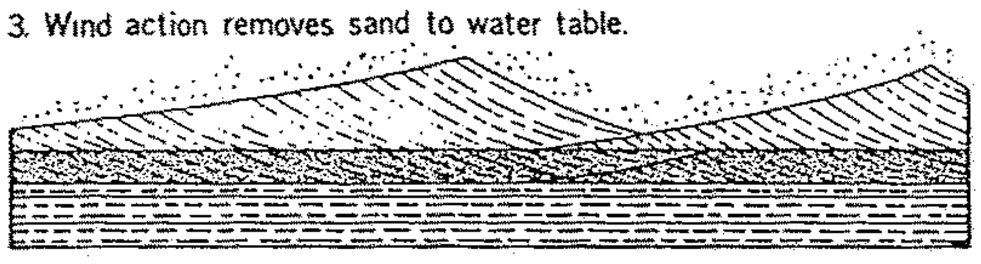

4. Second dune field accumulates on water table surface.

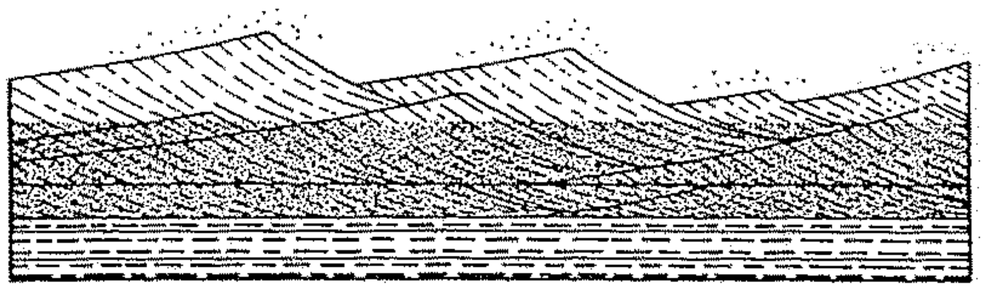

5. Water table rises to new position in dune field.

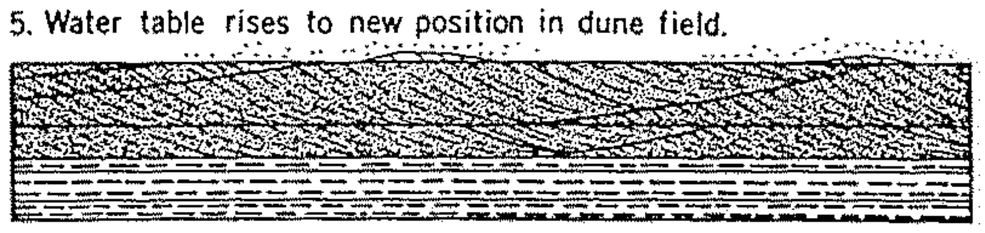

6. Wind action removes sand to second water table.

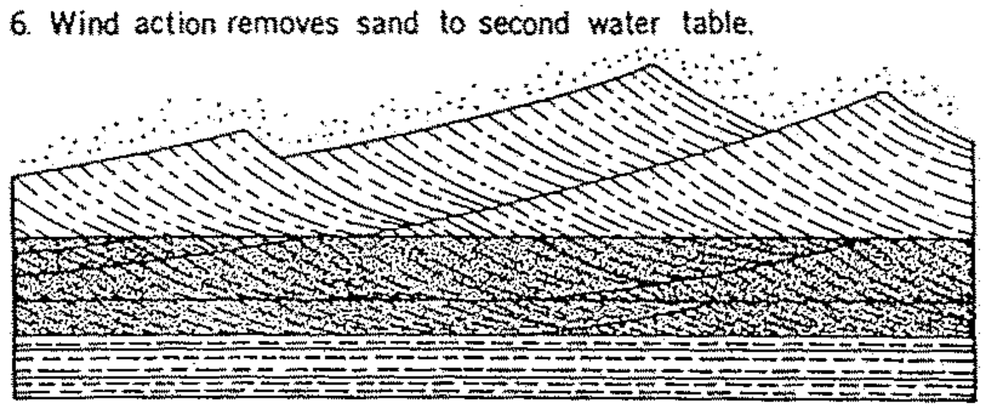

7. Third dune field accumulates, etc.

Fig. 328. Scheme showing horizontal truncation surfaces in a sand dune deposit. (After Stokes 1968)

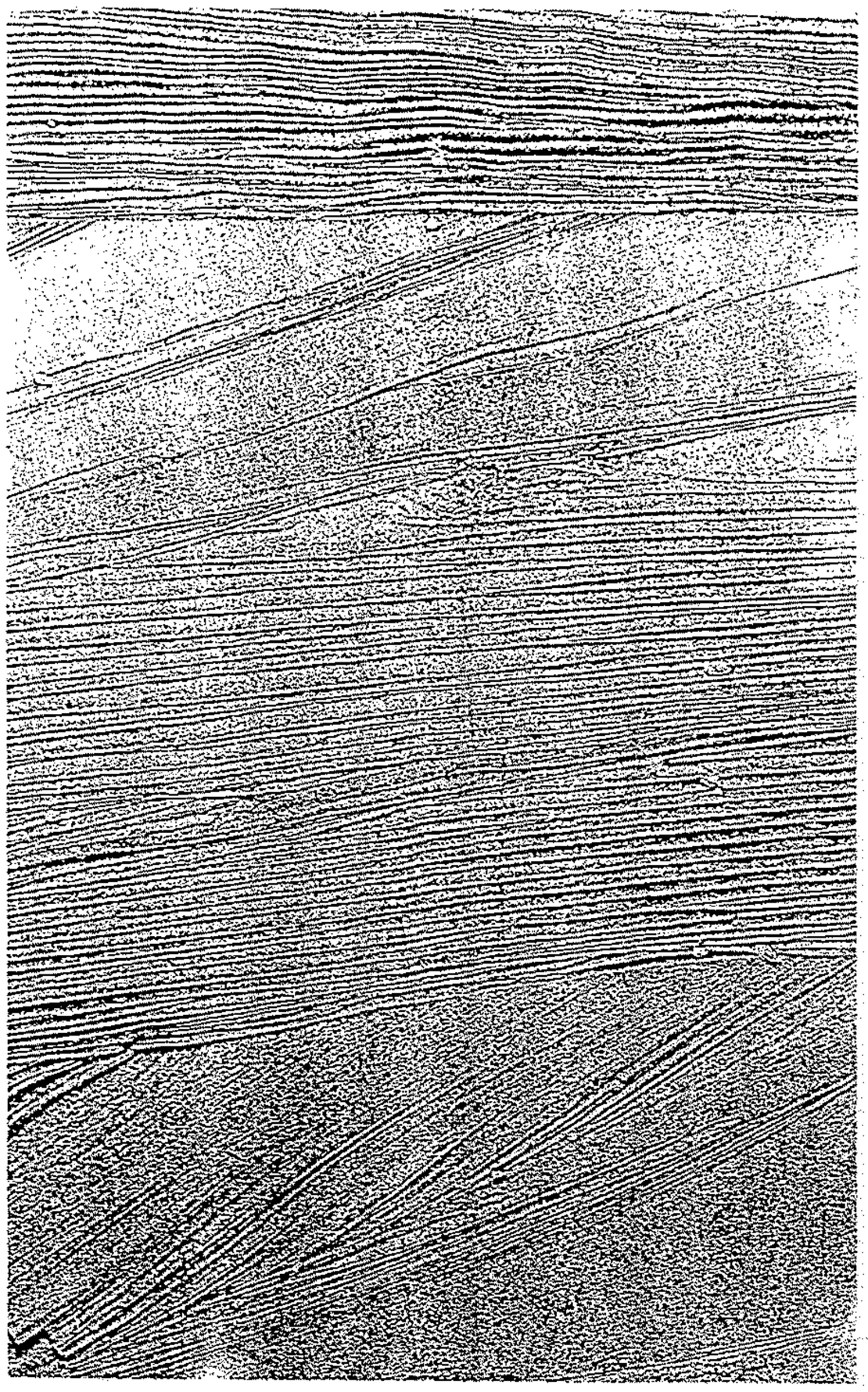

Fig. 349. Bedding features of a sand dune as lacquer peel. Dubai, Trucial coast. (After Glennie 1970)

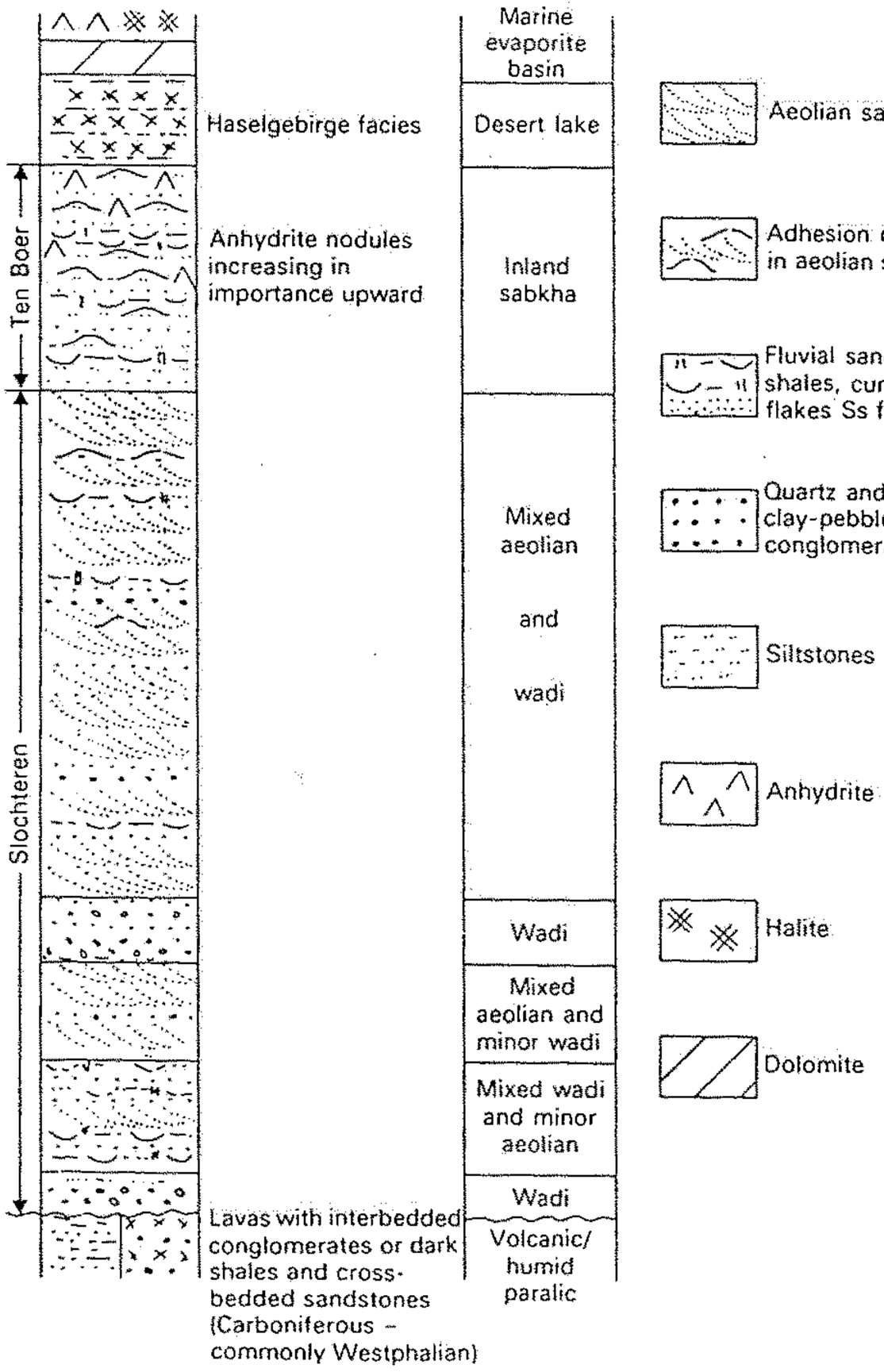

Fig. 5.16. Schematic section of the Upper Rötliegendes in north-west Europe from the south-central Rötliegendes basin. The section is composite and not all facies are present at any one place (after Glennie, 1972).

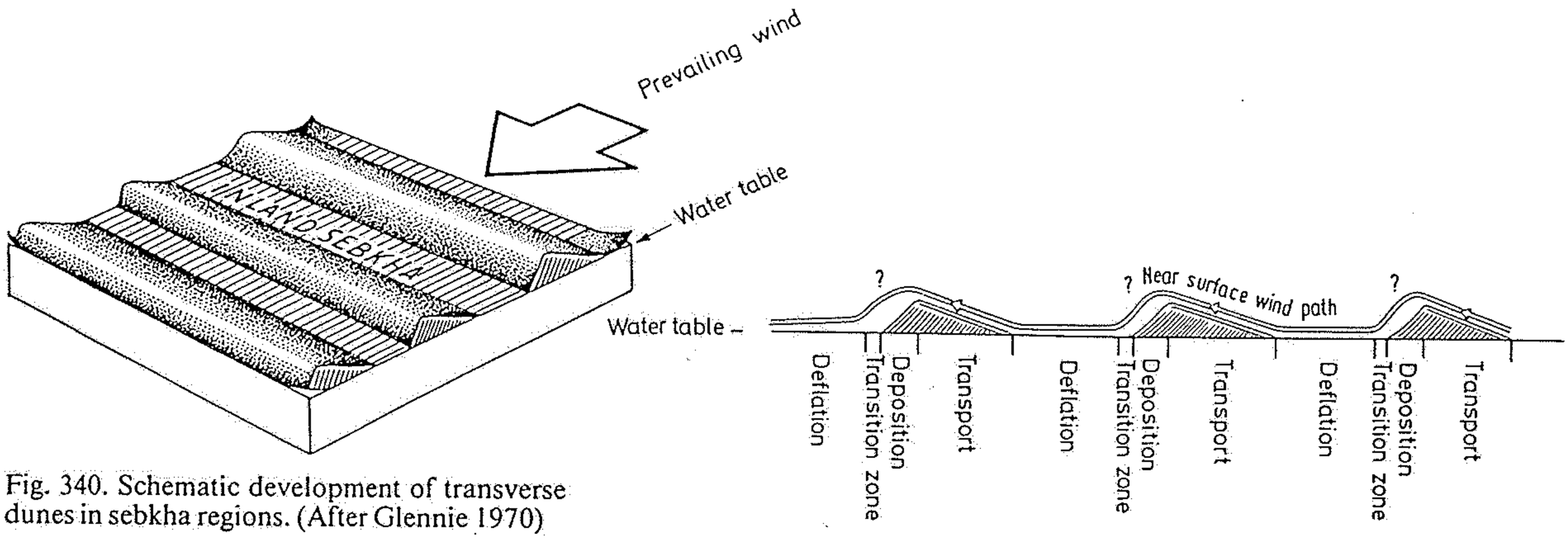

Fig. 340. Schematic development of transverse dunes in sebkha regions. (After Glennie 1970)

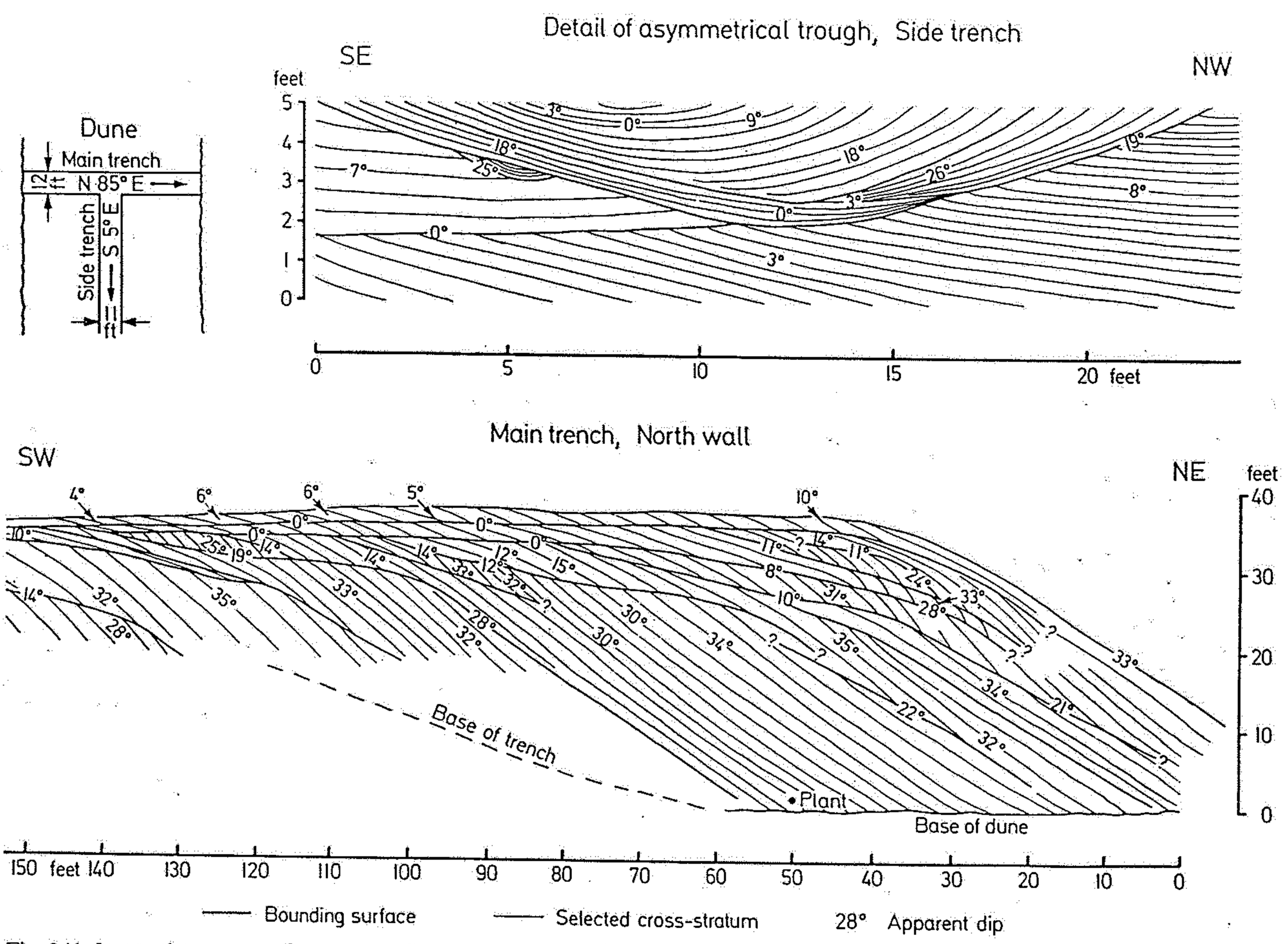

Fig. 341. Internal structure of transverse dunes as seen in sections in various directions. (After McKee 1966b)

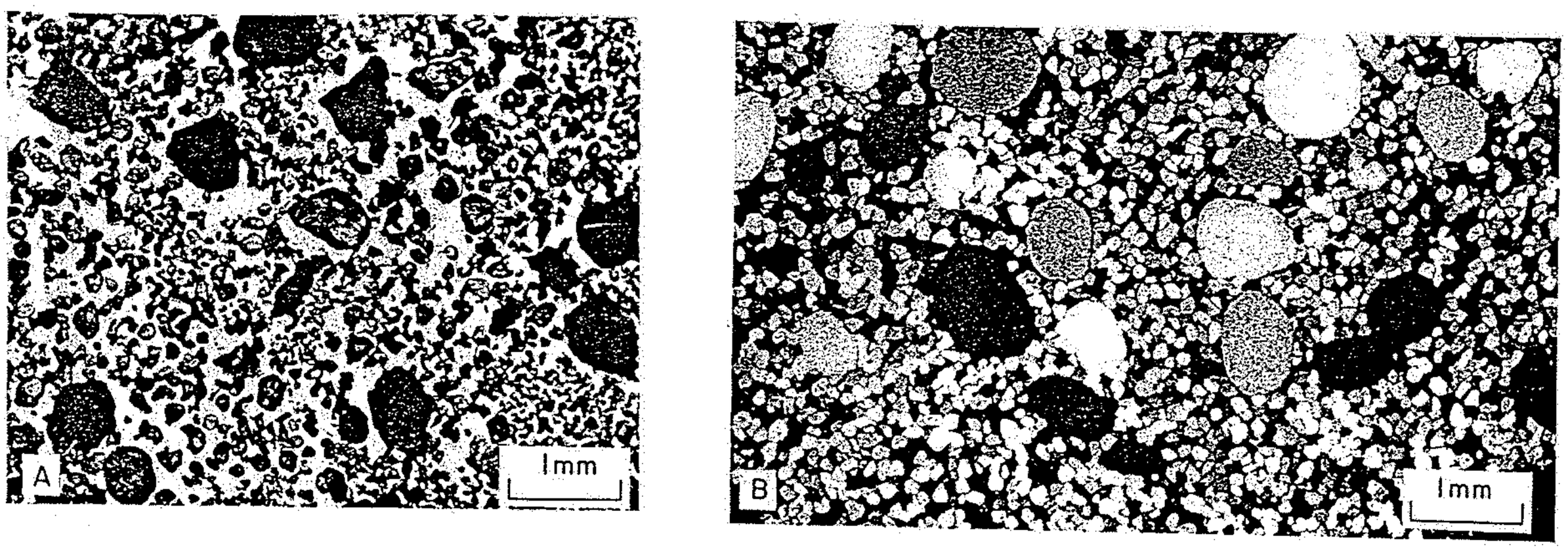

Figure 8-19 *Photomicrographs of modern reg sediment compared with thin-section view of sandstone inferred to be an ancient reg.*

A. *View through binocular microscope in ordinary light coming from below of particles of modern reg, one particle layer thick, Simpson Desert, Australia, collected by pressing a piece of Scotch tape against the ground surface.*

B. *View in plane-polarized light of thin section cut from specimen of Lander Sandstone (Ordovician), Wyoming, United States. (R. L. Folk, 1968; A, Fig. 4, p. 16; B, Fig. 1, p. 10.)*

Fig. 333. Complex barchan dunes, Sudan (After Solle 1966)

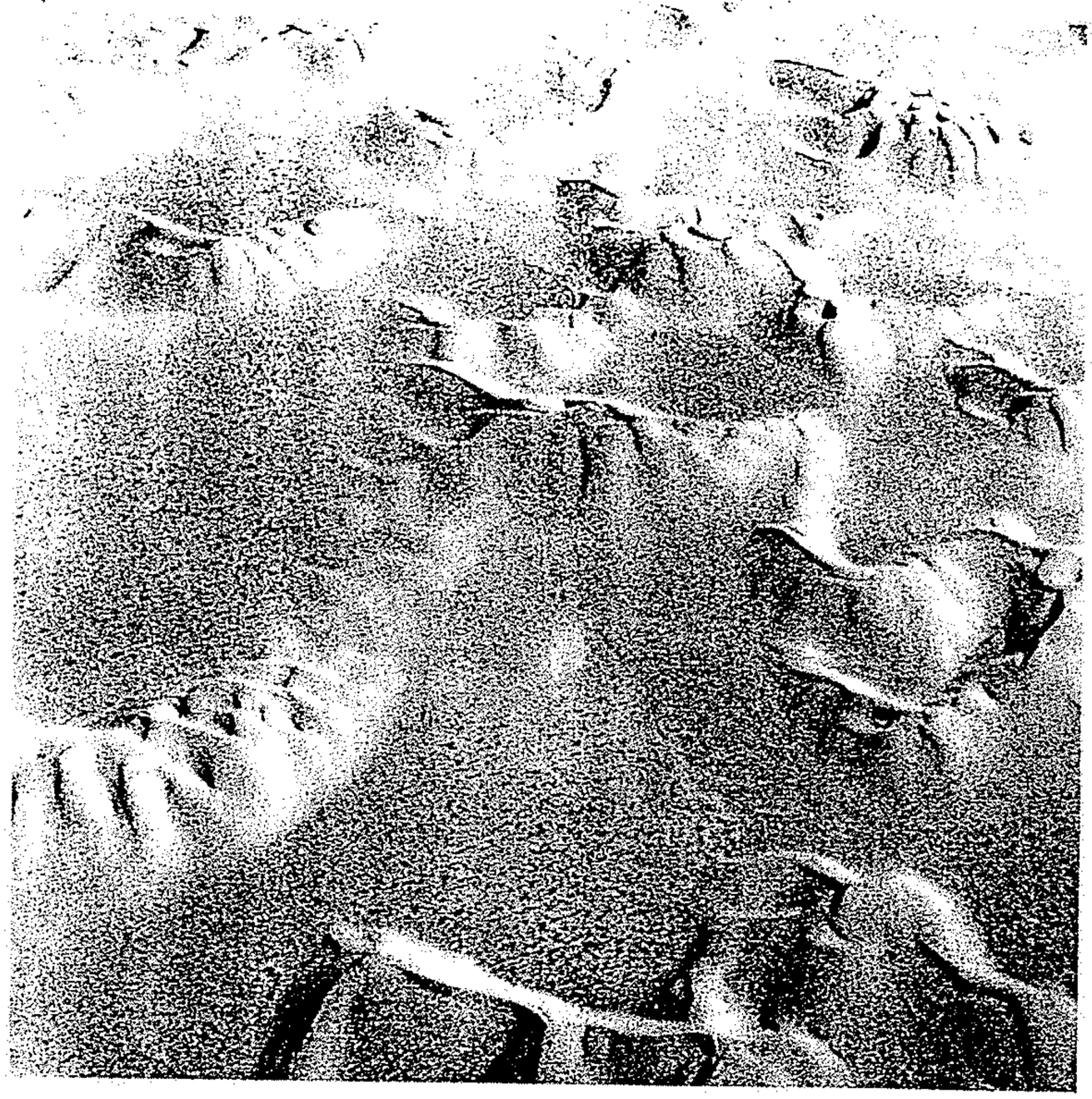

17.18 These shoreline dunes form complex patterns behind the beach at Coos Bay, Oregon. The beach serves as a source of sand, and this source is continuously renewed by longshore currents of ocean water. Onshore winds (from the left) drive the beach sand inland. The photograph shows about 450 m of shoreline.

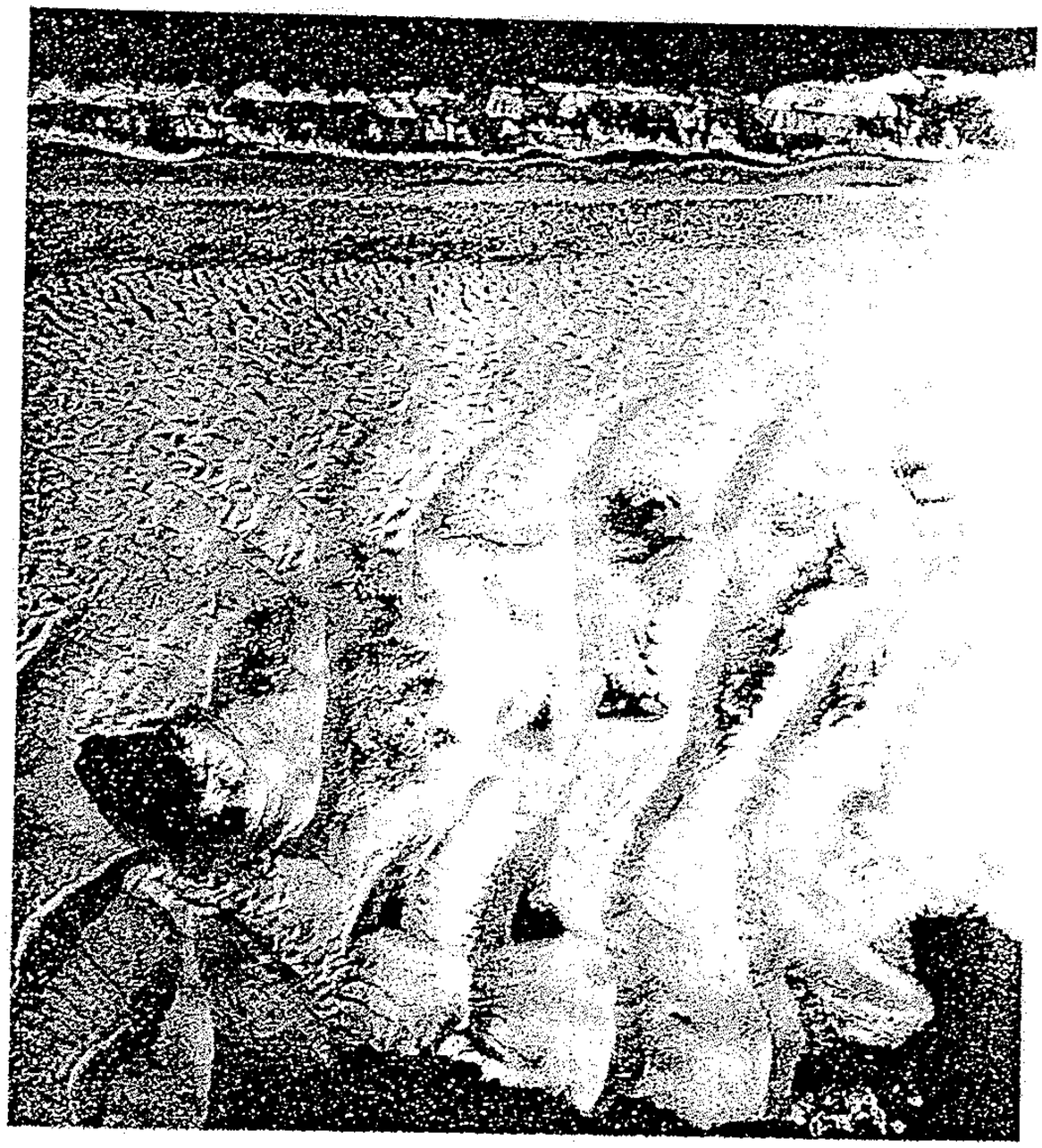

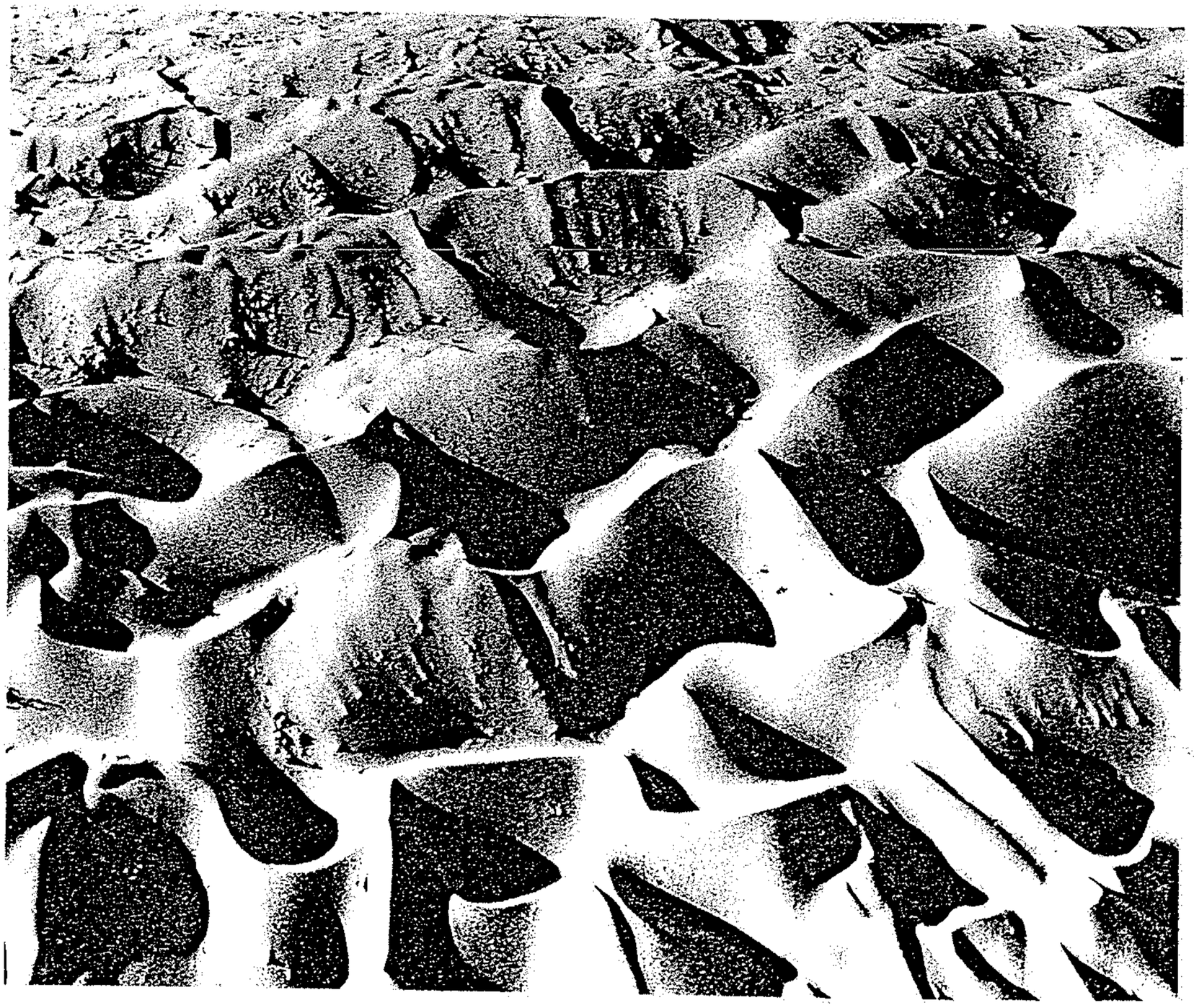

Figure 9-27

Aerial photograph of transverse dunes on the Saudi Arabian desert, aligned in a general direction at right angles to the prevailing wind direction. [From Arabian American Oil Co.]

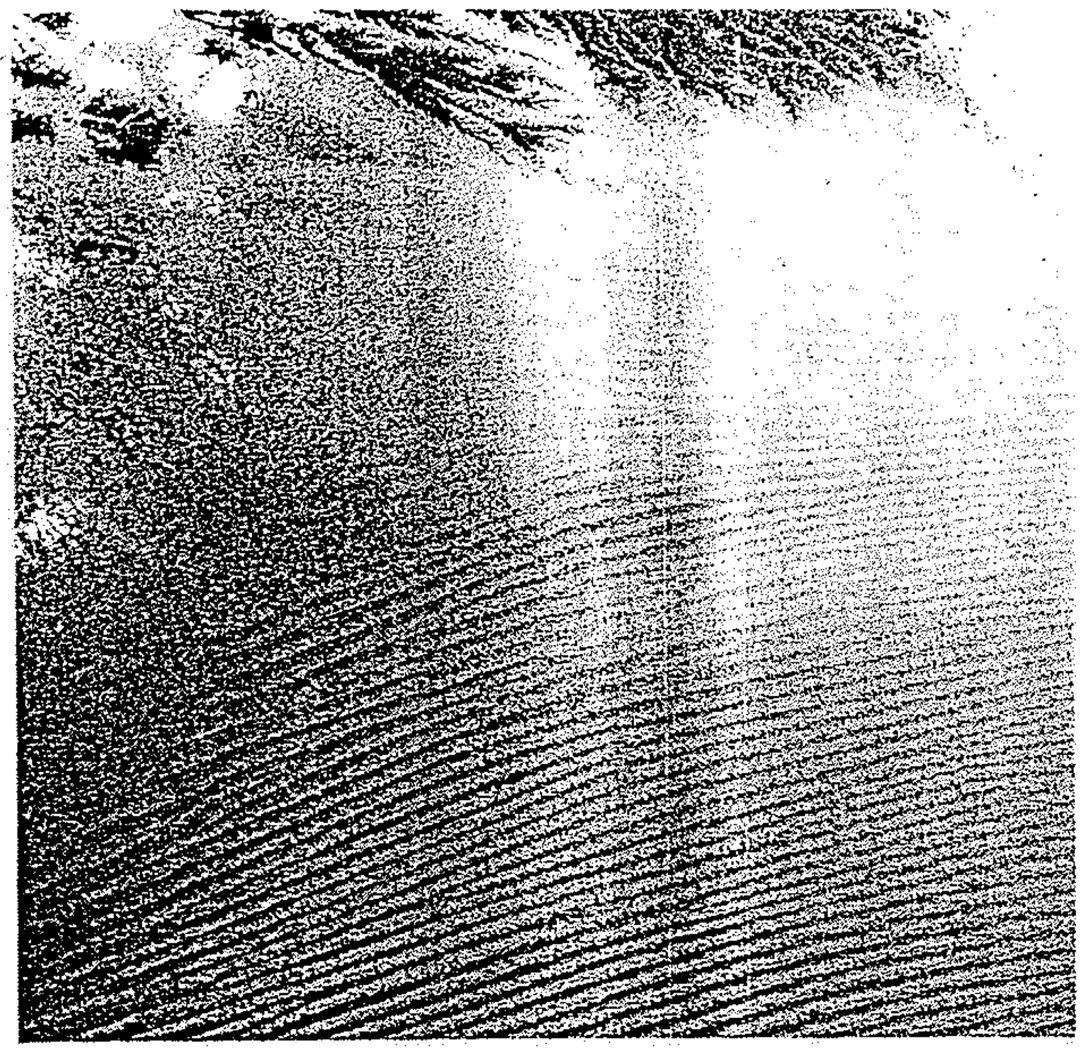

(a)

(b)

Figure 9-28

Longitudinal dunes parallel to the prevailing wind direction in the Saudi Arabian desert. Photograph (a) is a view of the dunes as seen from the great height of a satellite (Gemini IV); (b) is a low-altitude airplane photograph. [From Arabian American Oil Co.]

17.20 This transverse dune in the Sahara Desert south of the Atlas Mountains is nearly 1 km wide. Its surface exhibits a complex pattern characteristic of many smaller dunes. [U.S. Army Air Corps.]

17.21 These barchans are moving across the Pampa de Islay, Peru, in the direction in which their horns point. [Aerial Explorations, Inc.]

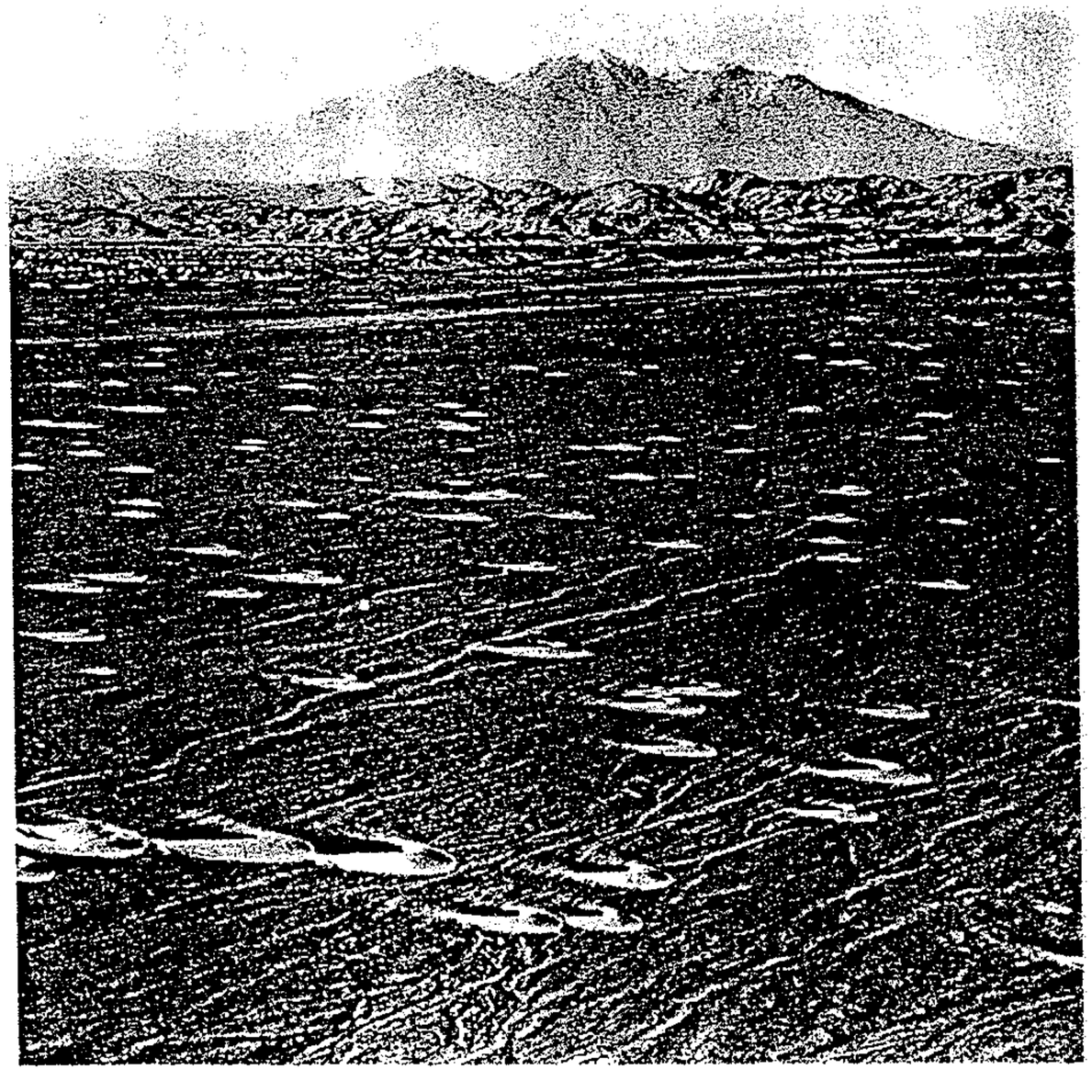

Fig. 302. A general view of a desert environment showing bare rocks and wadi systems. Coarse-grained debris usually accumulates near the exposed rocks. Sudan (After Solle 1966)

Fig. 319. Deposition of sand behind an obstacle, making a sand drift deposit. (After Gripp 1968)

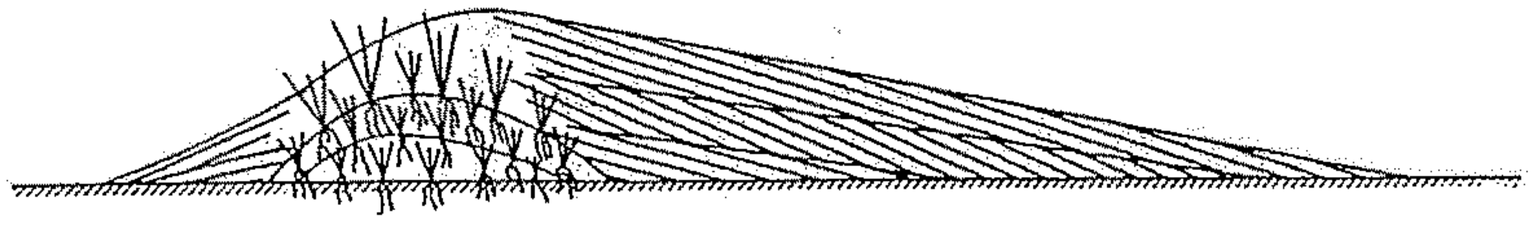

Fig. 320. Scheme showing cross-bedding developed in sand drift deposits

Figure 9-15

Death Valley, California, a desert playa. Surrounded by mountains and filled with debris from them, playas are intermittently occupied by lakes. The light-colored areas are salts, deposited by a Pleistocene lake. The lower slopes of alluvial fans grade into mudflats at the borders of the playa. [Photo by H. E. Malde, U.S. Geological Survey. Courtesy of C. B. Hunt.]

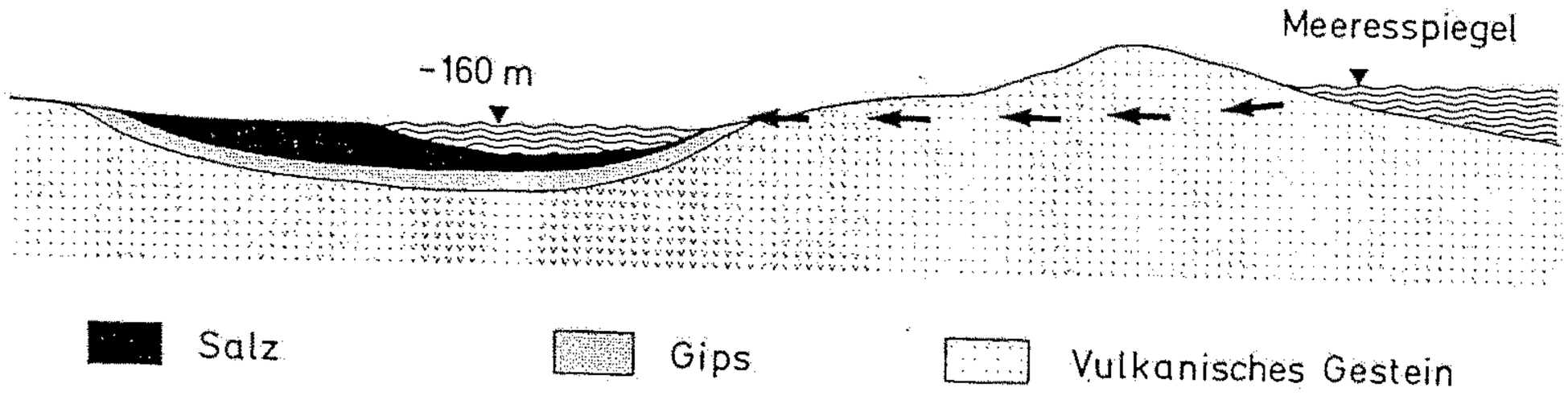

Abb. 47 Profil durch das Gebiet des Assalsees. Franz.-Somali. Maßstab 1 : 200 000, sechsfach überhöht (nach *M. Dégoutin*)
Der schwerer lösliche Gips scheidet sich näher, das leichter lösliche Steinsalz ferner der Einsickerungsstelle aus

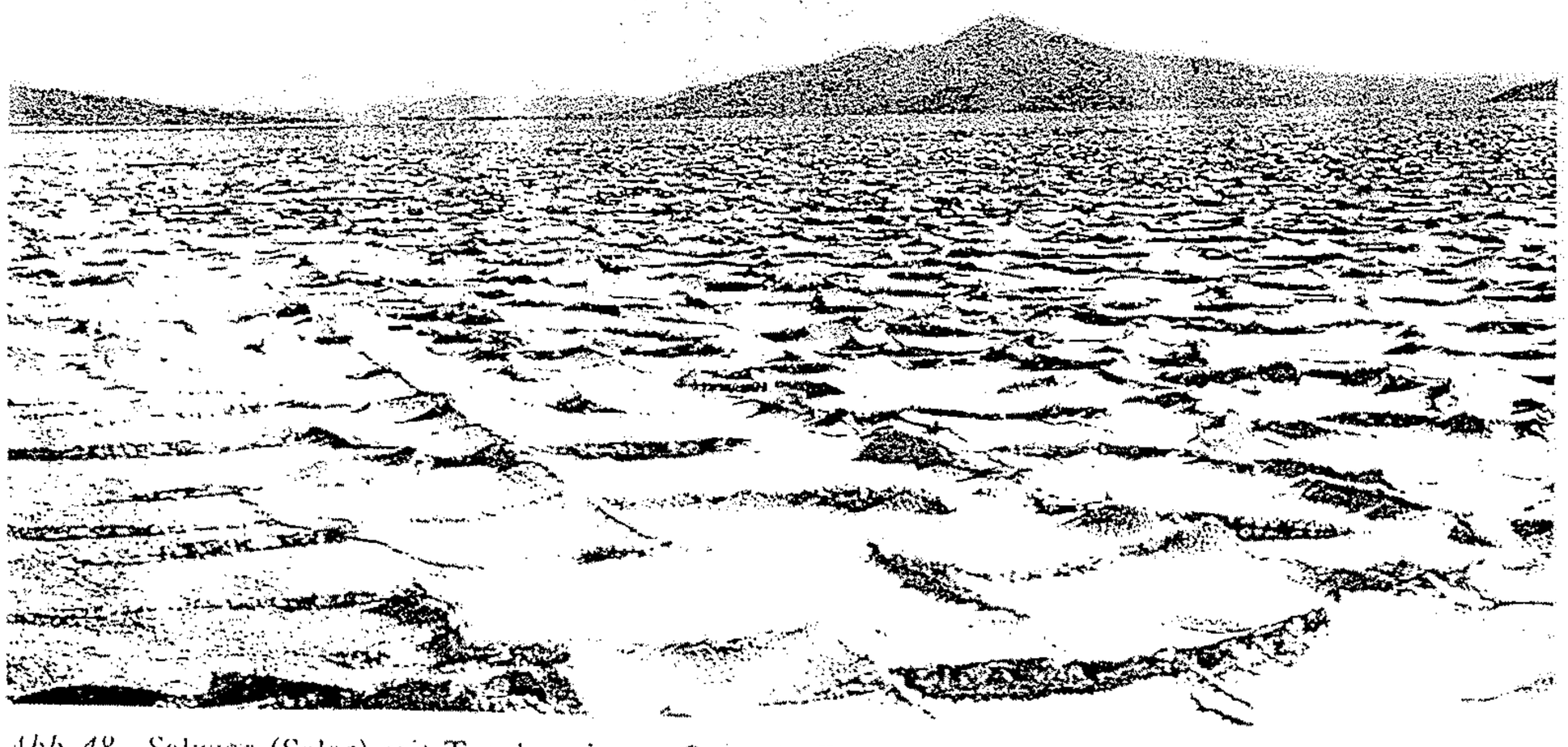

Abb. 48 Salzsee (Salar) mit Trockenrissen. Salar de Empexa, Bolivien

13. Sequence of the Al Jir Formation (limestone facies) — Az Zahrah fault. Qárat ar Reqúbah. Photo B. Záruba.

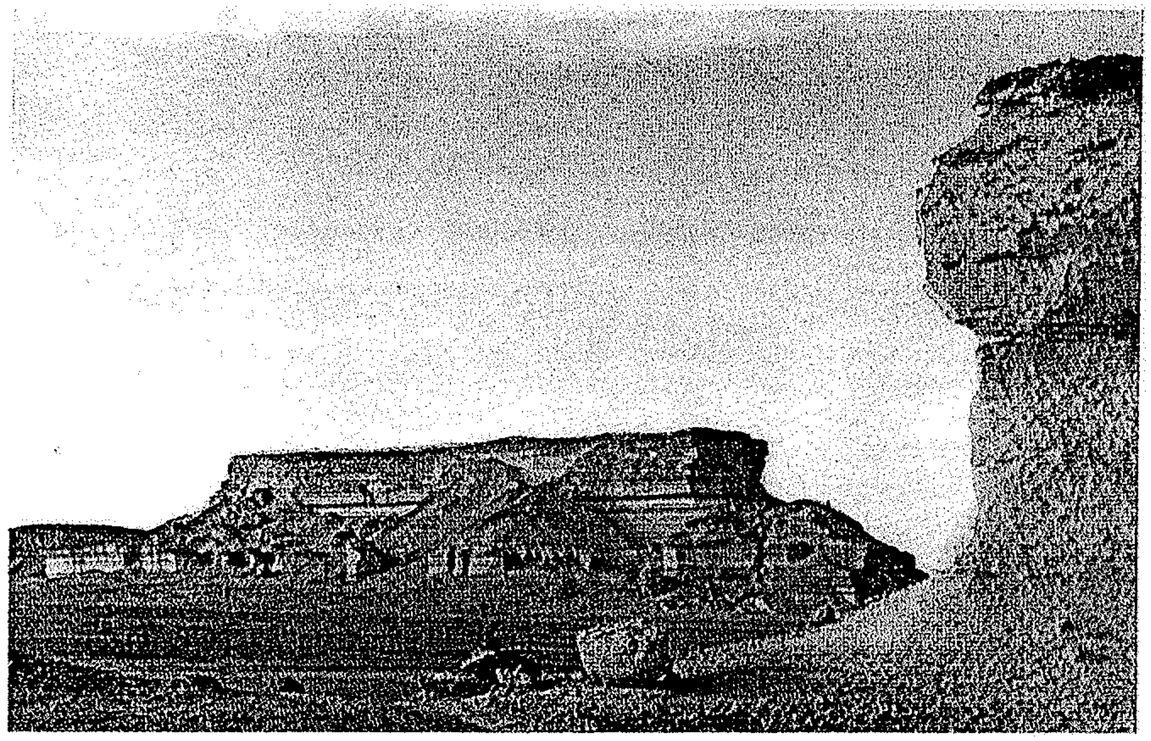

14. Al Gata Member (lower part of the residual hill) is overlain by the Thmed al Qusúr Member. Qarárat Umm Lidám. Photo J. Veselý.

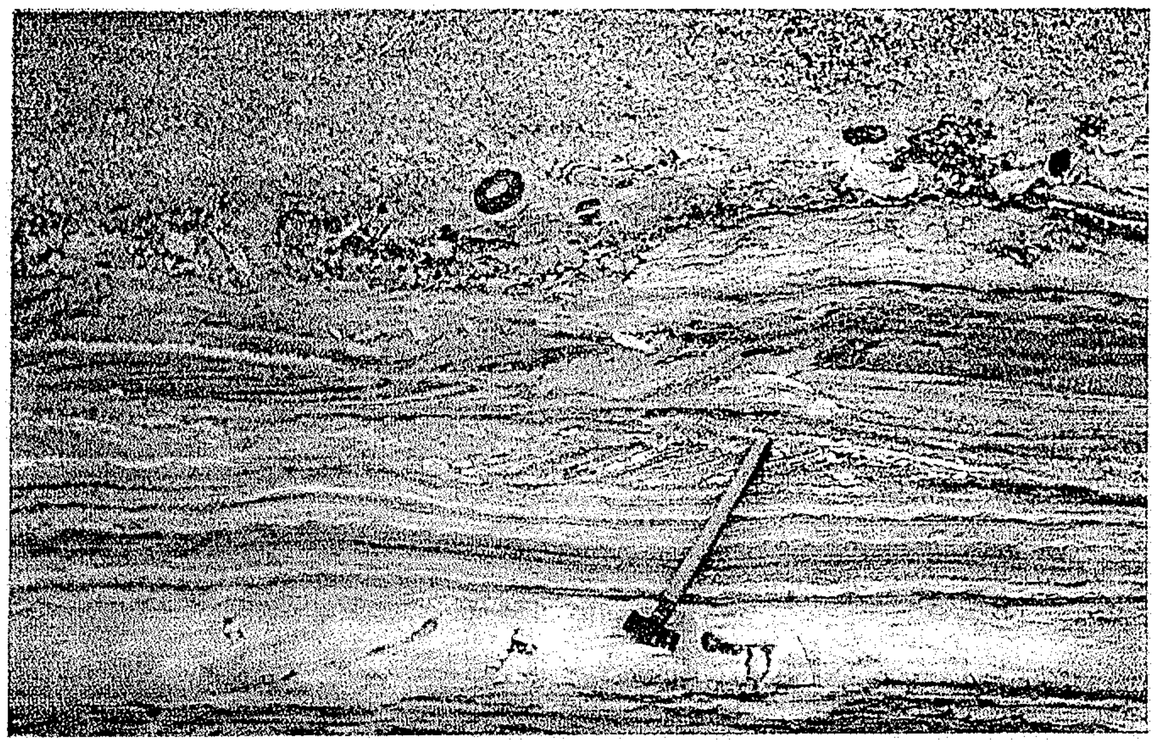

15. Continental and transitional marine deposits (crossbedded sandstone overlain by conglomerate), Oligocene. 7 km SE of Zallah. Photo J. Veselý.

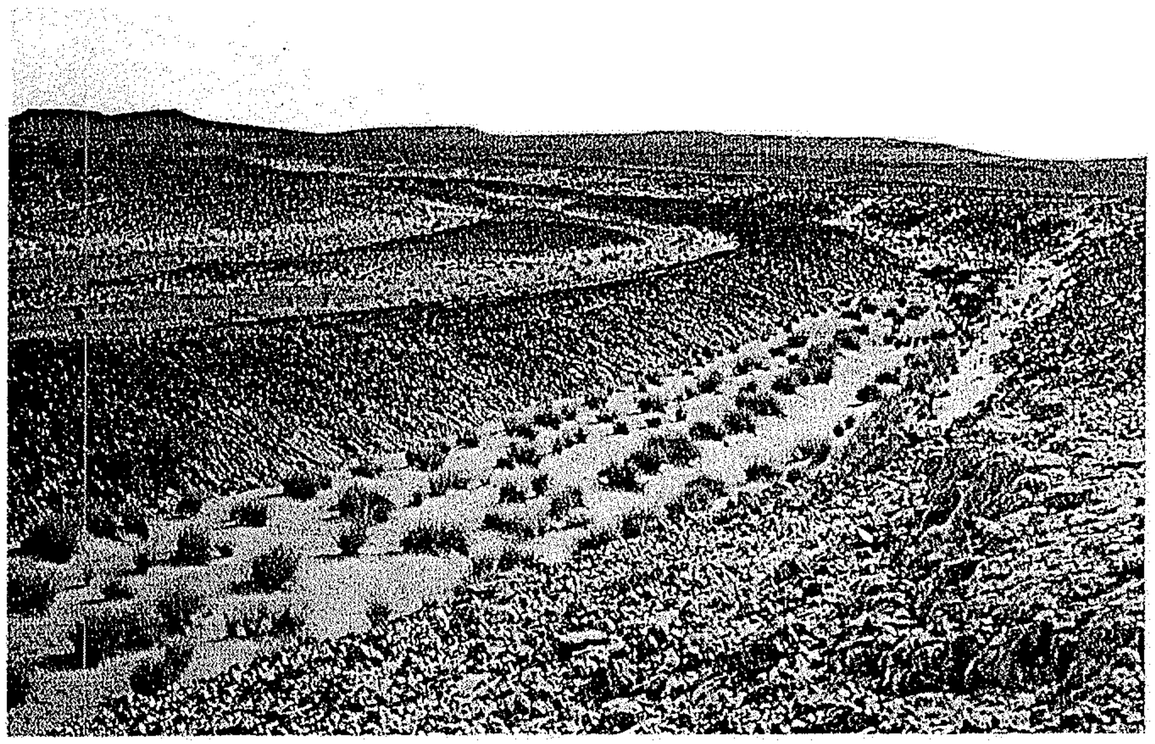

16. Basalt flow type f2 filling a paleowádí north of Ra's al Abyad. Photo B. Záruba.

Staré tamaryšky si vytvořily kolem své kořenové soustavy vrstvu humusu, která celý keř uchránila v době odvátí okolního sypkého materiálu. Tyto kopcovité útvary mají své vlastní označení — nebky ▶

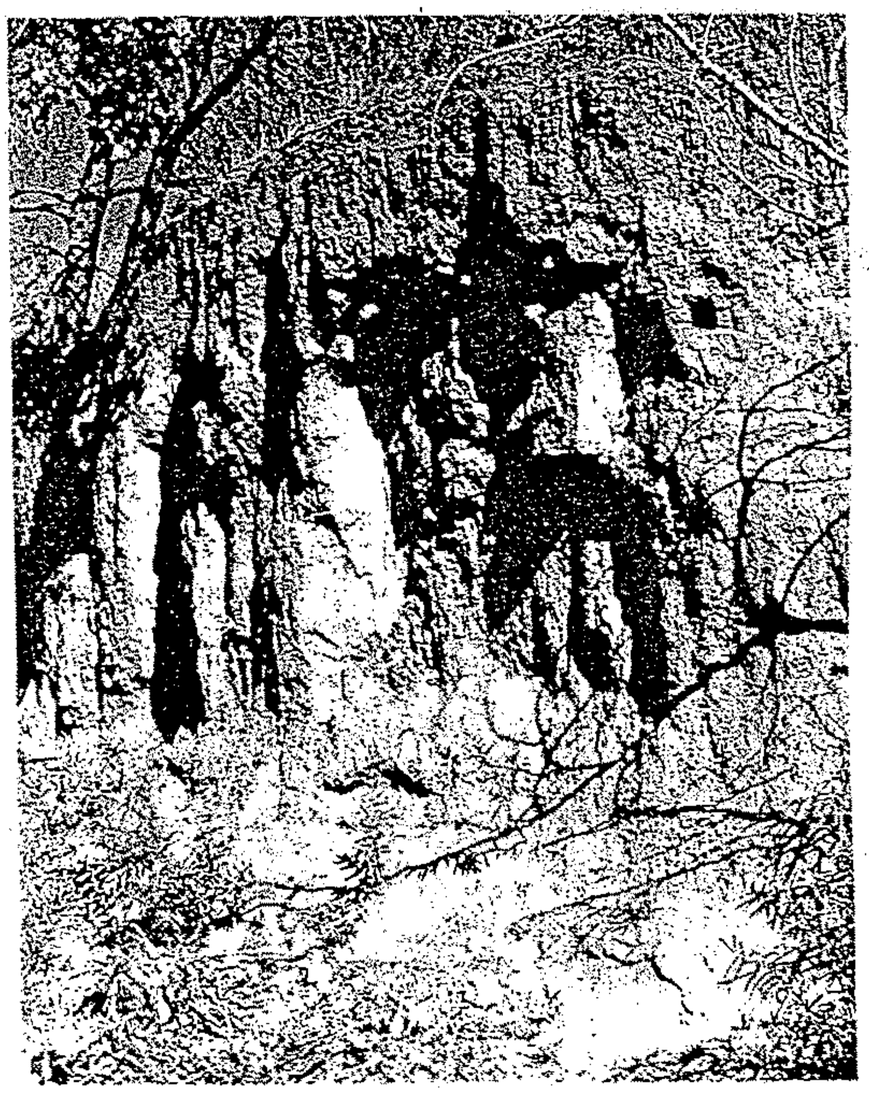

Figure 9-29

Pleistocene loess, showing prismatic jointing, in Colorado. [Photo by H. E. Malde, U.S. Geological Survey.]

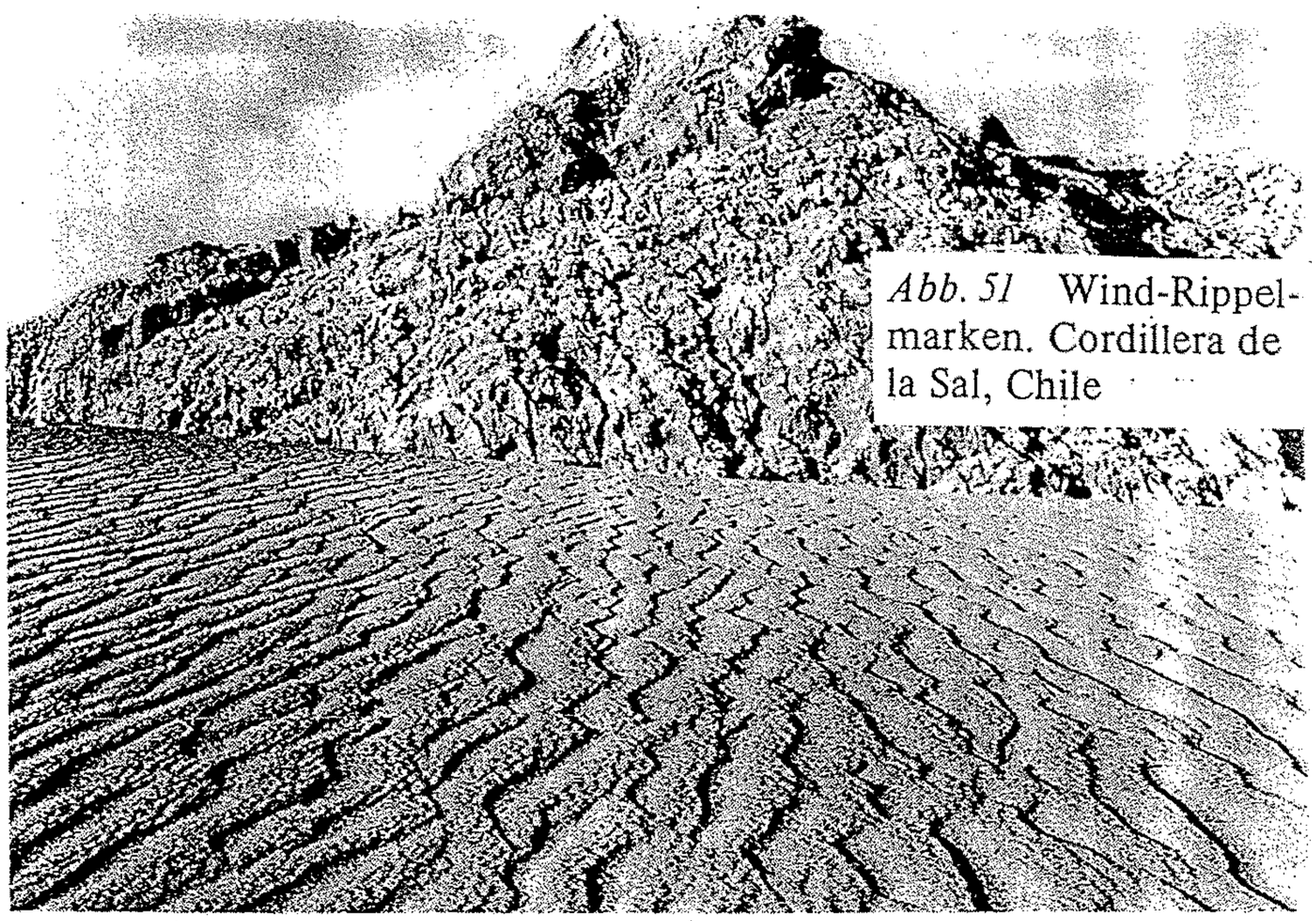

Abb. 51 Wind-Rippelmarken. Cordillera de la Sal, Chile

Figure 3

Set of low angle cross bedding showing asymptotic passage of foresets into bottomsets. Note length and thickness of bottomsets: exposed thickness of set about 2m. White Rim Sandstone (Permian, Utah).

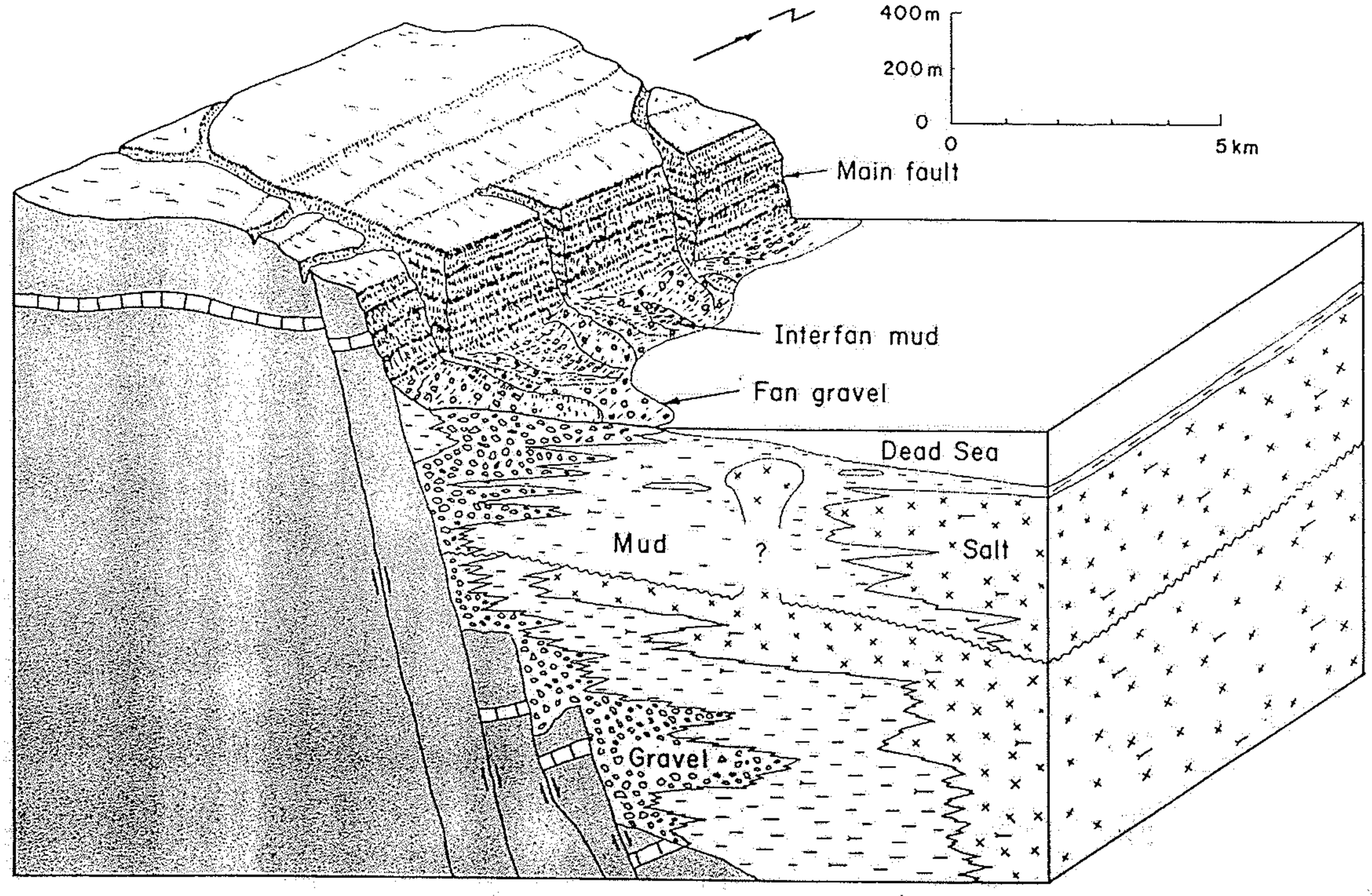

Figure 8-11 *Schematic block diagram between Judaean Mountains and Dead Sea, Israel, showing partial view of sediment filling of graben. Proximal fans consist of gravel; and distal fans, of interbedded gravel and muds (Fig. 4-3, A). Center of basin is occupied by lake muds and salts. (Modified from Y. Langozky,* in *Y. Langozky and A. Sneh, 1966, Fig. 2, p. 9.)*

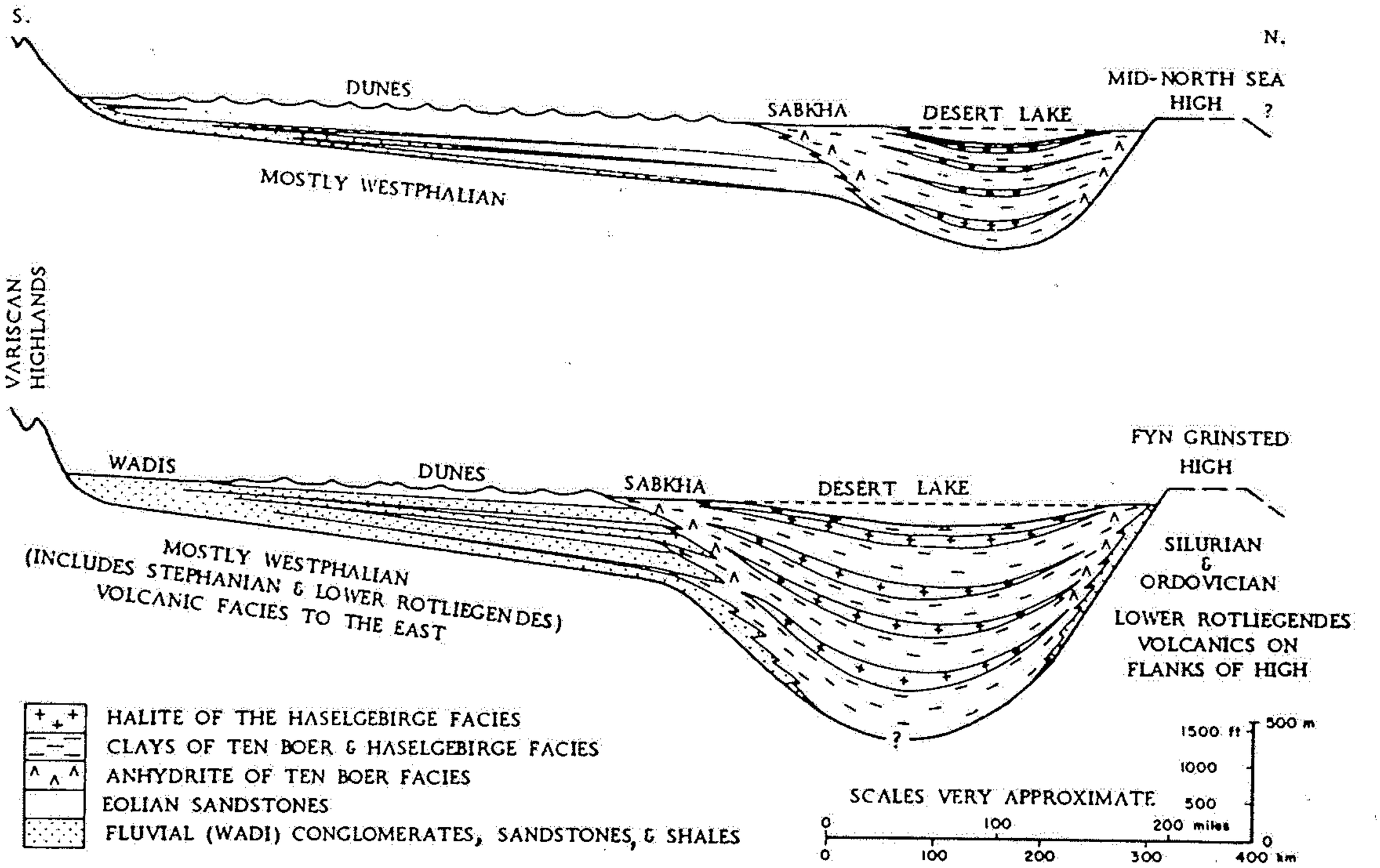

Figure 8-34 *Conceptual cross sections through Permian Rotliegendes Basin in southern North Sea and eastern Netherlands just prior to Zechstein (Permian) transgression. Interfingering products of several depositional environments are indicated. (K. W. Glennie, 1972, Fig. 17, p. 1067.)*

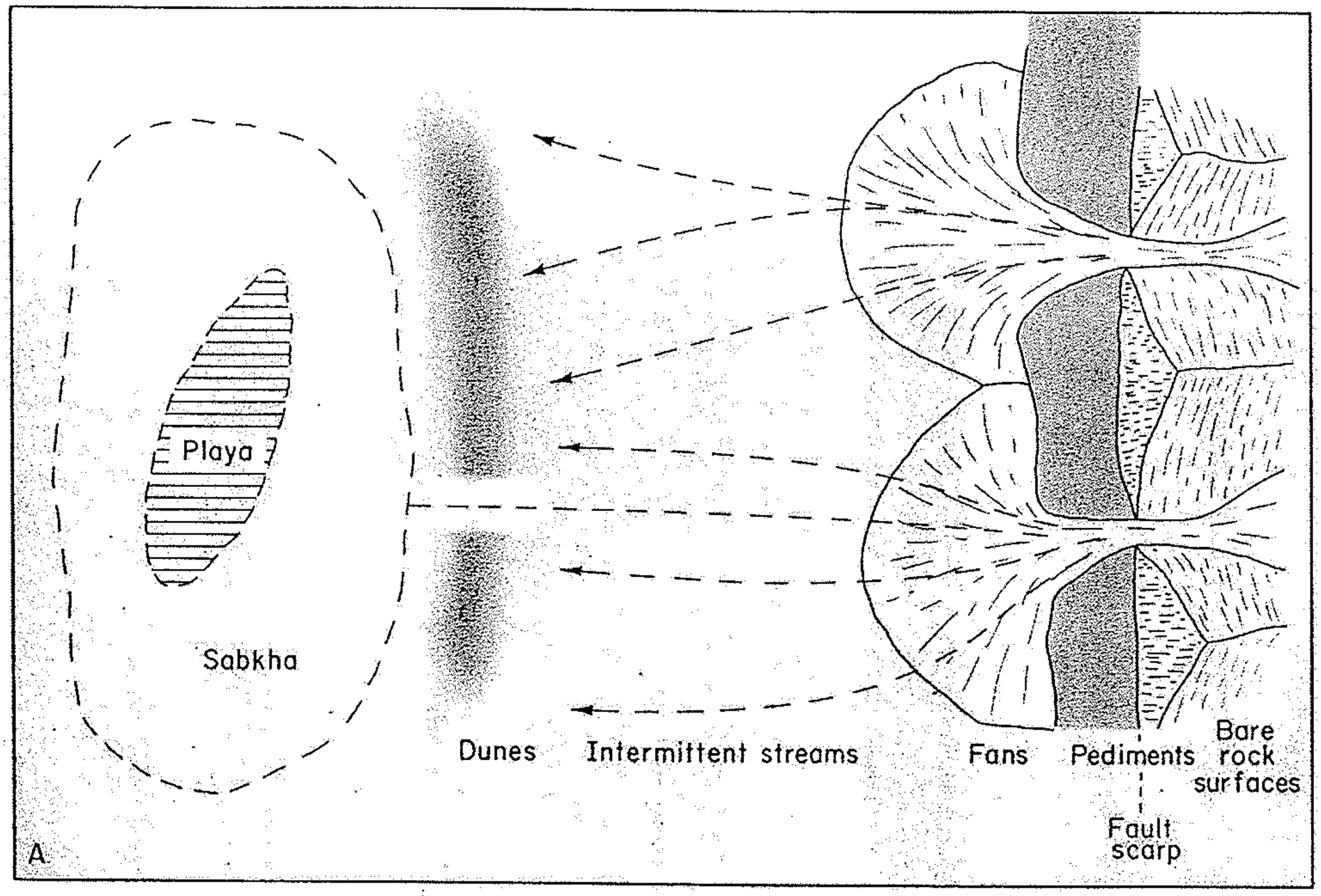

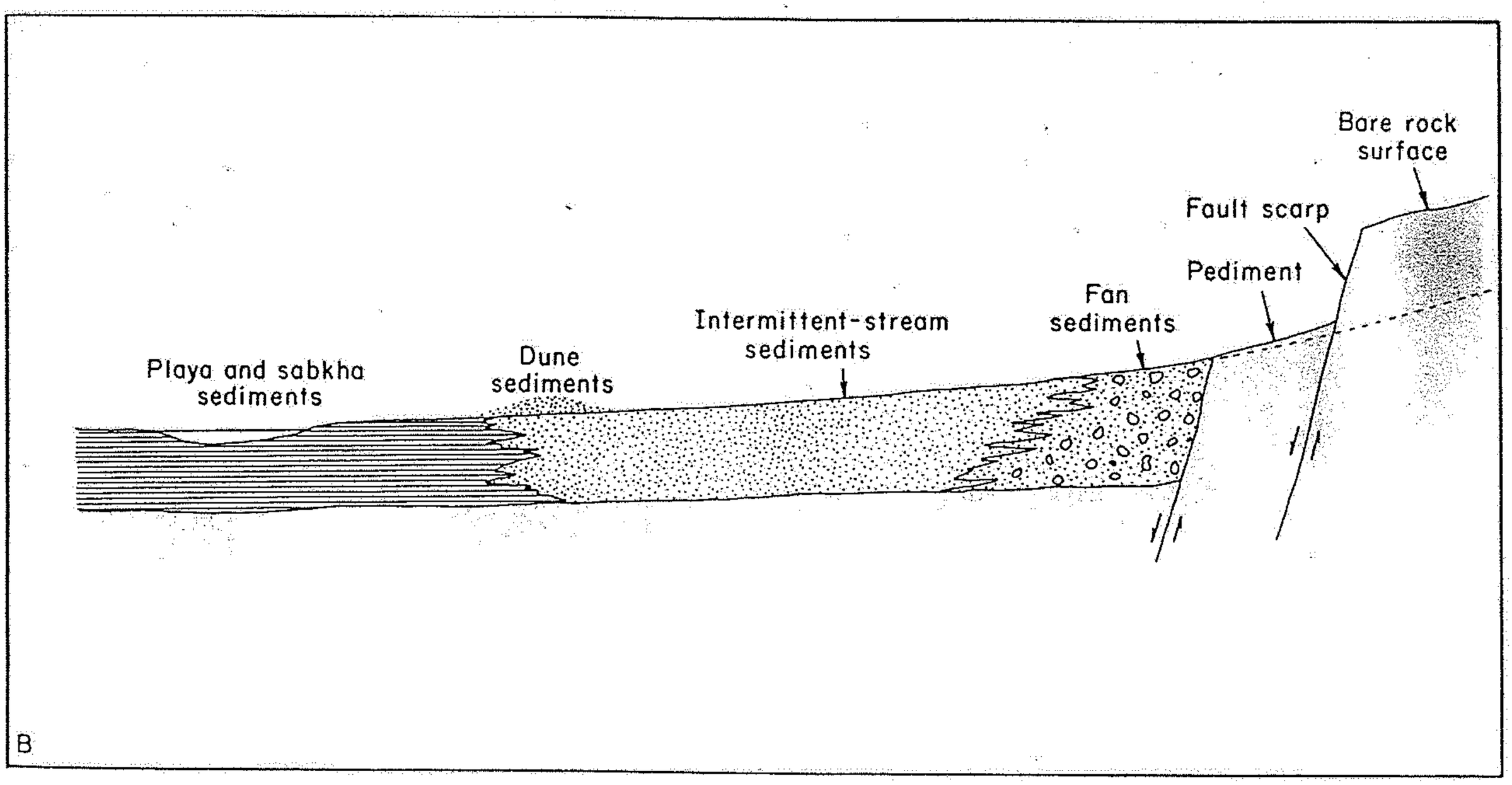

Figure 8-5 *Schematic view of map and section of sedimentary environments in a desert basin adjoining a steep mountain block.*

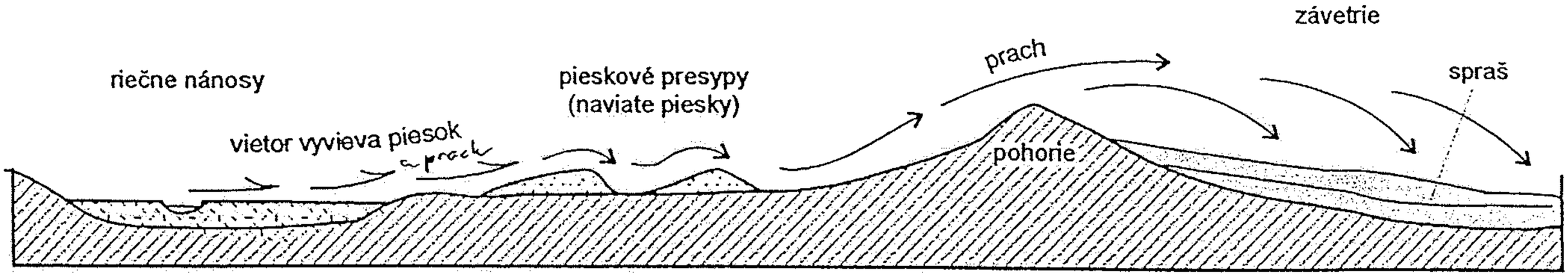

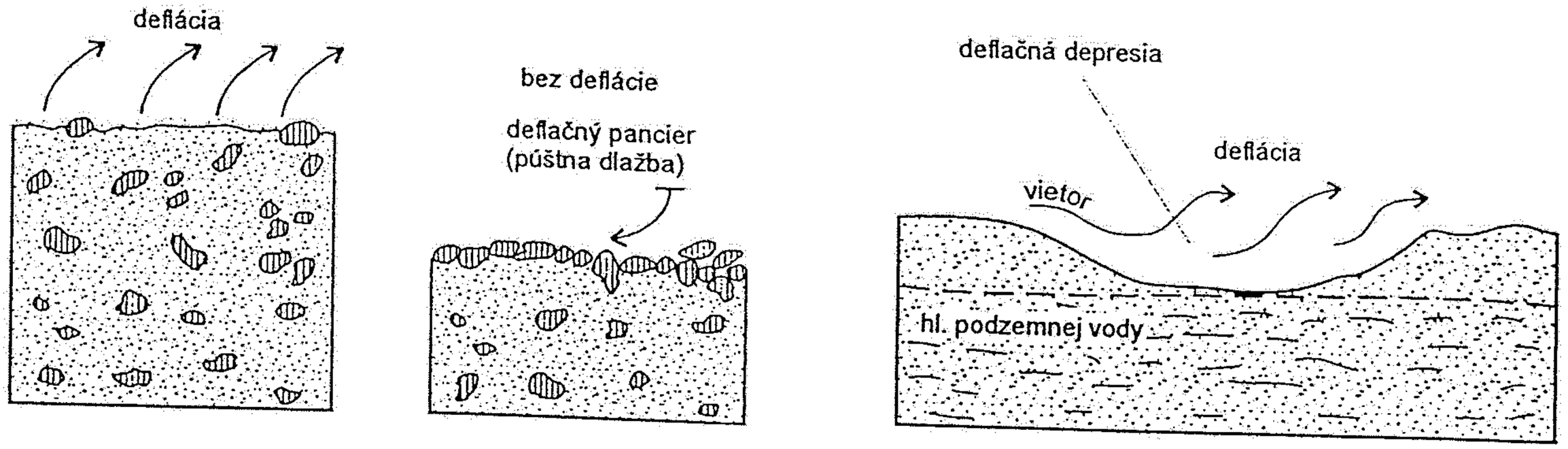

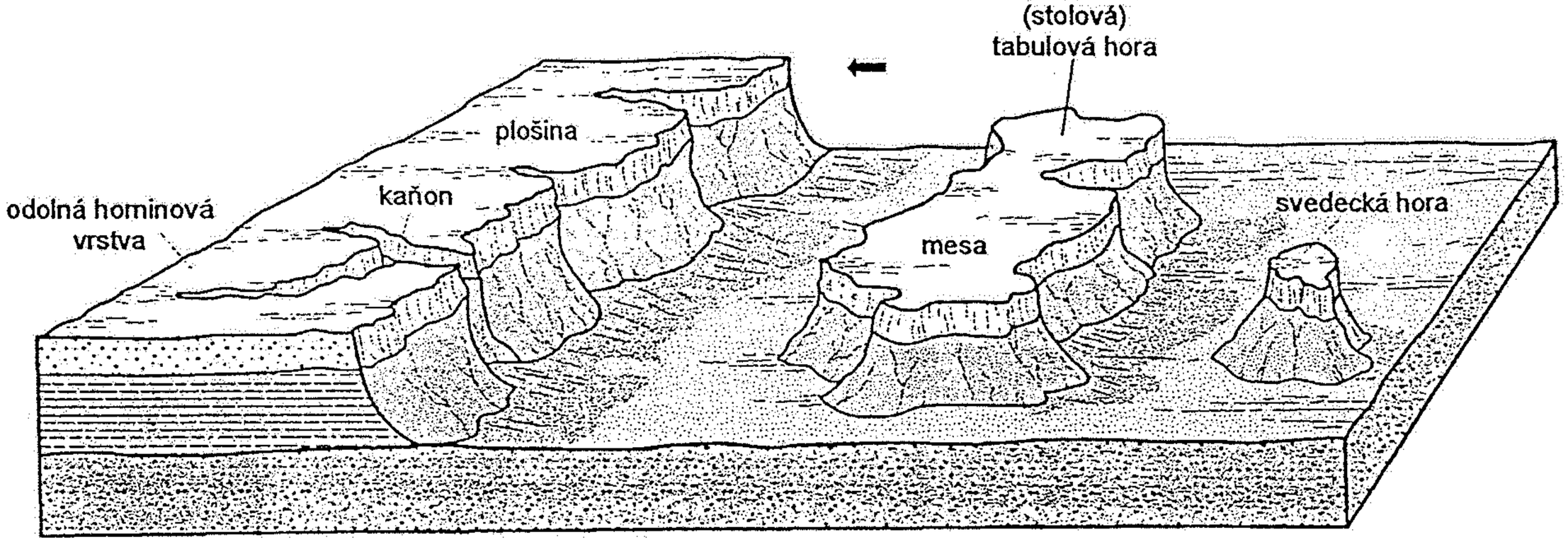

20.13 Vetrom modelovaná krajina

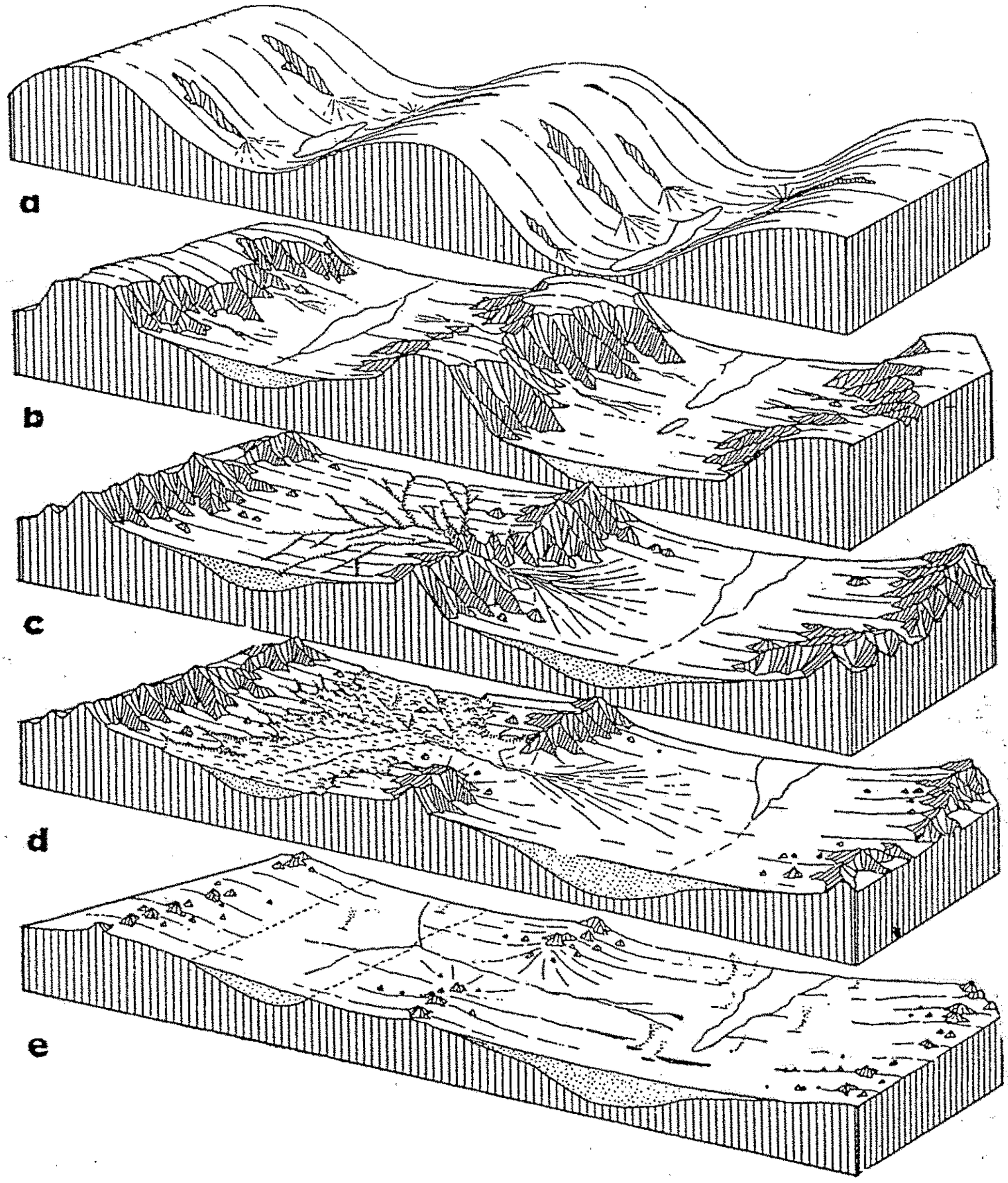

Obr. 114. *Schematické znázornění erosivního cyklu v aridní oblasti.*
(Podle R. F. Flinta.)

a) *Počáteční stadium: Horské hřbety jsou odděleny korytovitými kotlinami; přívalové vody vyrývají ve svazích rýhy, při jejichž vyústění do kotlin se tvoří dejekční kužele drti; v kotlinách vznikají bezodtoká jezera — playas.*

b) *Stadium mladosti: Horské hřbety jsou erosí značně rozryty, kotliny se zaplňují horninovou drtí.*

c) *Stadium zralosti: Nižší (pravá) kotlina stává se erosivní základnou kotliny vyšší (levé) a načepovává ji.*

d) *Stadium pozdní zralosti: Povrchové vody odtékající z vyšší (levé) kotliny do kotliny nižší (pravé) rozrývají nánosy vyplňující vyšší kotlinu četnými rýhami a vytvářejí v nich krajinný typ zvaný Bad Lands.*

e) *Stadium staroby: Zarovnání reliefu; z původních horských hřbetů zbývají jen ojedinělé svědecké pahorky. Zánik vodních toků značným úbytkem srážek. Silná deflace projevuje se na četných drobných vělrných vírech (smrštích) zvedajících sloupy jemného písku a prachu.*